CHARACTERISTICS OF FLOW PAST BLUFF CAVITATING SOURCES

Pandompatam Bhaskaran

A Thesis

in the

Faculty of Engineering

Presented in Partial Fulfilment of the Requirements
for the degree of Doctor of Engineering at
Concordia University
Montréal, Québec, Canada

October, 1977

ABSTRACT

CHARACTERISTICS OF FLOW PAST BLUFF CAVITATING SOURCES

Pandompatam Bhaskaran, D. Eng.
Concordia University, 1978.

An experimental programme has been carried out to study the drag, vortex shedding, erosion and noise characteristics of cavitating flow past circular and triangular sources. The latter shapes are chosen to eliminate Reynolds number effects in interpreting the results. Direct surface pressure measurements are made to estimate the drag force. The vortex shedding frequency of the cavitating bodies was recorded with the help of a pressure transducer. The drag coefficient and Strouhal number are found to increase due to wall interference for moderately large cavitation numbers. The gap velocity u_1 and the contracted jet velocity u_j are shown to be the proper velocity scales to form the drag coefficient, the Strouhal number and the cavitation number in order to account for blockage effects for moderately large blockage conditions.

Part of the study was aimed at evaluating the effects of flow velocity on erosion and noise due to cavitation. To this end, tests were conducted using a rotating disk and a venturi test rig in which soft aluminium test specimens were mounted in the wake of a cavitating source. For a given velocity, a critical size of the cavitation source was

noticed for which the erosion in the specimen was a maximum.

For a fixed source, the peak values of erosion and noise occur in a narrow band of cavitation numbers for the range of test velocities used. An excellent correlation appears to be present between erosion and noise due to cavitation in the range of velocities tested. At peak erosion conditions, the velocity exponents for the weight loss due to erosion and the intensity of noise were found to have an approximate value of 5.45. Further, a splitter plate set in the rear of a cavitating source was shown to reduce both the erosion and noise due to cavitation.

ACKNOWLEDGMENTS

The author wishes to express his gratitude to Professor A.S. Ramamurthy for suggesting the problem and for his guidance in the course of the investigation.

It gives great pleasure for the author to extend his appreciation to Mr. Harald von Cramon, Manager, Engineering and Construction Dept., Union Carbide Canada Ltd., Beauharnois, Québec, for his encouragement in carrying out the project to completion.

The work was supported under the National Research Council of Canada Grant No. 040-204.

Grateful acknowledgment is made to Messrs L. Stankevicius, D. Roy, T. Dugdale and the staff members of the machine shop for their assistance in fabricating the experimental set up.

Thanks are due to Mrs L. Dubé and Miss D. Beaudoin for typing the thesis.

TABLE OF CONTENTS

LIST OF FIGURES

LIST OF TABLES

NOMENCLATURE

b	source size (for cylinders: diameter; prisms: width)
B	width of test section
b/B	blockage (constraint)
c	sound velocity (cm/sec)
C_1	empirical constant
C_c	contraction coefficient
C_D	drag coefficient normalized by u
$C_D(0)$	drag coefficient at $\sigma = 0$
C_{D_1}	drag coefficient normalized by u_1
C_{D_j}	drag coefficient normalized by u_j
C_D'	drag coefficient normalized by v (ref. 41)
C_p	pressure coefficient based upon u
C_{pf}, C_{pb}	pressure coefficient of forebody and pressure coefficient of afterbody
D	erosion criterion (weight loss, volume loss, number of pits/sec/sq inch).
f	frequency
I	noise intensity ($p^2/\rho c^2$)
K	an empirical constant ($= u_s/u$)
K_1, K_2, K_3	constants
ℓ	cavity length
L	characteristic length
m, n_1, n_2	velocity exponents
P	pressure in the undisturbed approaching flow

P_b	minimum pressure on the tunnel wall
P_c	cavity pressure
P_{ref}	reference pressure ($0.0002 dyn/cm^2$)
P_v	vapour pressure
p	r.m.s. sound pressure (dyn/cm^2)
R	Reynolds number (ub/ν)
S	Strouhal number normalized by u ($= fb/u$)
S_1	Strouhal number normalized by u_1 ($= fb/u_1$)
S_j	Strouhal number normalized by u_j ($= fb/u_j$)
SPL	sound pressure level (dB) $= 20 \log_{10} (p/P_{ref})$
t	test duration
u	mean velocity of the undisturbed approaching flow
u_o	incubation velocity
u_1	mean gap velocity (fig. 3)
u_j	contracted jet velocity (fig. 3)
u_s	velocity along the separation streamline (fig. 3)
v	velocity corresponding to the minimum pressure on the tunnel wall
W	weight loss due to erosion (mg)
x	splitter plate (wake interference element) length
θ	angular measurement degrees
λ	non-dimensional cavity length
ν	kinematic viscosity
ρ	density of fluid
σ	cavitation number $(P-P_v)/(\frac{1}{2}\rho u^2)$
σ_1	cavitation number $(P-P_v)/(\frac{1}{2}\rho u_1^2)$
σ_j	cavitation number $(P-P_v)/(\frac{1}{2}\rho u_j^2)$

σ'	cavitation number $(P-P_c)/(\frac{1}{2}\rho v^2)$
σ^*	cavitation number (ref. 87)
σ_i	incipient cavitation number
σ_{ch}	choking cavitation number normalized by u
σ_{ch_1}	choking cavitation number normalized by u_1
σ_{ch_j}	choking cavitation number normalized by u_j

INTERRELATIONS

$$k = u_s/u = \frac{B}{C_c(B-b)}$$

$$u_1 = u/(1 - b/B)$$

$$u_j = u_1/C_c$$

$$C_{D_1} = (1 - b/B)^2 C_D$$

$$C_{D_j} = C_D/k^2 = C_c^2 C_{D_1}$$

$$S_1 = (1 - b/B)S$$

$$S_j = S/k = C_c S_1$$

$$\sigma_1 = (1 - b/B)^2 \sigma$$

$$\sigma_j = \sigma/k^2 = C_c^2 \sigma_1$$

$$\sigma_{ch_1} = (1 - b/B)^2 \sigma_{ch}$$

$$\sigma_{ch_j} = \sigma_{ch}/k^2 = C_c^2 \sigma_{ch_1}$$

CHAPTER 1

INTRODUCTION

CHAPTER 1

INTRODUCTION

In liquid flow systems, when the pressure reaches a value close to the vapour pressure of the liquid, vapour or vapour and gas filled bubbles are formed. The process of formation, growth and subsequent collapse of these bubbles in regions of higher pressure is generally termed as cavitation. Some of the important factors that govern the formation of bubbles are indicated below:

1. Tensile Strength of liquid
2. Nuclei Content
3. Turbulence and boundary layer
4. Physical properties of the liquid
5. Shape and texture of the surface from which the bubbles can be initiated

Due to turbulence and pressure fluctuations that always accompany cavitation, the speed of vaporization, the release of dissolved gases and the subsequent collapse of the bubbles are very complex and statistical in nature. The effect of cavitation has been studied for many years in many diverse fields including hydraulic structures, hydraulic machines, hydrodynamic lubrication, human physiology, space vehicles and nuclear reactors. Initial interest was promulgated by cavitation erosion observed in marine engineering problems in connection with the ship pro-

pellers operating at high speeds. Occurrence of cavitation in hydraulic turbines and pumps usually affects the performance of the machine adversely from the point of view of efficiency and power. This can be traced to the alteration of the flow passage size and the direction of guidance. Further, the life spans of the machine parts are reduced due to cavitation erosion. The power and efficiency characteristics of cavitating machines are generally not well defined. Except in the field of ultrasonic cleaning, destruction of bacteria, depolymerisation and emulsification techniques, cavitation is a hydrodynamic phenomenon whose effects are predominantly undesirable and often destructive.

It is usually difficult or impossible to make direct observations of cavitation when it occurs in prototype hydraulic machines. This necessitates the study of the cavitation phenomenon using special equipment. The following three types of equipment (35) are generally used to study the various effects of cavitation:

1. Flow Apparatus:

   Here, cavitation is produced in constricted passages such as venturi meters, nozzles, or on objects moved at high speeds through the liquid such as a rotating disk or a towing tank.

2. Vibratory Methods:

Cavitation is generated by vibratory means with erosion test specimens attached to the magnetostriction oscillators on the piezoelectric transducer drives.

3. Acoustic-field Generators:

The apparatus consists of a cylindrical glass beaker containing the test liquid, fitted with a Barium Titanate ring just below the free surface of the liquid. When an alternating electric field of sufficient intensity is applied across the conductive coating on its inner and outer surfaces, a standing wave pattern is set up in such a way that a large pressure amplitude is built-up at the centre of the bottom of the beaker. Erosion test specimens are mounted at the bottom of the beaker.

In all these devices, cavitation is produced under controlled conditions in specified locations where observations can be readily made. The present experimental investigations are performed using devices under the first category in order to study the erosion, noise and hydrodynamic characteristics for flow past cavitating bluff bodies.

CHAPTER 2

REVIEW OF EXISTING LITERATURE

CHAPTER 2

REVIEW OF EXISTING LITERATURE

2.1 HYDRODYNAMIC CHARACTERISTICS OF FLOW PAST CAVITATING SOURCES

Considerable data have been published on the hydrodynamic characteristics of flow past cavitating sources (25, 35, 78, 84, 86, 93) mounted in water tunnels. The ratio of the model area to the test section area is generally denoted as blockage and it determines the influence of the side walls on the flow characteristics. A number of studies have been made to determine the effect of blockage on bluff body wakes (49, 63, 76, 77) under non-cavitating conditions. Recently, a few studies have been made to determine the effects of blockage in cavitating flows (14, 57, 88, 91, 92). However, in the tests reported, two-dimensional cylindrical sources were often used (57, 70) and the test conditions spanned the critical Reynolds number of the cylindrical source. Consequently, the test results were highly Reynolds number dependent.

2.1.1 VORTEX SHEDDING CHARACTERISTICS FOR CAVITATING SOURCES

Shalnev (56) used high speed movies to study the wake flow and cavitation characteristics for flow past a cylindrical source in a two-dimentional water tunnel. He states

that the formation and breaking away of the cavity obeys the Strouhal's law in the initial stage of cavity development. At comparable Reynolds numbers, the magnitude of the Strouhal number and also the drag coefficient were found to be close to the established non-cavitating values. In the developed stages of cavitation, the Strouhal number was observed to reach a value of zero. Young and Holl (93) measured the vortex shedding frequency and the spacing of vorticies in the wake of cavitating symmetric wedges using stroboscopic light techniques and high speed movies. The vortex shedding frequency was expressed as a function of the normalized cavitation number σ/σ_i for four different wedges. The Strouhal number based on the vortex shedding frequency was essentially constant from the inception state down to as low as half the incipient cavitation number σ_i. With a further decrease of the cavitation number, a maximum was observed subsequent to which no regular vortex shedding was noted. The geometry of the vortex street was also determined by Young and Holl (93) to understand the near wake structure of the source. Varga and Sebestyen (84) correlated the Strouhal number with the cavitation number for circular cylinders mounted in a water tunnel. For supercritical Reynolds numbers, the following relation was found to be true:

$$S = C_1 \sqrt{\sigma} \qquad (1)$$

where C_1 is a constant and σ is the cavitation number.

According to Varga and Sebestyen, the Strouhal number varied progressively from about 0.32 to 0.24 when the cavitation number was varied from 2.5 to 1.5 for circular cylinders.

Hammitt & Kemppainen (25) studied the vortex shedding characteristics of a cavitating cylindrical pin held in a venturi diffuser with the help of high-speed photography. Rao et al. (68) have also conducted tests to determine the vortex shedding frequency for cavitating two-dimentional circular cylinders ($25{,}000 < R < 800{,}000$) using high-speed photography. Their results confirm the observations of Varga (84) about the progressive reduction of the Strouhal number with the reduction of the cavitation number during the early stages of cavitation. However, the data of Rao et al. (68) also indicate that the Strouhal number for cylyndrical cavitating sources increases abruptly as choking conditions ($\sigma \rightarrow \sigma_{ch}$) are reached. On the other hand, for flow past cavitating wedges, Young and Holl (93) state that the vortex shedding frequency (and hence the Strouhal number S) decreases with decreasing cavitation number and assert that "the wake flow becomes steady and the shedding frequency vanishes as the asymptotic zero cavitation number is approached". It may be appropriate to add that the results of Young and Holl do in fact provide a more representative dependence of Strouhal number on cavitation number since their results are not very much influenced by the effects of the Reynolds number.

In a subsequent section in chapter 4, it will be shown that for partially cavitating conditions, one can associate a predominant frequency to the vortices shed by the cavitating source. On the other hand, as fully cavitating conditions are approached, ($\sigma \rightarrow \sigma_{ch}$) the vortex shedding by the cavitating source will be intermittent to begin with and will vanish when choking conditions prevail.

2.1.2 DRAG COEFFICIENT FOR CAVITATING SOURCES

A number of theoretical and experimental results have been published on the drag coefficient for cavitating sources at very low values of σ ($\sigma \rightarrow 0$). A brief summary of the drag coefficient values for different source shapes, compiled from the various published theoretical and experimental data is available in reference (35). For small cavitation numbers, Birkhoff (6) expressed the drag coefficient as a function of σ as follows:

$$C_D(\sigma) = C_D(0) \quad (1 + \sigma) \qquad (2)$$

Equation 2 is found to be increasingly accurate as σ approaches zero. Varga (83) observes that the drag coefficient for cavitating circular cylinders increases as the cavitation number is reduced, reaches a maximum and then decreases with further reduction of σ. Since the flow around the circular cylinder is highly Reynolds number dependent, the dependence of drag coefficient on cavitation number may be obscured.

2.1.3 BLOCKAGE EFFECTS

2.1.3.1 Non-cavitating sources

In wind tunnel and water tunnel tests, the side walls of the test section can alter the hydrodynamic force coefficients and the vortex shedding frequency of the model set in the test facility. Several studies have been made to determine the effects of blockage on the drag coefficient (49, 63) and the Strouhal number (13, 49, 75, 76, 77) of non-cavitating bluff bodies. It has also been shown that the separation velocity u_s (fig. 3) is the characteristic velocity scale that should be used to normalize the drag coefficient when the blockage effects are severe (49, 50, 63). According to Shaw (62, 63), the contracted jet velocity u_j fig. 3) is equal to the separation velocity u_s when the blockage is at least moderate. The value of u_j is known when the jet contraction coefficient C_c is known. The use of u_j for scaling the velocity in constrained flows is also suggested by Birkhoff (6, 7).

2.1.3.2 Cavitating Sources

Excellent reviews of the wall effects in cavitating flows are given by Plesset and Shaffer (46), Cohen and Diprima (14) and Wu et al (91, 92). Very recently, Popp (48) has analyzed the wall effects problem in cavity flows and her conclusions are in very good agreement with those of

Wu et al. (91, 92). Some of the existing test results (64, 86, 92) confirm the theoretical predictions about the effect of side wall interference on the drag coefficients of bluff bodies at low cavitation numbers.

To account for the blockage effects in his tests on hydrofoils, Meijer (41) used the minimum pressure P_b on the tunnel wall and the corresponding velocity V to form the cavitation number σ' and the drag coefficient C_D'. Both the theoretical predictions of Wu, Whitney and Lin (91) and the experimental results of Whitney (88) indicate that Meijer's procedure generally imparts an over-correction while accounting for blockage. Whitney (87) suggested an empirical correction rule given by equations 3 and 4 for cavitation number and drag coefficient. He also showed that his correction rule was effective for tests on flow past wedges at low cavitation numbers.

$$\sigma^* = \sigma - \frac{(1 + \sigma)}{\sigma} C_D (\sigma, b/B) \frac{b}{B} \qquad (3)$$

$$C_D (\sigma^*, 0) = C_D' (\sigma, b/B) \cdot \frac{(1 + \sigma^*)}{(1 + \sigma)} \qquad (4)$$

However, the effects of blockage on the drag of bluff bodies under partially cavitating conditions (moderately large σ) have not been explored fully. Shalnev (56, 57) had suggested the use of extrapolation techniques to unify the drag coefficient data for cavitating cylinders subject to blockages at higher cavitation numbers.

2.2 VELOCITY DEPENDENCE OF EROSION AND NOISE

2.2.1 CAVITATION EROSION

It has been established by many investigators that the flow velocity has an extremely strong influence on cavitation erosion of test specimens. Laboratory studies indicate that damage due to cavitation varies exponentially with velocity. The two common types of velocity exponents discussed in literature are the following:

$$K_1 u^{n_1} = \text{volume or weight loss} \qquad (5)$$

$$K_2 (u - u_o)^{n_2} = \text{volume or weight loss} \qquad (6)$$

where u_o is an arbitrary incubation velocity under which there is no measurable cavitation erosion.

Table 1 shows the various reported values for the velocity exponents n_1 and n_2, together with the damage criteria used by the various investigators. For the velocity exponent, Knapp (33, 34) and Kerr (32) obtained a good agreement between the water tunnel and field turbine tests. The average value of the exponent was close to 6. Other investigators (21, 25, 27, 29, 56, 74) reported the exponent to be in the range of 4 to 8. The experimental data of Wood (90) and Kozirev (36) indicate that the velocity exponent decreases when the test duration is increased. However, Varga (80), Hammitt (22, 23, 24) and Shalnev (60) assert that the value of the exponent increases with test duration. Hammitt

(23, 24) has also demonstrated that the exponent is highly dependent on the cavitation number. Hobbs (28) has presented a limited amount of data to show that cavitation erosion on a cylindrical source is a function of blockage.

At peak erosion conditions, Ilichev (29) states that the value of the velocity exponent n_1 for cavitation erosion attains a minimum value of 5. On the other hand, Syamala Rao (67) claims that the exponent n_1 attains a maximum value of 17 at peak erosion conditions. Such disagreements in the published data related to the velocity exponent may be partly due to Reynolds number effects associated with the use of cylindrical cavitating sources. Thiruvengadam (74) has reported a value of 6 for the velocity exponent for cavitation damage on rotating hydrofoils and has proposed several scaling laws for cavitation erosion. His erosion results also indicate that the size of the cavitation source and the cavitation number may influence the intensity of erosion.

Some of the recent tests (52) have indicated that the maximum cavitation erosion is associated with an optimum source size when the cavitation number and the velocity are fixed. These results are discussed in a subsequent section in chapter 4. In these tests, the effects of Reynolds number on the flow characteristics were eliminated by choosing the equiangular shape for some of the models tested. It should be added that Reynolds number effects can be severe when the

separation point of the cavitating source shape is not fixed, as in the case of some of the earlier studies (9, 20, 29, 33, 56, 65, 67, 71, 74).

2.2.2 CAVITATION NOISE

A number of investigators have indicated that the change in sound pressure level of the radiated sound could be used to determine the inception of cavitation during tests in water tunnels (16, 29, 59, 85), pumps (16, 44, 85, 89) and water turbines (10, 44). The theoretical spectral density of the noise radiated by a single spherical cavitation bubble is given by Fitzpatrick (19). He has indicated that the noise spectra corresponding to the early stages of cavitation contain much of the energy in the high frequency range. This may be partly attributed to the existence of relatively large number of smaller bubbles. Recently, Blake (8) obtained the cavitation bubble histories for flow past a hydrofoil using movie pictures and got a theoretical estimate of the noise spectra which agreed qualitatively with the spectra associated with the direct sound pressure measurements.

The normalized mean square value of the sound pressure is generally denoted as the intensity of noise I, which is given by equation 7,

$$I = \frac{p^2}{\rho c^2} \qquad (7)$$

In most of the studies related to cavitation noise, the noise level meter registers the sound pressure level SPL (see notation) with reference to an arbitrary reference pressure. Equation 8 gives the commonly used relationship between the intensity of noise I and the velocity exponent m:

$$I = K_3 \, u^m \tag{8}$$

The dependence of noise level on the flow velocity for cavitating flows has been studied in the past to a limited extent. In the analysis reported by Fitzpatrick (19), it has been shown that the sound pressure level caused by the bubbles streaming past a cylinder should increase exponentially with the free stream velocity. Specifically, the exponent was stated to be equal to 4. Blake (8) found experimentally the value of this velocity exponent for cavitation noise for flow past a hydrofoil to be in the range of 3 to 4. For cavitation tests behind a rear-facing step, Lush (39) measured the sound pressure level and filtered the signal in an octave band at 8 KHz. His results indicate that the velocity exponent is close to 4. Ilichev's water tunnel tests (29) on cavitating cylinders show that the velocity exponent depends on the cavitation number and varies from 5 to 8. For similar tests on cavitating circular cylinders and wedges, Varga (85) reported the velocity exponent for cavitation noise to vary from 4.9 to 5.3 in the neighbourhood of the cavitation number at which cavitation erosion is maximum. For flow past a cavitating hydrofoil, Barker (2)

has stated that the value of the exponent varied from 6 at the low frequency end (f< 1KHz) to 10 at the high frequency end of the spectra (10 KHz < f < 100 KHz)

2.3 SCOPE OF THE PRESENT INVESTIGATION

The following aspects of the problem of flow past a cavitating source are studied in the present investigation.

1. The effects of blockage on the following hydrodynamic characteristics in the upper range of cavitation numbers (large σ):
   a) Drag Coefficient
   b) Strouhal Number
2. The effects of the source size and velocity on cavitation erosion.
3. The effects of cavitation number and velocity on the following:
   a) Cavitation Erosion
   b) Cavitation Noise
4. The effects of wake interference elements on the following characteristics:
   a) Cavitation Erosion
   b) Cavitation Noise

CHAPTER 3

EXPERIMENTAL SET UP AND PROCEDURES

CHAPTER 3

EXPERIMENTAL SET UP AND PROCEDURES

A brief description of the equipment used in the present study is outlined below. A venturi apparatus was used to study the blockage effects for flow past cavitating sources. Both the erosion and noise studies were conducted in a modified test section of the venturi apparatus. A rotating disk apparatus was used to study the effects of source size and velocity on cavitation erosion.

3.1 VENTURI FLOW APPARATUS

The venturi flow apparatus (fig.1) is characterised by a two dimensional test section in which the model source can be housed to study its cavitation characteristics.

3.1.1 BLOCKAGE EFFECTS ON DRAG AND VORTEX SHEDDING CHARACTERISTICS

The studies on drag coefficient and Strouhal number were conducted in the two-dimensional test section of the venturi apparatus. It was 154 mm wide and 6 mm deep. Polished brass cylinders and equilateral prisms formed the basic shapes for the cavitation source (fig. 2). The minimum size of the model was 16 mm. The models were mounted as struts across the test section (fig. 3). Peripheral pressure taps were housed in the cavitating sources and these were connected in turn to a bank of manometers and pressure transducers. The drag force was obtained by direct

integration of the steady pressure around the cavitating source. Great care was taken to properly orient the source. The requirement of symmetry of the pressure distribution was used as a check in this context. The flow was measured with the help of a calibrated venturi meter.

The vortex shedding frequency was obtained with the help of a pressure transducer located in the edge of the wake region of the source. The location of the transducer for different shapes and sizes of the model was determined by trial and error to register the primary vortex shedding frequency. The associated instrumentation is shown in figure 4. The amplified signal was recorded on a strip chart recorder and the recorded data were often checked with the help of a frequency counter. The transducer signals were also recorded on a tape recorder. An analyser fitted with a level recorder was used for spectral analysis of the recorded data, especially when the frequency of vortex shedding was not discernible from direct records of the strip chart. For this purpose, large enough time samples were chosen. If the frequency of vortex shedding was f, the sample length in seconds was generally in excess of 500/f. The upper range of the cavitation numbers covered in the test spanned both noncavitating and partially cavitating conditions.

3.1.2 EROSION AND NOISE TESTS

Erosion and noise tests were conducted in the venturi apparatus in a modified test section (fig. 5). The test section was similar to the test section described in section

3.1.1. In order to achieve a wider range of velocities, a narrower cross section was adopted for all the erosion tests (61mm X 5.59mm). A polished equilateral prism of sides 19.1 mm fixed with its apex facing downstream was used as the cavitation source. The test specimens were made of 6.4 mm soft aluminium plates (1100-F). These specimens were cleaned, dried and weighed with the help of a precision balance whose least count was 0.1 mg and fixed in the downstream section of the cavitating prismatic source. Following the test for a set duration, the loss of weight of the specimen was determined. The pressure and velocity at the test section were changed independently to obtain a wide range of cavitation numbers.

Preliminary tests were conducted to determine the effect of test duration on the erosion rate (fig. 6). The results were in general agreement with published data (40, 47). Generally, one would prefer to keep the test duration long enough to improve the accuracy of weight measurements. However, for tests longer than 120 minutes, it was difficult to keep the water temperature constant and further, a through hole was formed in the test specimen for some tests. Hence, a test duration of 75 minutes was chosen for the subsequent tests. This duration was also in a region where the erosion rate was not highly dependent on time (fig. 6).

A precision sound level meter (Bruel and Kjaer) was located at about 300mm from the face of the test section in

3.1.1. In order to achieve a wider range of velocities, a narrower cross section was adopted for all the erosion tests (61mm X 5.59mm). A polished equilateral prism of sides 19.1 mm fixed with its apex facing downstream was used as the cavitation source. The test specimens were made of 6.4 mm soft aluminium plates (1100-F). These specimens were cleaned, dried and weighed with the help of a precision balance whose least count was 0.1 mg and fixed in the downstream section of the cavitating prismatic source. Following the test for a set duration, the loss of weight of the specimen was determined. The pressure and velocity at the test section were changed independently to obtain a wide range of cavitation numbers.

Preliminary tests were conducted to determine the effect of test duration on the erosion rate (fig. 6). The results were in general agreement with published data (40, 47). Generally, one would prefer to keep the test duration long enough to improve the accuracy of weight measurements. However, for tests longer than 120 minutes, it was difficult to keep the water temperature constant and further, a through hole was formed in the test specimen for some tests. Hence, a test duration of 75 minutes was chosen for the subsequent tests. This duration was also in a region where the erosion rate was not highly dependent on time (fig. 6).

A precision sound level meter (Bruel and Kjaer) was located at about 300mm from the face of the test section in

3.1.1. In order to achieve a wider range of velocities, a narrower cross section was adopted for all the erosion tests (61mm X 5.59mm). A polished equilateral prism of sides 19.1 mm fixed with its apex facing downstream was used as the cavitation source. The test specimens were made of 6.4 mm soft aluminium plates (1100-F). These specimens were cleaned, dried and weighed with the help of a precision balance whose least count was 0.1 mg and fixed in the downstream section of the cavitating prismatic source. Following the test for a set duration, the loss of weight of the specimen was determined. The pressure and velocity at the test section were changed independently to obtain a wide range of cavitation numbers.

Preliminary tests were conducted to determine the effect of test duration on the erosion rate (fig. 6). The results were in general agreement with published data (40, 47). Generally, one would prefer to keep the test duration long enough to improve the accuracy of weight measurements. However, for tests longer than 120 minutes, it was difficult to keep the water temperature constant and further, a through hole was formed in the test specimen for some tests. Hence, a test duration of 75 minutes was chosen for the subsequent tests. This duration was also in a region where the erosion rate was not highly dependent on time (fig. 6).

A precision sound level meter (Bruel and Kjaer) was located at about 300mm from the face of the test section in

the horizontal plane containing the axis of the cavitation source (fig. 5). The sound level meter had a built-in octave filter set with eleven band pass filters in the range of 31.5 Hz to 31.5 KHz. A complete spectrum of the sound pressure level was taken for each erosion test in order to correlate the erosion data with the noise data.

3.1.3 STUDY OF WAKE INTERFERENCE ELEMENT TO REDUCE CAVITATION EROSION AND NOISE.

For wake interference tests, the test section described in section 3.1.2 was used. A brass circular cylinder formed the cavitating source. Its diameter was 19.1 mm. Wake interference elements of varying lengths (35.05 and 95.5mm) in the form of a splitter plate were attached to the rear of the cavitation source. The length ℓ of the cavity in the rear of the source was always recorded during the tests. It is well known that the non-dimensional cavity length λ ($= \ell/b$) is closely related to the cavitation number σ (59,82). As such, λ was chosen as a parameter in place of σ. The test specimen consisted of 1100-F aluminium plates (6 mm thick). The duration of the test to determine the weight loss due to cavitation erosion was chosen to be one hour for the wake interference tests. Tests were repeated to check the consistency of results.

The light flicker of a stroboscope was synchronized with the vortex shedding frequency f of the cavitating test body. The trail of vapour bubble clusters were ren-

dered clearly visible by this method, especially when the test body was not fitted with a splitter plate. When longer splitter plates were attached to the source to cause wake interference, no visible trails of vapour clusters were present in the section downstream of the source. A noise meter was located close to the plexiglass cover of the test section (fig. 5) to record the noise data.

3.2 ROTATING DISK APPARATUS

The rotating disk apparatus (fig. 7) consisted of a circular disk attached to a rotating horizontal shaft. The disk itself was housed in a chamber filled with water. During the test run, a constant supply of fresh tap-water was maintained in order to keep the water temperature nearly constant. Settling vanes mounted in the chamber on either side of the disk inhibited induced circulation of water. Triangular prisms and circular cylinders were adopted as the basic forms for the source of cavitation (fig. 7). The former shape is associated with the flow characteristics that are independent of the Reynolds number. The sizes of the source were limited to 38.1 mm so that excessive velocity gradients were absent across the face of the source. Downstream of the cavitation source soft aluminium (1100-F) test pieces (3 mm thick) were fixed flush on the disk.

For each test, both the specimen and the cavitation source were mounted at a predetermined radius. The peripheral velocity of the source was readily obtained by noting

the angular velocity of the disk. Tests were conducted at different controlled chamber pressures to obtain a constant cavitation number. The test specimens were cleaned, dried in a dessicator and weighed on a precision balance to an accuracy of 0.1 mg in order to obtain the weight loss due to cavitation erosion. For purposes of visual observation, a stroboscope was used.

Tests were also conducted to determine the effect of test duration on cavitation damage (fig. 8). A through hole was formed in the specimen for test durations longer than 40 minutes in some tests. At the same time one would prefer to stay away from the threshold value of test duration (approximately 9 minutes). Consequently, a test duration of 30 minutes was chosen for the other tests in this series.

3.3 EXPERIMENTAL UNCERTAINTIES

The error ranges of the observed or computed data presented in the following sections are given in Appendix II in a tabular form. The error range of the individual variables are considered in order to compute the error range of non-dimensional variables.

CHAPTER 4

ANALYSIS OF RESULTS

CHAPTER 4

ANALYSIS OF RESULTS

4.1 HYDRODYNAMIC CHARACTERISTICS OF CAVITATION

In the ensuing discussions the drag and vortex shedding characteristics of cavitating cylindrical and prismatic sources are considered with an emphasis on blockage correction.

4.1.1 DRAG COEFFICIENT

4.1.1.1 Cylindrical Sources

While studying the effect of blockage on the drag coefficient and vortex shedding frequency of cavitating bodies, the influence of Reynolds number on the test results should be reduced or eliminated. For most of the normal test facilities that are in use, the Reynolds number ranges of the tests span the critical Reynolds number of a cylindrical source. As stated earlier, in this range, the Strouhal number S and drag coefficient C_D are very sensitive to Reynolds number changes (4,12,42).

Figure 9 indicates that the drag coefficient characteristics of cylindrical sources under noncavitating constrained flow conditions (large σ) do follow the trends reported earlier (49,75,76). The discrepancies between the present test data (noncavitating) and those reported elsewhere can be attributed once again to the fact that C_D is very sensitive to Reynolds number effect in the neighbourhood of the critical Reynolds number.

The drag coefficient for circular cylinders in the lower range of cavitation number which included the minimum value of σ attainable in the present test set-up is shown in figure 10. The numerals in these graphs correspond to the pressure distribution graphs of figures 12 and 13. The line demarking cavitation condition in figure 10 refers to the presence of visual initiation of cavitation as seen with the help of a stroboscope. The value of the drag coefficient increases with the reduction of cavitation number up to a critical value and thereafter tends to decrease significantly as the cavity length approaches its upper limit in the tests.

As one reduces the cavitation number of the flow, the flow separation point starts moving upstream for the test conditions shown in figure 11 and gradually the area enveloped by the cavity spans a bigger segment of the afterbody and in the limit (case 3), the separation points reach the crown points of the cylinder. As a result of this, the deceleration of the flow in the afterbody is limited. Consequently, the pressure coefficient of the afterbody section C_{pb} is lower for case 3 (partially cavitating) as compared to case 1 (noncavitating). Since the forebody pressure coefficient C_{pf} is the same in both cases, a slight increase in the drag coefficient is registered for partially cavitating conditions. Further reduction of the cavitation number by increased velocity or a general decrease in the ambient pressure (case 3 to 6, fig. 10)

corresponds to situations wherein the flow accelerations on the forebody require very low pressures at the separation point. The pressure at the separation point has a lower bound which is close to the vapour pressure of water. As the velocity is increased from case 3 to 6 (at a fixed ambient pressure), the limiting forebody pressure and hence the separation point for case 6 occur at a location upstream of the separation point for case 3. The forebody pressure coefficient C_{pf} is hence reduced and the net result is a reduced drag coefficient value for cases 4,5 and 6. Silberman (64) and Varga (83) have presented experimental data which also indicate that a decrease in cavitation number is accompanied by a decrease in the drag coefficient of circular cylinders when the cavitation numbers are very low. Since the effects of surface roughness and Reynolds number can be significant for flow past cylindrical sources, the comparison of the different results in figure 13 must be made only on a qualitative basis.

It may be remarked that abrupt changes in the drag coefficients reported by Varga (83) were not registered in the present tests (fig. 13) when the cavitation number was lowered. Roshko's model (55) for cavitating cylinders is also included in figure 13. According to him, the value of C_D is equal to 0.5 for zero cavitation number (unbounded flow). Further, at low cavitation numbers ($\sigma<0.5$), the drag coefficient is found to vary linearly with the cavitation number. Waid's test data (86) for very low

blockage (b/B = 0.027), agrees very well with Roshko's model (55). Table 2 and figures 38, 39 and 40 indicate the choking cavitation numbers (σ_{ch}) associated with the different shapes tested. For the smaller sizes of the test bodies, available information from other studies is shown.

When the gap velocty u_1 (fig. 3) is used as the characteristic velocity, the resulting drag coefficient C_{D_1} is nearly constant for non-cavitating flows (fig. 9). However, for the developed stages of cavitation, it seems to depend on blockage.

4.1.1.2 Prismatic Sources

The drag coefficients for noncavitating prismatic sources determined in the present investigation agree well with those reported in the earlier studies (49,50,75). This is shown in figures 14 and 16 for both orientations of the prism. The dependence of the drag coefficient on cavitation number for those two bodies for different blockages is shown in figures 15 and 17. The numerals on the curves correspond to the pressure distribution curves given in figures 19 to 24. When the cavitation number σ is lowered progressively to reach fully cavitating conditions, the value of the suction pressure at the separation points will be reduced. Further, the larger suction pressure registered near the mid-section of the afterbodies at higher cavitation numbers will disappear (fig. 19). Hence the drag coefficient C_D will be reduced as fully cavitating

conditions are reached. Due to the limitations of the experimental set-up, the back pressure was relatively high and the smaller bodies (b/B = 0.196 and 0.103) could not be tested for choking conditions (table 2). Figure 17 includes some of the existing experimental and theoretical results for 30° and 90° wedges (35,86) for low blockages and low cavitation numbers.

For the prism set at 0° orientation, a similar comparison of the present test data with earlier results (35,86) is shown in figure 18. The mean curves shown are adopted from figure 15.

It should be noted that the drag coefficient for a blunt body such as a flat plate or a prism ($\theta = 0^{\circ}$) increases with blockage when the cavitation number is sufficiently high and the flow is noncavitating. As blockage increases, the flow gets accelerated near the front edges where flow separation occurs and as a consequence of this, the average value of the forebody pressure coefficient gets lowered. However, at higher blockage, the decrease in the average value of afterbody pressure coefficient more than compensates for the loss of thrust on the forebody and this in turn increases the drag coefficient. On the other hand, as choking conditions are approached ($\sigma \rightarrow \sigma_{ch}$), the suction pressures on the surface of the afterbody reach a limiting value close to the vapour pressure. Moreover, "the lateral constraints of the tunnel wall must make the flow velocity somewhat higher, and hence the pressure lower, than their

corresponding values for unbounded flows over the wetted body surface away from the stagnation point, provided the comparison is made for the same cavitation number" (91). Consequently, increased blockage yields a lower drag coefficient at choking conditions, since the average value of the back pressure coefficient does not change significantly and compensate for the decrease in the average value of the forebody pressure coefficient. Away from choking conditions, the pressure on the afterbody will not have reached the limiting value (vapour pressure) and hence the blockage effects tend to follow the trend for noncavitating flows.

An attempt was made to use the gap velocity u_1 and the contracted jet velocity u_j to normalize the drag force of the two prisms subjected to blockages. One can use u_1 in place of u_j if the contraction coefficient C_c is a weak function of blockage as in the case of the triangular prism (15) set at 60°. The graphs in figures 15 and 17 show that the values of C_{D_j} and C_{D_1} denoting the prism drag coefficients based on u_1 and u_j are indeed invariant over a large range of cavitation numbers. It may be noted that the value of u_j is equal to the separation velocity u_s ($= ku$). Equation 9 yields the value of k in terms of C_c and b/B,

$$k = \frac{B}{C_c(B-b)} = \frac{u_j}{u} = \frac{u_s}{u} \qquad (9)$$

For the prismatic sources set with their apex facing downstream (0^{o} orientation), the value of k and the contraction coefficient C_c for a flat plate (62) were used to compute u_j. This was based on the assumption that the afterbody of the prism has marginal effect on the jet contraction.

There is a minimum value of k for each body shape. Hence, at very low blockages, equation 9 will underestimate the value of k. For instance, the limiting value of k (=1.46) for a flat plate (62) is reached when the blockage is close to 0.12. Consequently, for blockages which are well below the limiting value ($b/B << 0.12$), adoption of u_j based on equation 9 may not be effective as the velocity scale to account for blockage. Hence, no attempt was made to reduce the experimental results from other studies related to drag characteristics at extremely low blockages. Further, for flow past a source at low cavitation numbers, C_D decreases with an increase in blockage (87,88) and as such u_j (= ku) cannot be used to yield a constant drag coefficient C_{D_j} at very low cavitation numbers, since k is always greater than unity for all sources.

4.1.2 VORTEX SHEDDING CHARACTERISTICS

4.1.2.1 Cylindrical Sources

Figure 25 shows the blockage effects on the vortex shedding frequency of circular cylinders at large cavitation numbers (noncavitating). The Strouhal numbers S and S_1 are formed using the undisturbed velocity u and the gap

velocity u_1 respectively (fig. 3). The experimental results denoting the Strouhal numbers for cavitating cylinders are plotted against cavitation number in figure 26. Due to the limitations of the test set-up, the smaller source (b/B = 0.165) could not be tested for choking conditions. The trend towards the choking condition is indicated by the dotted lines in this figure. Since the Reynolds number of the flow was close to the critical Reynolds number, the vortex shedding frequency and hence the Strouhal numbers S and S_1 display a wide scatter (figure 26). Consequently, no clear dependence of S and S_1 on cavitation number or blockage can be established. When the cavitation number was gradually reduced to reach choking conditions, vortex shedding occurred intermittently. A few typical pressure pulsation records and power density spectra for the cavitating cylinder (b/B = 0.165) are shown in figures 27 and 28. The test results of other investigators are compared with the general trends displayed by the present data in figure 29. In some earlier investigations (68, 70) it was shown that the Strouhal number for cavitating cylinders reaches a minimum and starts rising again as the cavitation number is reduced. However, in the present tests, the Strouhal number continuously decreased following a small increase as choking conditions were approached. Such a dependence of Strouhal number on cavitation number has also been reported in some of the studies related to cavitating flow past two dimensional wedges (93) and cylinders (56,

61, 81).

The mean curves denoting S_1 for the two cylinders tested tend to merge into a single curve for non-cavitating (fig. 25) flows. Except in the vicinity of choking conditions, this characteristic holds even for partially cavitating conditions (fig. 26).

4.1.2.2 Prismatic Sources:

The effect of blockage on the vortex shedding frequency of cavitating prisms is clearly seen in figures 31 and 33. Here, the source shape chosen eliminated Reynolds number effects. A sequence of pressure records and corresponding power density spectra for the triangular prism set at 60° orientation ($b/B = 0.326$) is shown in figures 34 and 35. These figures provide a clear contrast between the type of signals registered for the prisms and the cylinders. The dip in the vicinity of 63 cps and 200 cps in all the spectral graphs (figs. 28 and 35) is due to the shift registered by the level recorder as the different band widths are scanned. As such, this dip should be ignored while interpreting the spectra.

When the choking conditions are approached (fig. 34), the pressure pulsations occur only intermittently. The trend indicates that the pressure pulsations and hence, the vortex shedding will cease when choking occurs. The high speed movie pictures show that little or no interaction occurs between the separated sections of the flow when

choking conditions are approached. This observation is found to be true for all the three source shapes tested. As one approaches choking stage, it is difficult to analyze the vortex shedding phenomena using high speed movies and this difficulty is expressed by other investigators too (68, 70, 93). To get reliable data, especially for the cylindrical sources, numerous strips of photographs are to be taken, since the vortex shedding is irregular near choking conditions. The need to keep a minimum film speed (frames per second) to ensure proper resolution, often restricts the sample lengths that can be obtained. On the other hand, the continuous recording of the pressure signals enables one to obtain a large enough sample without sacrificing resolution. The spectral plots (fig. 35) of the pressure signals are characterized by well defined peaks for the prisms when the cavitation numbers are sufficiently high. However, for conditions in the vicinity of choking flow, the spectral plots are characterized by wide band noise and are indicative of the absence of vortex shedding. Young and Holl (93) have also stated that vortex shedding ceases for cavitating wedges when choking conditions prevail. The absence of vortex shedding in the vicinity of choking has also been reported for cavitating flow past cylinders (56) and spheres (66).

The values of S_j and S_1 are nearly invariant for the prisms set at 0^o and 60^o respectively for a wide range of cavitation numbers (figs. 31 and 33). The agreement of the

Strouhal number data (figs. 30 and 32) with earlier results is quite close. In the fully cavitating region, the curves denoting different blockages are expected to reach choking conditions ($\sigma \rightarrow \sigma_{ch}$, $S = 0$) at different values of the cavitation number (table 2).

4.1.3 BLOCKAGE CORRECTION FOR CAVITATION NUMBER

As discussed already in the previous sections, it is clear from figures 10, 15, 17, 26, 31 and 33 that the dependence of the modified parameters C_{D_1}, C_{D_j}, S_1 and S_j on blockage is limited to very low cavitation numbers ($\sigma \rightarrow \sigma_{ch}$). However, an attempt is made to remove this dependence by replacing σ by the modified cavitation numbers σ_1 and σ_j as shown in figures 36 and 37. Since the present experimental results for choking conditions are confined to the higher blockages, additional experimental data from another source (43) is also included in figures 36 and 37. It may be of interest to note that the reduced form of vortex shedding data of Young (93) shown in figure 37 starts departing from the general trend at lower cavitation numbers, since the flow constraint was extremely weak ($b/B = 0.02$) for these tests (see section 4.1.1.2, page 27).

4.1.4 BLOCKAGE CORRECTION FOR CHOKING CAVITATION NUMBERS

For flow past a cavitating source fixed in the test section of a water tunnel, the minimum value of the cavitation number attainable is a function of the blockage and the source shape. As the cavitation number decreases, the

cavity lengthens and eventually becomes extremely long at a cavitation number greater than zero. Under these conditions, the tunnel is said to be choked and it is not possible to further reduce the value of the cavitation number. The effect of choking is important since it limits the ability of a water tunnel to operate at low cavitation numbers. Theoretical (7, 14, 79) and experimental (11, 37, 43) evidence indicates that a larger blockage is associated with a higher value of the choking cavitation number σ_{ch}. Figures 38, 39 and 40 show the choking cavitation numbers for circular cylinders and prismatic shapes. Since the present test results for choking conditions are limited to larger blockages, data from other sources (7, 11, 37, 43) are also included. An attempt is made to examine the effect of the use of u_l and u_j to reduce or eliminate the blockage effects on σ_{ch}. The resulting modified choking cavitation numbers σ_{ch_l} and σ_{ch_j} are also indicated in figures 38, 39 and 40. It is clear from these figures that σ_{ch_l} and σ_{ch_j} are nearly independent of blockage except at low blockages

4.2 EROSION AND NOISE CHARACTERISTICS OF CAVITATION

4.2.1. EROSION DUE TO CAVITATION

4.2.1.1 General Remarks

The high transient pressure and shock waves associated with cavitation erode the material in the proximity

of a collapsing bubble. Earlier studies related to cavitation erosion in a variety of metal specimens indicate that structural damage can occur due to high intensity pressures caused by blows (33, 73). Direct evidence has been provided by a few investigators to show that large mechanical stresses develop at the region of bubble collapse (5, 18). Single blow cratering is not uncommon due to cavitation collapse (22, 33). However, a flow phenomenon capable of generating a pulsating pressure field can accentuate the damage potential of the cavitation system. This is especially true when one recognizes that structural damage has been attributed to fatigue failure (20, 71) at stress intensities which are inadequate to cause damage by single blows (35).

At fixed cavitation numbers and test specimen material characteristics, one should expect both the size of the cavitation source and the frequency of pressure pulsations to significantly influence the intensity of erosion and noise due to cavitation. The results of the study undertaken to determine the effects of source size and velocity on the cavitation erosion characteristics are outlined below.

4.2.1.2 Effect of Source Size and Velocity on Erosion

The erosion studies conducted in the rotating disk apparatus provided the variation of weight loss due to cavitation for specimens mounted in the rear of the cavitation sources. The cavitation data was obtained at

fixed cavity length. The latter denotes fixed cavitation numbers (33).

Figure 41 shows the cavitation damage test data for three sets of velocities in which a circular cylinder was used as the cavitating source. Since the test range spans the critical Reynolds number for all the present tests, the frequency of vortex shedding and the pressure pulsations in the source wake depend highly on the Reynolds number. In the vicinity of the critical Reynolds number, the change in the Reynolds number is accompanied by significant shifts in the location of the separation point. This in turn will alter the frequency of vortex shedding and hence, the frequency of pressure pulsations. This characteristic of the flow has been confirmed for both cavitating and non-cavitating cylindrical sources (30, 51, 53). Consequently, for the tests related to the effect of source size and velocity on cavitation erosion, it is desirable to choose a source shape for which the Reynolds number is not a primary factor determining the behaviour of the flow.

The loss of weight data for the triangular source is shown in figure 42. The prismatic sources have fixed flow separation points and the flow characteristics are not dependent on Reynolds number. When the cavitation number and the source velocity are fixed, a decrease in the source size increases the frequency of pressure fluctuations. This is reflected in the increased damage

(weight loss) up to a certain limiting source size (fig.42). Clearly, when the source size is made extremely small, its effect is local and no serious damage should be expected. In other words, for a given set of controlled conditions (fixed velocity and cavitation number), there is a combined effect of source size (scale) and frequency of pressure pulsations which render the weight loss (cavitation damage) to be a maximum. This trend was confirmed for three sets of velocities.

The flow field associated with a rotating disk facility at the location of the cavitating source is rather complex in view of the fact that the flow is highly sheared This necessitated more controlled tests in a two dimensional water tunnel to study the effect of cavitation number and the velocity exponent for erosion and noise. Consequently, some tests were also conducted in a venturi test section using a prismatic cavitation source. The results of these tests are discussed in the following section.

4.2.1.3 Effect of Cavitation Number and Velocity on Cavitation erosion

Since Reynolds number effects were eliminated with the use of the prismatic cavitating source in the present tests, the variations in both the cavitation erosion and cavitation noise recorded can be directly traced to the variations in the flow velocity and the cavitation number.

Figure 43 shows the erosion of the test specimen as a function of the cavitation number. The flow velocity has been used as the group parameter. Due to equipment limitations, the erosion data for the highest velocity could not be obtained for higher cavitation numbers. Nevertheless, the cavitation number for maximum erosion can be identified for all the cases reported. Figure 43 shows that cavitation erosion depends strongly on the cavitation number at a given velocity. As the cavitation number is decreased, the erosion increases, reaches a maximum and then decreases with decreasing cavitation number. This characteristic of the erosion curves (fig. 43) can be attributed to the following facts.

It has been observed that the cavitation bubbles move approximately at the same speed as the liquid (31). The length of cavity increases when the cavitation number is reduced beyond the point of inception. As the cavitation number is reduced by decreasing the ambient pressure P at a fixed velocity, the dominant bubble size becomes larger, since the time available for bubble growth is longer. The larger bubbles penetrate the high pressure regions and their damage potentials are higher. On the other hand, reduction of P also results in a reduced collapse pressure (72). This amounts to a reduced damage potential at lower cavitation numbers. In fact, very little damage is sustained when the cavitation region entirely envelops the test specimen (22). Consequently,

the overall damage potential of the bubbles will increase to a maximum and then decrease due to the effect of the two opposing variables, namely the size of the bubbles and the ambient pressure at which they collapse.

The dependence of erosion on the cavitation number is similar for the five velocities tested in the present study. The cavitation numbers at which the peak erosion occur, stay within a narrow band ($2.7 < \sigma < 2.9$) and this is qualitatively in agreement with the earlier published data (9, 22, 29, 69, 74, 85). However, the choice of circular cylinder as a cavitation source often may lead to ill-defined relationships between cavitation erosion and cavitation number (9, 52, 69).

4.2.2 NOISE DUE TO CAVITATION

4.2.2.1 General Remarks

It is well known that hydrodynamic cavitation is always associated with a loud hissing sound as a result of the growth and collapse of the vapour cavities. The magnitude of erosion due to cavitation and the sound pressure level are determined by the distribution of cavitation bubbles with respect to their number, size, spacial location and implosion rate. Hence, it is reasonable to expect a close relationship between the extent of cavitation erosion and the intensity of cavitation noise. It is beneficial to study the effects of flow velocity and cavitation number on cavitation noise besides cavitation ero-

sion. Hence, a few tests were conducted to determine the effect of velocity and cavitation number on cavitation noise for a fixed cavitating prismatic source set in the test section of the venturi apparatus.

4.2.2.2 Effect of Cavitation Number and Velocity on Cavitation Noise

Sound pressure levels were obtained for different cavitation numbers at fixed flow velocities. Figure 44 shows a typical spectral distribution of sound pressure levels at a fixed velocity for various cavitation numbers. An estimate of the background noise was obtained by registering the sound pressure levels for test conditions at which there was no visible cavitation. The background noise levels were relatively very weak at higher frequencies. Figure 45 shows the spectra of the sound pressure levels for different flow velocities at a fixed cavitation number. At fixed cavitation numbers, the sound pressure levels in the high frequency range ($f > 2000$ cps) appear to increase with velocity. The drastic reduction in the sound pressure levels at 31,500 cycles per second is attributed to the frequency response (20-20,000 cps) characteristics of the microphone.

For the test series aimed at correlating erosion and the associated noise, the sound pressure levels were registered after setting the center frequency of the octave filter at 8,000 cycles per second in order to limit

the interference of low frequency background noise.

Figure 46 shows the measured sound pressure levels of cavitation noise (f = 8000 cps) for the same test conditions as for the erosion tests (fig. 43). Beyond the inception point, the sound pressure levels increase with the reduction of cavitation number, reach a peak value and decrease with further reduction of the cavitation number. At the inception of cavitation, the sound pressure level increases due to the formation and collapse of vapour bubbles. This is especially true in the high frequency range of the spectra, since the smaller bubbles are associated with higher frequencies. As the cavitation number is reduced further, the number of bubbles and their collapse pressures increase and this in turn increases the radiated sound pressure. The formation of longer cavities at lower cavitation numbers promote the growth of larger bubbles at the expense of smaller ones. As the bubbles grow bigger, they absorb more and radiate less noise in the high frequency range. Hence, the rise of the sound pressure levels at the high frequency band is limited, as one approaches the lower range of cavitation numbers. This also accounts for the reduction of the high frequency noise as choking conditions are approached.

4.2.3 CAVITATION EROSION AND NOISE CORRELATION

The peak erosion and peak noise occur in the same narrow band of cavitation numbers for the present test

series (figs. 43 and 46). Although the noise peaks are less well defined than the erosion peaks, an attempt was made to correlate the peak erosion with the peak noise (fig. 47). The vertical bands in figure 47 show the ranges of cavitation numbers with which the peak noise (fig. 46) can be associated. Clearly, there is a very close correlation between peak erosion and peak noise, which is in agreement with the results of earlier investigations (16, 29, 45, 51, 85).

4.2.4 VELOCITY EXPONENT

With the help of the results shown in figures 43 and 46, the velocity exponents n_1 and m corresponding to to peak erosion conditions were obtained for the weight loss W and the noise intensity I respectively. Figure 48 shows the dependence of both the peak noise and the peak erosion as functions of the flow velocity. It is clear that the velocity exponents n_1 and m are almost identical and possess a value of 5.45 in the velocity range tested.

In the present test series, it must be noted that the exponents n_1 and m corresponding to peak erosion conditions were obtained when the source size and blockage were fixed. Further tests are required to study the effects of blockage and source size on the velocity exponents since peak erosion also depends on the source size (52) and blockage (28).

As part of the general study related to the hydrodynamic characteristics of flow past cavitating sources, it was felt desirable to explore a method by which cavitation erosion and noise can be reduced based on a principle of drag reduction. The following section is related to this aspect of the general problem.

4.2.5 EFFECT OF WAKE INTERFERENCE ELEMENT ON CAVITATION EROSION AND NOISE

The results of the experiments are related to a specific problem of cavitating flow past a two dimensional cylindrical body to which a wake interference element in the form a splitter plate is attached at the rear. It is well known (1, 3, 54) that considerable reduction of the fluid dynamic drag of a bluff body occurs when a splitter plate is attached to the rear of the body. This change is a result of the lack of pressure communication on either side of the line of symmetry in the near wake. The splitter plate permits a reattachment of the flow which separates from the main body and prohibits the interaction of the shear layers.

Figures 49 and 50 indicate the effectiveness of the splitter plate in reducing cavitation damage. In the case of bodies fitted with an appropriate splitter plate only a superficial damage occurs. This damage is restricted to the removal of the surface shine. The attack on the test specimen is considerable for the same duration

when there is no splitter plate.

Figure 51a shows the graph of weight loss W due to cavitation damage as a function of cavity length λ with the splitter plate length x/b as the family parameter. The reduction of weight loss is particularly significant for the test body with a splitter plate length of x/b equal to 5 or more, for all cavity lengths.

The near synchronization of vortex shedding and the discrete pulse frequency of the stroboscopic light confirms the existence of a predominant frequency f_s in the frequency spectra of the near wake flow of the cavitating body reported by other investigators (81, 93). As stated earlier, the visible wake trail of vapour bubbles was not present for the case where longer splitter plates were attached to the test body. This may in part be due to the higher base pressures associated with cylinders carrying splitter plates.

Figure 51b shows the results of noise analysis in a wide band width (2000 to 20000 cps). The lower limit of this band width was chosen to eliminate the influence of background machinery noise which was significant up to 2000 cps. The frequency response of the microphone imposed a restriction on the upper limit of the band width of analysis. The close correlation between the reduction of cavitation noise and cavitation erosion in figure 51 also upholds the results discussed in section 4.2.3. Table 3 summerizes the results of these tests.

CHAPTER 5

SUMMARY AND CONCLUSIONS

CHAPTER 5

SUMMARY AND CONCLUSIONS

5.1 CONCLUSIONS

1. The drag coefficients of partially cavitating bodies such as circular cylinders and triangular prisms increase due to wall interference effects when the cavitation numbers are relatively large. The trend of the present drag data indicates that the wall interference effects are small near zero cavitation number. For constrained flow past triangular prisms set at 60° and 0° orientations, the gap velocity u_1 and the jet contraction velocity u_j are the proper velocity scales that yield nearly constant drag coefficients over a wide range of cavitation numbers.

2. For constrained flow past prisms ($\theta = 60^{\circ}$ and 0°), the Strouhal number of the flow is nearly constant until choking conditions are reached. The Strouhal number increases slightly with decreasing cavitation number as choking conditions are approached and later reaches the zero value. The shedding of vortices stops when choking conditions prevail. The velocity scales u_1 and u_j provide a nearly constant Strouhal number for constrained flow past prisms ($\theta = 60^{\circ}$ and 0°), over a broad range of cavitation numbers (except in the neighbourhood of choking conditions). The corresponding tests for studying the characteristics of constrained flow past cylindrical sources are inconclusive as the Strouhal number of the flow is highly dependent on the cylinder Reynolds number.

The velocity scales u_l and u_j can be utilized to form the modified cavitation numbers to unify the drag and vortex shedding data for constrained flows for moderately large blockages for all cavitation numbers. For moderately large blockages, modified choking cavitation numbers (σ_{ch_l} and σ_{ch_j}) which are nearly constant can be obtained if u_l and u_j are used as the velocity scales.

2. Although the flow associated with the rotating disk is very complex in view of the fact that the flow is highly sheared, erosion test results indicate that the cavitation erosion caused by prismatic cavitation sources in the aluminium specimens can be explained in terms of the size (scale) and the fluid dynamic variable (velocity). Specifically, for fixed cavitation numbers and velocities, there is a critical source size for maximum erosion of the test specimen when the flow characteristics are independent of Reynolds number. The variation of weight loss with the size of the cavitating source is very regular for the prismatic source and it contrasts with the inconclusive results obtained for the cylindrical source.

3. For a fixed velocity, both the weight loss due to cavitation erosion and the corresponding sound pressure levels measured in the high frequency range depend on the cavitation number. The variations of erosion and sound pressure level with cavitation number are very similar for all the velocities tested. At fixed velocities, the peak

erosion and the peak noise appear within a narrow band of cavitation numbers. There is an excellent correlation between the cavitation number at which the peak erosion occurs and the cavitation number at which the peak noise occurs.

Increased weight loss and noise are observed at increased velocity for both the cylindrical and the prismatic sources. The velocity exponents n_1 and m are found to be close to 5.45 at peak erosion conditions.

4. Cylindrical structural components can be fitted with simple wake interference elements such as a splitter plate to reduce cavitation erosion and noise.

5.2 FURTHER REMARKS

The results of the present study provide useful information to the investigators who are obliged to use large models of structural elements of hydraulic machinery in water tunnel studies.

As a further extension of the present investigation, one could explore the effects of dissolved gas and free nuclei on cavitation erosion, cavitation noise and choking cavitation number.

REFERENCES

1. Apelt, C.J., West, G.S. and Szewczyk., "The Effects of Wake Splitter Plates on the Flow Past a Circular Cylinder in the range $10^4 < R < 5 \times 10^4$", J. Fluid Mech., Vol. 61, Part 1, 1973, pp. 187-198.

2. Barker, S.J., "Measurements of Radiated Noise From Cavitating Hydrofoils", ASME Cavitation and Polyphase Flow Forum, 1973.

3. Bearman, P.W., "Investigation of Flow Behind a Two-dimensional model with a blunt trailing edge and Fitted with Splitter Plates", J. Fluid Mech., Vol. 21, Part 2, 1965, pp. 241-255.

4. Bearman, P.W., "On vortex Shedding from a Circular Cylinder in the Critical Reynolds Number Regime", J. Fluid Mech., Vol. 37, 1969, pp. 577-585.

5. Benjamin, T.B. and Ellis, A.T., "The collapse of Cavitation Bubbles and the Pressure thereby Produced Against Solid Boundaries", Phil. Trans. Royal Soc. (London), Vol. A, No. 260, 1966, pp. 221-240.

6. Birkhoff, G., "Hydrodynamics", Princeton University Press, Princeton, N.J., 1950.

7. Birkhoff, G., Plesset, M. and Simmons, N., "Wall Effects in Cavity Flow", Part 1: Quarterly of Applied Mathematics, Vol. 8, No. 2, 1950, pp. 151-168; Part 2, Vol. 9, No. 4, 1952, pp. 413-421.

8. Blake, W.K., Wolpert, M.J. and Geib, F.E., "Cavitation Noise and Inception as Influenced by Boundary Layer. Development on a Hydrofoil", J. Fluid Mech., 1977, 80, 4, pp. 617-640.

9. Canavelis, R., "Effects of Velocity and Static Pressure on Cavitation Damage", ASME, Cavitation Forum 1968.

10. Causon, G.J. and Aust, M.I.E., "Sonic Cavitation Studies on Model and Prototype Water Trubines", Inst. Engrs. Australia, Mech. and Chem. Engr. Trans. 1972, MC8, 1, pp. 24-30.

11. Chandrasekhara, D.V., Syamala Rao, B.C., "Effects of Pressure on Length of Cavity and Cavitation Damage Behind Circular Cylinders in a Venturi", Trans. ASME, Paper No. 72-WA/FE-6, 1972.

12. Chen, Y.N., "Properties of the Karman Vortex Street", Sulzer Research, 1972, pp. 68-80.

13. Chen, Y.S., "Effects of Confining Walls on the Periodic Wake of 90° Wedges", M. Thesis, Department of Engineering Mechanics and Hydraulics, University of Iowa, 1967.

14. Cohen, H. and Di Prima, R.C., "Wall Effects in Cavitating Flows", 2nd Symposium on Naval Hydrodynamics, (ONR) Aug. 1958, pp. 367-390.

15. Daily, J.W. and Harleman, D.R.F., "Fluid Dynamics" Addison Wesely Publishing Co. Reading, Mass., 1966.

16. Deeprose, W.M., King, N.W., McNulty, P.J. and Pearsall, I.S., "Cavitation Noise, Flow Noise and Erosion", Cavitation Conf. Inst. Mech. Engrs., Edinburg, Sept. 1974.

17. Eisenberg, P., "Modern Developments in the Mechanics of Cavitation", Applied Mechanics Surveys, Edited by Abrahamson, H.N., et al., Mcmillan Co. Ltd., 1966, pp. 915-924.

18. Ellis, A.T., Gruber, G. and George, N., "An Experimental Investigation of Shock Wave-Bubble Interaction and Reflection Holograms of Long Polymer Molecules", Calif. Inst. Techl., Eng. and Appl. Science, Rep. E-115-A.1, 1968.

19. Fitzpatrick, H.M. and Strasberg, M., "Hydrodynamic Sources of Sound", 1956, 2nd Symp. Naval Hydrodyn., Washington, D.C., pp. 241-280.

20. Govinda Rao, N.S. and Thiruvengadam, A., "Prediction of Cavitation Damage", J. Hyd. Div., Proc. ASCE, Vol. 87, No. Hy5, Sept. 1961, pp. 915-924.

21. Hackworth, J.V. and Arndt, R.E.A., "Preliminary Investigation of the Scale Effects of Cavitation Erosion in a Flowing Media", ASME Cavitation and Polyphase Flow Forum 1974.

22. Hammitt, F.G., "Observation on Cavitation Damage in a Flowing System", Trans. ASME, Ser. D, 85, Sept. 1963, pp. 347-359.

23. Hammitt, F.G., Barinka, L.L., Robinson, M.J., Pehlke, R.D, and Siebert, C.A., "Initial Phases of Damage to Test Specimens in a Cavitating Venturi", Trans. ASME, Ser. D, 87, 1965, pp. 453-464.

24. Hammitt, F.G., "Damage to Solids Caused by Cavitation", Royal Soc. London, Phil. Trans. A, 260, 1966, pp. 245-255.

25. Hammitt, F.G. and Kemppainen, D.J., "Cavitation Flow Past Transverse Cylinder in Venturi Diffuser with Water and Mercury", Proc. Third Conf. on Fluid Mechanics and Fluid Machinery, Budapest, Sept. 1969, pp. 255-265.

26. Hansen, B.W. and Rasmussen, R.E.H., "Cavitation Damage Experiments in a Rotating Disk Apparatus Especially with regard to Gas Content of Water", J. Ship Research, June 1968, p. 83.

27. Hobbs, J.M., "Practical Aspects of Cavitation", Royal Soc. London, Phil. Trans. A, 260, 1966, pp. 267-275.

28. Hobbs, J.M., "Constricted Tube Cavitation Erosion Tests", ASME Cavitation Forum 1969.

29. Ilichev, V.I. and Kurietsov, G.N., "Relation between Acoustic Noise and Erosion in Hydrodynamic Cavitation", Soviet Physics, Doklady 13, 4, Oct. 1968, pp. 313-316.

30. Itaya, S. and Yasuda, Y., "Experiments on Strouhal Number", Bull. JSME, Vol. 4, No. 14, 1961, pp. 1-5.

31. Ivany, R.D., Hammitt, F.G. and Mitchell, I.M., "Cavitation Bubble Collapse Observation in a Venturi", Trans. ASME, Ser. D, Sept. 1966, pp. 649-657.

32. Kerr, S.K. and Rosenberg, K., "An index of Cavitation Erosion by means of Radioisotopes", Trans. ASME, 80,6, 1958, pp. 1308-1314.

33. Knapp, R.T., "Recent Investigations of the Mechanics of Cavitation and Cavitation Damage", Trans. ASME, 77, Oct. 1955, pp. 1045-1054.

34. Knapp, R.T., "Accelerated Field Tests of Cavitation Intensity", Trans. ASME, 80, 1, 1958, pp. 91-102.

35. Knapp, R.T., Daily, J.W. and Hammitt, F.G., "Cavitation", McGraw Hill Book Co., 1970.

36. Kozirev, S.P., Discussion on "The Effect of Velocity of Sound in Liquid on Impact Erosion" and "A Dimensional Grouping for Assessing the Extent of Cavitation Erosion", ASME Cavitation Forum 1971.

37. Lakshmana Rao, N.S., "Scale Effects in Cavitation", Cavitation and Polyphase Flow Forum, 1973, pp. 14-16.

38. Lichtman, J., Kallas, D., Chatten, C. and Cochran, E., "Cavitation Erosion of Structural Materials and Coatings", J. Corrosion, Vol. 17, No. 10, 1961, pp. 119-127.

39. Lush, P.A., "Cavitation", Inst. Mech. Engrs. Conf., Edinburgh, Sept. 1974, Discussion of Papers, pp. 405-409.

40. Matsumura, M., Seuzawa, R. and Tsuda, K., "On the Time Dependence of the Rate of Erosion", ASME Polyphase Flow Forum, 1972.

41. Meijer, M.C., "Pressure Measurements on Flapped Hydrofoils in Cavity Flows and Wake Flows", J. Ship. Res. 11, 3, 1967, pp. 170-189.

42. Morkivin, M.V., "Flow Around Circular Cylinder - A Kaleidoscope of Challenging Fluid Phenomena", ASME Symp. Fully Separated Flows, 1964, pp. 102-118.

43. Palanichamy, K., Syamala Rao, C. and Lakshmana Rao, N.S., "Investigations on Cavitation Inception in a Venturi with Transverse Pins", Cavitation, Inst. Mech. Engrs., London, Conference, Edinburg, Sept. 1974, Paper C/162/74.

44. Pearsall, I.S., "Acoustic Detection of Cavitation", Proc. Inst. Mech. Engrs. 181, 3A, Paper 14, 1966-67.

45. Pearsall, I.S. and McNulty, P.J., "Comparison of Cavitation Noise with Erosion", ASME Cavitation Forum 1968.

46. Plesset, M.S. and Shaffer, P.A. Jr., "Cavity Drag in Two and Three Dimensions", U.S. Navel Ordinance Test Station, Navord., Report No. 1014, Pasadena, Oct. 1949; see also Journal of Applied Physics, Vol. 19, Oct. 1948, pp. 934-939.

47. Plesset, M.S. and Devine, R.E., "Effect of Exposure Time on Cavitation Damage", Trans. ASME, D, 88, 4, 1966, pp. 691-705.

48. Popp, S., "Theoretical Investigations and Numerical Evaluations of Wall Effects in Cavity Flows", Journal Fluids Engineering, Trans ASME, Dec. 1975, Vol. 97, No. 4, pp. 482-491.

49. Ramamurthy, A.S. and Ng., C.P., "Effects of Blockage on Steady Force Coefficients", Journal of the Engineering Mechanics Division, ASCE, Vol. 99, No. EM4, Proc. Paper 9905, Aug. 1973, pp. 755-772.

50. Ramamurthy, A.S. and Lee, P.M., "Wall Effects on Flow Past Bluff Bodies", Journal of Sound and Vibration, 1973, 31 (4), pp. 443-451.

51. Ramamurthy, A.S., Bhaskaran, P. and Subramanya, K., "Use of Wake Interference Element to Reduce Cavitation Damage", ASME Cavitation and Polyphase Flow Forum 1974.

52. Ramamurthy, A.S. and Bhaskaran, P., "Source Size and Velocity Effects on Cavitation Damage", Trans. ASME, J. Fluids' Eng. 97, 3, 1975, pp. 384-386.

53. Ramamurthy, A.S. and Bhaskaran, P., "Constrained Flow Past Cavitating Bluff Bodies, Trans. ASME, J. Fluids Eng. (Accepted for publication).

54. Roshko, A., "On the Drag and Shedding Frequency of Two-dimensional bluff Bodies", NACA TN 3159, 1954.

55. Roshko, A., "A new Hodograph for Free Streamline Theory", NACA TN 3168, July 1954.

56. Shalnev, K.K., "Experimental Study of the Intensity of Erosion due to Cavitation", Proc. Symp. on Cavitation in Hydrodyn. NPL, 1955.

57. Shalnev, K.K., "Boundary Effect on Cavitating Flow Past a Cylinder", J. Applied Mechanics and Tech. Phys. No. 3 (Zhurnal Prikladnoi Meckniki i Tecnicheskoi. Fiziki, No. 3), 1965, pp. 103-108, pp. 73-76.

58. Shalnev, K.K., Varga, J. and Sebestyen, Gy., "Investigation of the scale effects of Cavitation Erosion", Royal Soc. London, Phil. Trans. A, 260, 1966, pp. 256-266.

59. Shalnev, K.K., Sebestyen, Gy. and Ilichev, V.I., "Intensity of Cavitation Noise caused by a Cylinder", Appl. Elect. Phenomena, 4, 1967, pp. 282-288.

60. Shalnev, K.K., Varga, J. and Sebestyen, Gy., "Accurate Determination of Scale Effect Formula for Cavitation Erosion", Acta. Tech. (Budapest) 66, 4, 1969, pp. 347-367.

61. Shalnev, K.K., "The Structure of Cavitation in Zones of Primary and Secondary Erosion Focuses", Acta Technica Academiae Scientiarum Humgaricae, Tomus 71 (3-4), 1971 pp. 241-265.

62. Shaw, T.L., "Steady Flow Past Plate in Channel", Journal of Hydraulic Division, Proc. ASCE, Hy 6, 1969, No. 6903, pp. 2013-2028.

63. Shaw, T.L., "Effect of Side Walls on Flow Past Bluff Bodies", Journal of Hydraulic Division, Proc. ASCE, Hy1, Jan. 1971, No. 7788, pp. 65-79.

64. Silberman, E., "Experimental Studies of Supercavitating Flow About Simple Two-dimensional Bodies in a Jet", SAF Hydraulic Lab., Report No. 59, Univ. of Minnesota, Apr. 1958.

65. Subirkar and Murthy, B.Y., "Dimensional Analysis of Cavitation Damage in a Flow System", ASME Cavitation Forum 1971.

66. Suezawa, Y., Matsumura, M., Nakagerna, M. and Tsude, K., "Studies on Cavitation Erosion", ASME, Paper No. 71, WA/FE-34, 1971.

67. Syamala Rao, B.C., Lakshmana Rao, N.S., Seetharamaiah K., "Cavitation Erosion Studies with Venturi and Rotating Disk in Water", Trans. ASME D, 1970, pp. 563-579.

68. Syamala Rao, B.C., Chandrasekhara, D.V. and Seetharamaiah, K., "A high Speed Photographic Study of Vortex Shedding behind Circular Cylinders in Cavitating Flows", 2nd Internat. JSME Symp. Fluid Machinery and Fluidics, Tokyo, Sept. 1972, pp. 293-302.

69. Syamala Rao, B.C. and Chandrasekhara, D.V., "Cavity and Damage Characteristics for Cavitation in a Venturi", Water Power, Jan. 1974, pp. 27-31.

70. Syamala Rao, B.C. and Chandrasekhara, D.V., "Some Characteristics of Cavity Flow Past Cylindrical Inducers in a Venturi", ASME Paper 75-WA/FE-7, 1975.

71. Thiruvengadam, A., "A Unified Theory of Cavitation Damage", ASME, Paper No. 62-Wa-118, 1962.

72. Thiruvengadam, A., "On Modeling Cavitation Damage", J. Ship Research, Sept. 1969, pp. 220-233.

73. Thiruvengadam, A., "Cavitation Erosion", Applied Mechanics Reviews, March 1971, pp. 245-252.

74. Thiruvengadam, A., "Scaling Laws for Cavitation Erosion", Tech. Rept. 233-15, Hydronautics, Dec. 1971.

75. Toebes, G.H., "The Frequency of Oscillating Forces Acting on Bluff Cylinders in Constricted Passages", Proceedings of the 14th Congress of Internat. Hydr. Res., Paris 1971, 2, B-7-58.

76. Toebes, G.H. and Ramamurthy, A.S., "Lift and Strouhal Frequency for Bluff Shapes in Constricted Passages", Proceedings of the Conference on Flow Induced Vibration in Nuclear Reactors, Argonne National Laboratory, Illinois, 1970, pp. 225-247.

77. Tozkas, A., "Effect of Confining Walls on the Periodic Wake of Cylinders and Plates", M.S. Thesis, Dept. of Eng. Mechanics and Hydraulics, University of Iowa, 1965.

78. Tulin, M.P., "Steady Two-Dimensional Cavity Flows about Slender Bodies", Davis Taylor Model Basin, Report 834, May 1952.

79. Tulin, M.P., "Supercavitating Flows", Handbook of Fluid Dynamics", Ed. Streeter, V.L., McGraw Hill, New York, 1961, Section 12-II.

80. Varga, J. and Sebestyen, Gy., "Observation on Cavitation Velocity Damage Exponent in a Flowing System", Periodica Polytechnica Eng. 8, 3, 1964, pp. 343-352.

81. Varga, J. and Sebestyen, Gy., "Determination of the Frequencies of Wakes Shedding from Circular Cylinders", Acta Technica 53 1966, pp. 91-108.

82. Varga, J. and Sebestyen, Gy., "Cavitation Noise Spectrum and Cavitation Damage", Acta Technica Vol. 57 (3-4), 1967, pp. 383-396.

83. Varga, J. "Einige Forschungsergebnisse auf dem Gebiete der Kavitationsstromung und der Kavitationserosion", Osterreichische Ingenieur-Zeitcehrift, August 1968, pp. 266-271.

84. Varga, J. and Sebestyen, Gy., "Cavity Shedding and Cavitation Erosion", Proceedings of the 3rd Conf., Fluid Mechanics and Fluid Machinery, Budapest, 1969 pp. 705-711.

85. Varga, J., Sebestyen, Gy. and Fay A., "Detection of Cavitation by Acoustic and Vibration Measurement Methods", La Houille Blanch. 2, 1969, pp. 137-147.

86. Waid, R.L., "Water Tunnel Investigations of Two-Dimensional Cavities", Hydrodynamics Lab. Report Cal. Inst. of Tech. No. E-73.6, Sept. 1957.

87. Whitney, A.K., "A Simple Correction Rule for Wall Effect in Two-Dimensional Cavity Flow"., Cavitation: State of Knowledge, ASME Publication, 1969.

88. Whitney, A.K., "Experimental Verification of Cavity-Flow Wall Effects and Correlation Rules." Calif. Inst. Tech. Rep. (U) No. E-97A-18, 1970.

89. Wolde, T.T., Moelker, W.H. and Mendte, K.W., "Experiences with Acoustical Methods for the Detection of Cavitation in Pumps", Cavitation, Inst. Mech. Engrs. Conf. Edinburgh, 1974, Paper C 187/74.

90. Wood, G.M., Knudsen, L.K. and Hammitt, F.G., "Cavitation Damage Studies with Rotating Disk in Water", Trans. ASME, 89, D, 1, 1967, pp. 98-110.

91. Wu, T.Y., Whitney, A.K. and Lin, J.D., "Wall Effects in Cavity Flows", Cal. Inst. of Tech. Pasadena, Calif. E-111, A.5, August 1969.

92. Wu, T.Y., Whitney, A.K. and Brennen, C., "Cavity Flow Wall Effects and Correction Rules", Journal Fluid Mechanics (49, 2) 1971, pp. 223-256.

93. Young, J.O. and Holl, J.W., "Effects of Cavitation on Periodic Wakes Behind Symmetric Wedges", Journal of Basic Engineering, Trans ASME, March 1966, pp. 163-176.

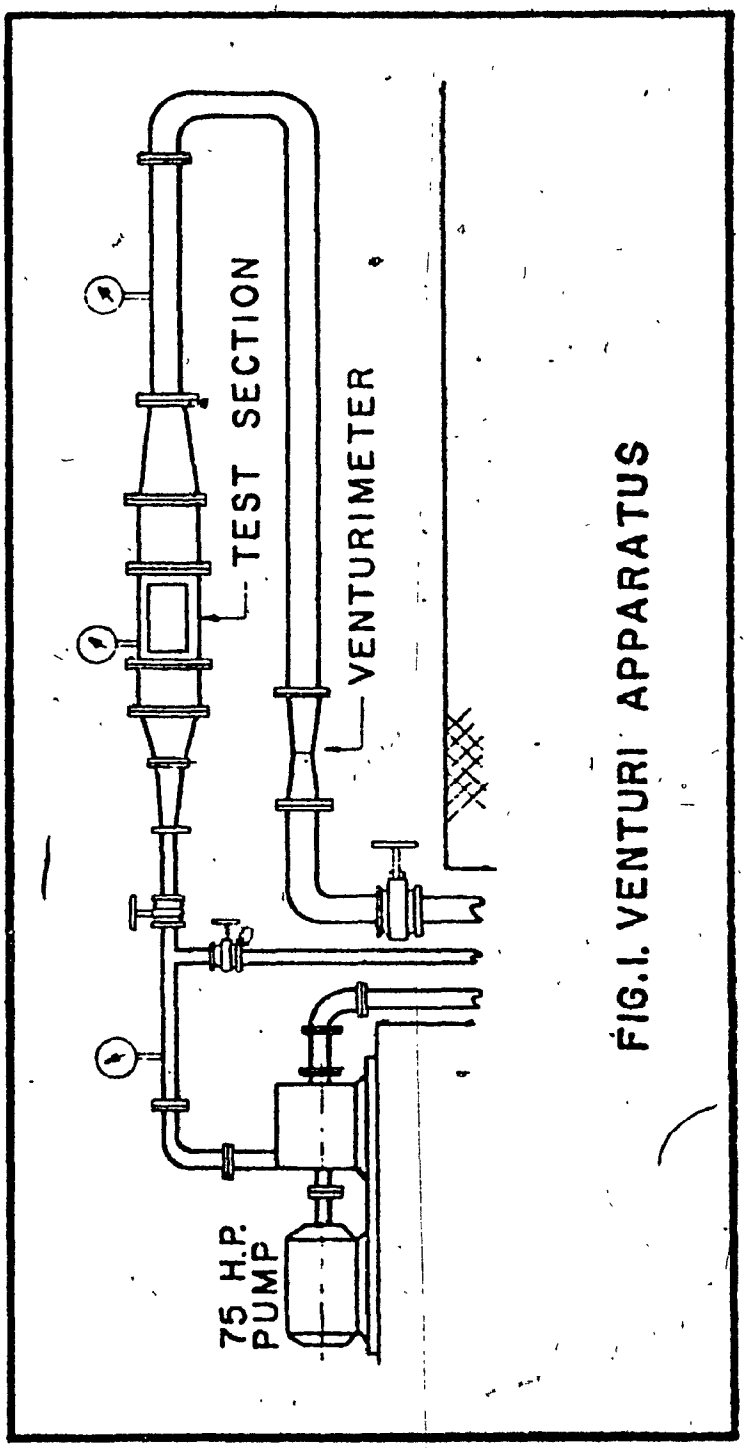

FIG.I. VENTURI APPARATUS

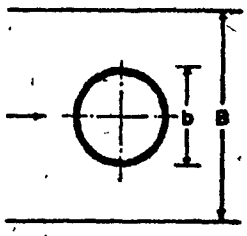

$b/B = \begin{cases} .165, & R = 1.0 - 5.0 \times 10^5 \\ .327, & R = 3.0 - 8.0 \times 10^5 \end{cases}$

CYLINDERS

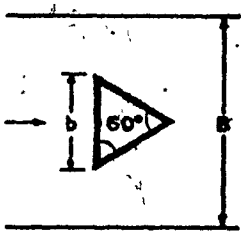

$b/B = \begin{cases} .103 \\ .196 \\ .326 \end{cases}$

PRISM $\Theta = 0°$

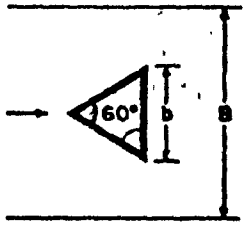

$b/B = \begin{cases} .103 \\ .196 \\ .326 \end{cases}$

PRISM $\Theta = 60°$

FIG. 2. CAVITATING BODIES

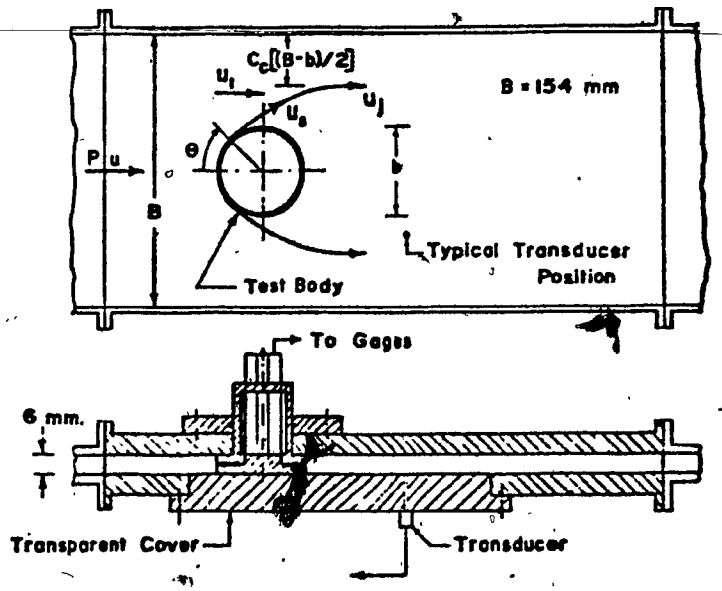

FIG. 3 CAVITATION TEST SECTION

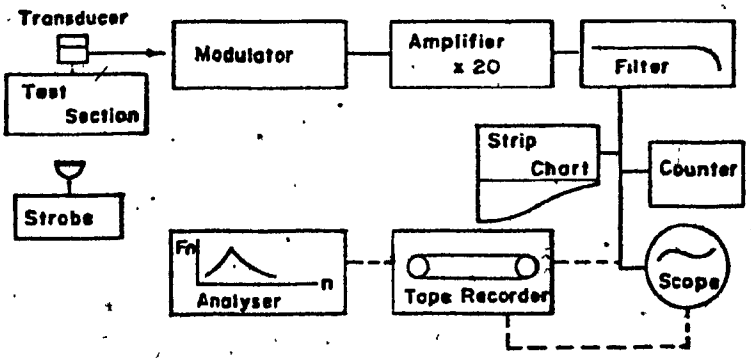

FIG. 4 INSTRUMENTATION

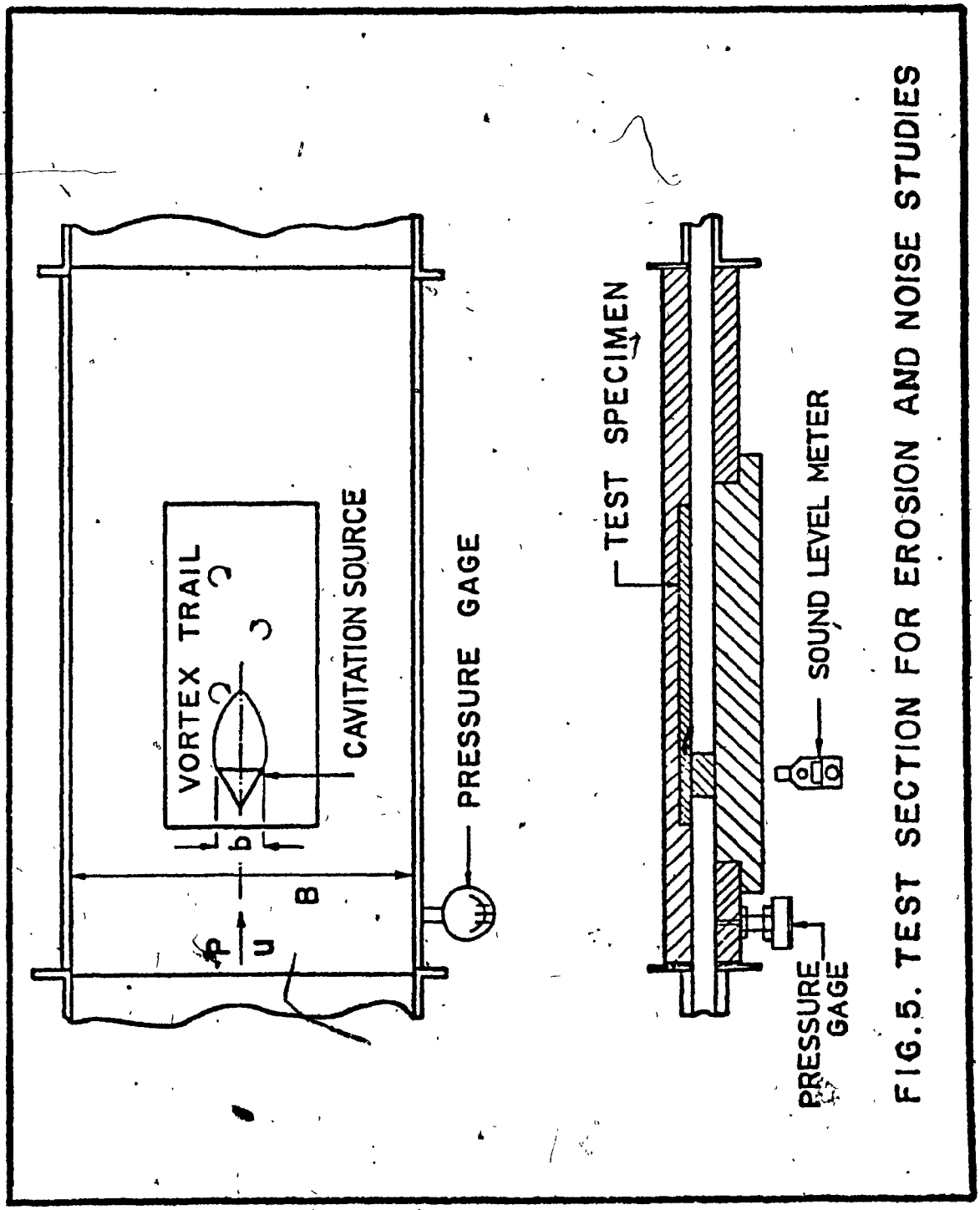

FIG.5. TEST SECTION FOR EROSION AND NOISE STUDIES

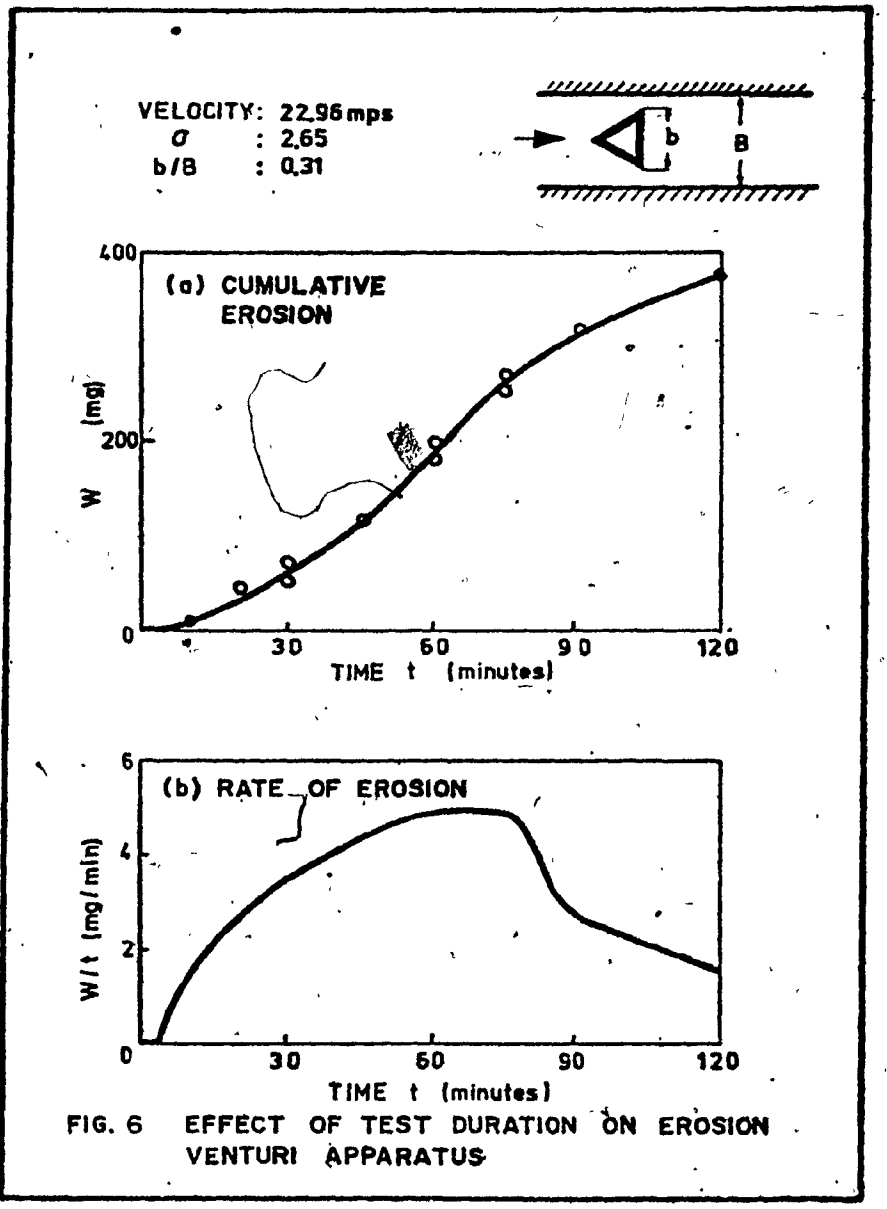

FIG. 6 EFFECT OF TEST DURATION ON EROSION VENTURI APPARATUS

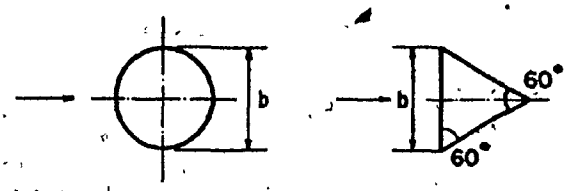

(a) CIRCULAR CYLINDER (b) EQUILATERAL PRISM

$Re = 4 \times 10^5 - 15 \times 10^5$

$\sigma = 0.196$

b(mm)= 7.37, 9.53, 12.7, 19.05, 22.23
25.4, 28.58, 31.75, 38.10

CAVITATION SOURCE SHAPES

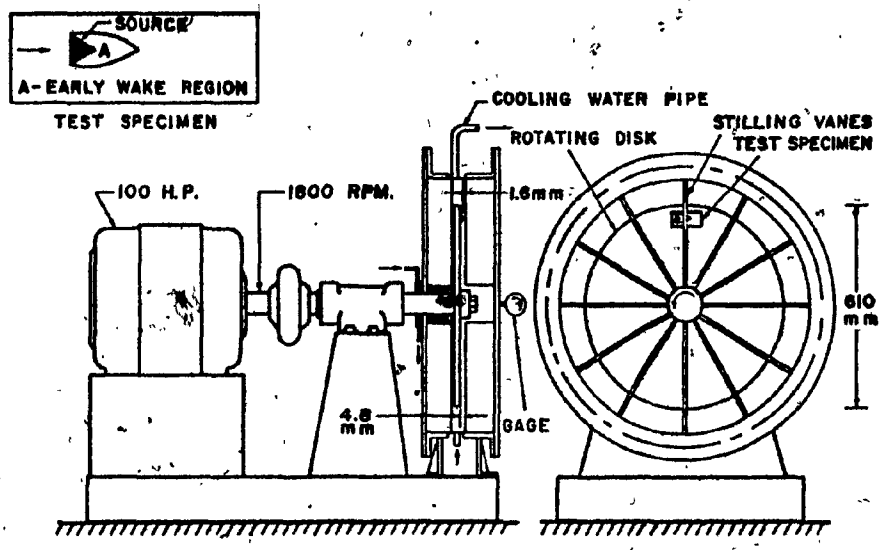

FIG. 7 ROTATING DISK FACILITY

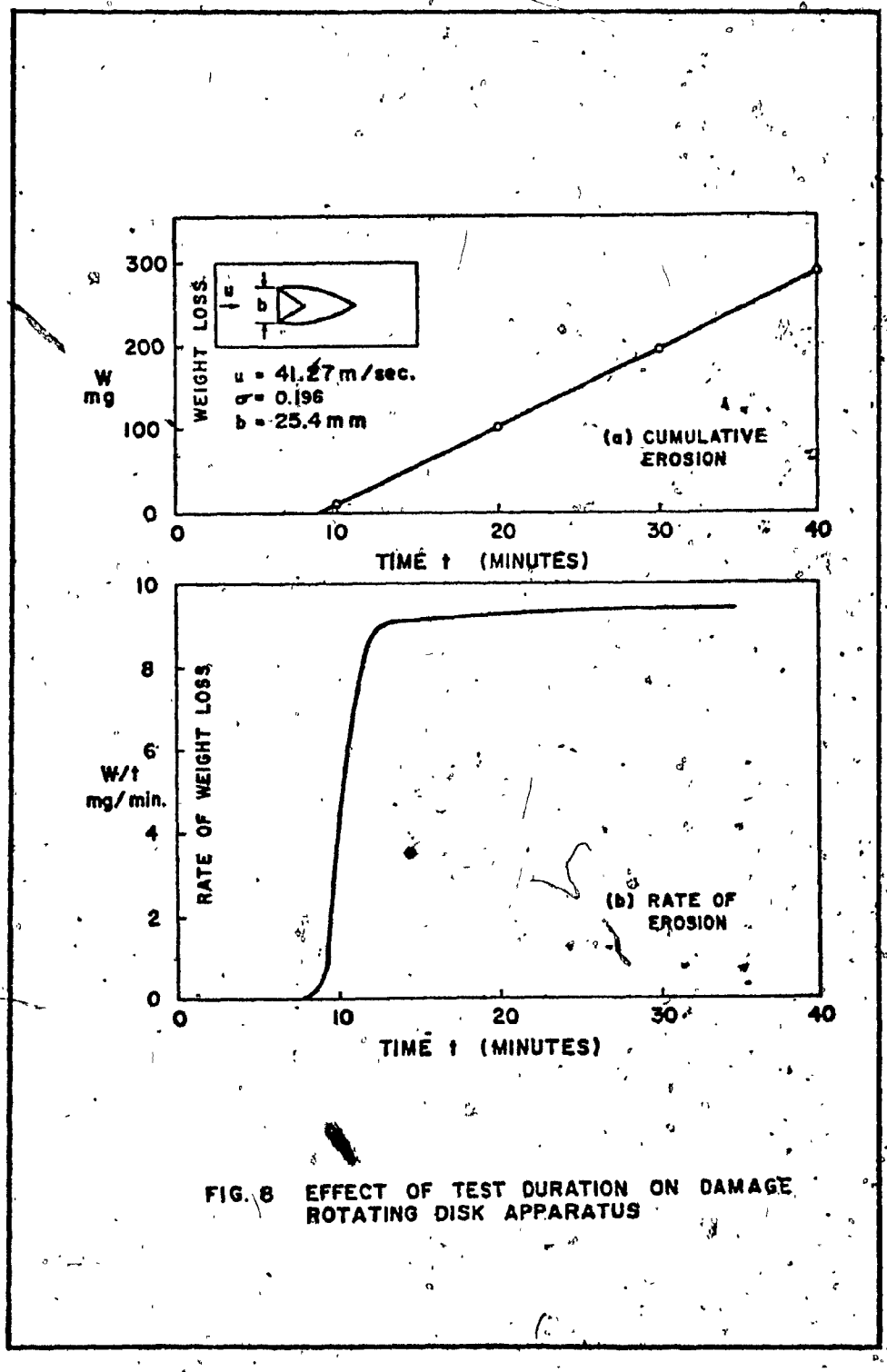

FIG. 8 EFFECT OF TEST DURATION ON DAMAGE ROTATING DISK APPARATUS

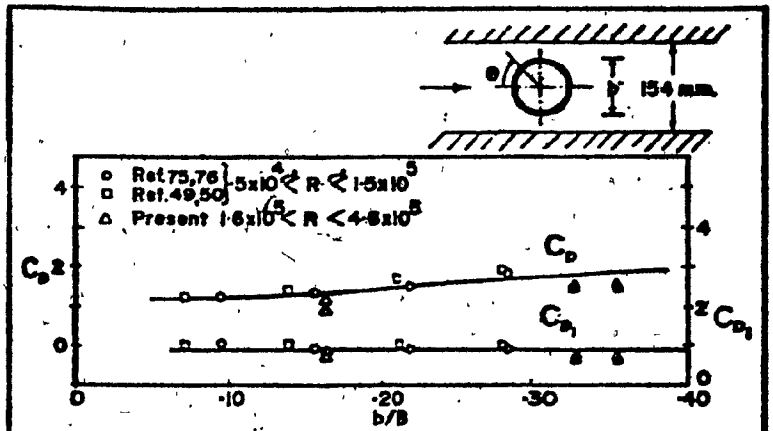

FIG. 9 DRAG COEFFICIENT, NONCAVITATING CYLINDER.

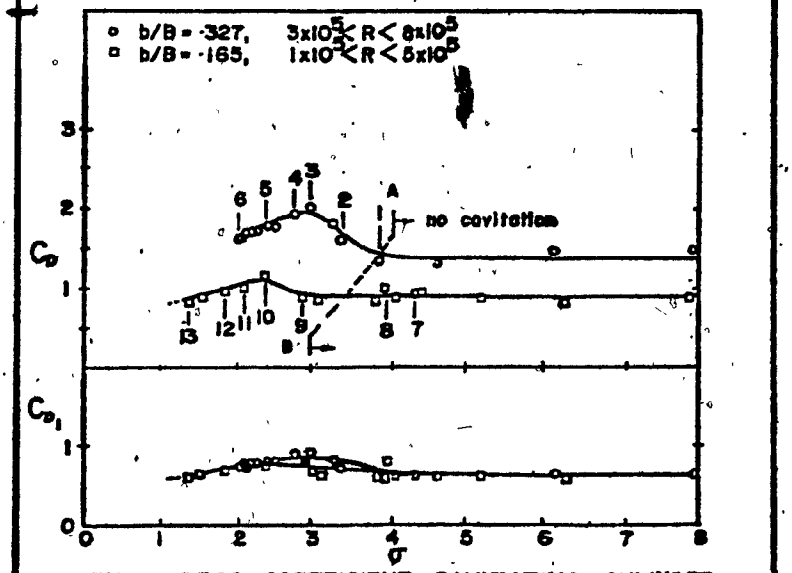

FIG.10 DRAG COEFFICIENT, CAVITATING CYLINDER.

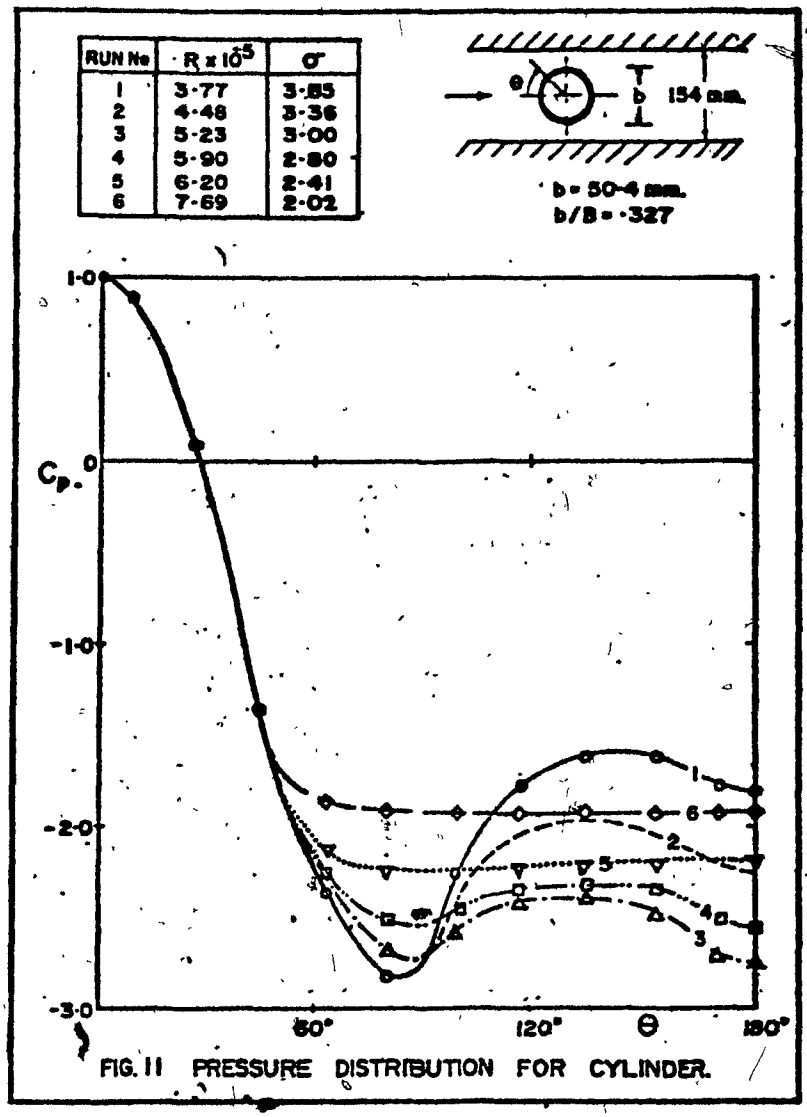

FIG. 11 PRESSURE DISTRIBUTION FOR CYLINDER.

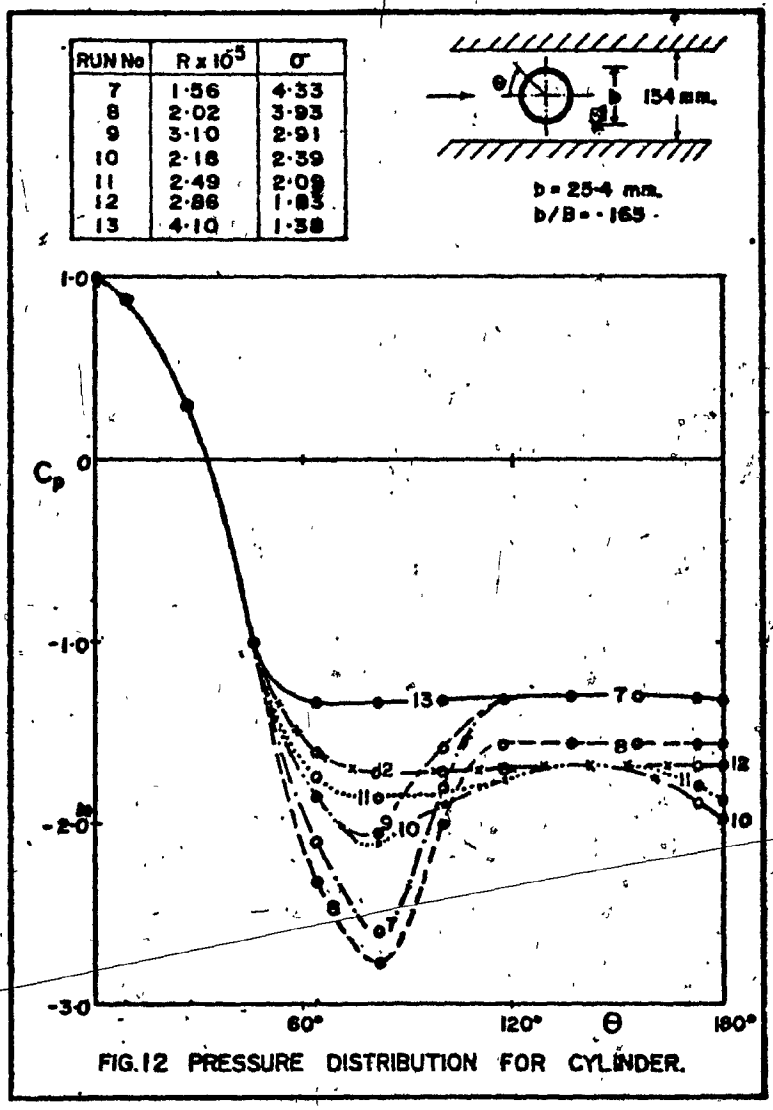
RUN No
R x 10^5
σ'
7
1·56
4·33
8
2·02
3·93
9
3·10
2·91
10
2·16
2·39
11
2·49
2·09
12
2·86
1·83
13
4·10
1·38
154 mm.
b = 25·4 mm.
b/B = ·165 ·
1·0
0
-1·0
-2·0
-3·0
Cp
60°
120°
θ
180°
13
7
8
12
11
10
9
6
FIG. 12 PRESSURE DISTRIBUTION FOR CYLINDER.

No	b/B	R x10^{-5}	REF.
1	·027	0·7 - 1·2	35,86
2	·037	>2·0	14
3	·120	1·0 - 3·0	83
4	·165	1·0 - 5·0	Present
5	·180	-	83
6	·240	-	83
7	·300	-	83
8	·327	3·0 - 8·0	Present
9	0	Theoretical	35,55

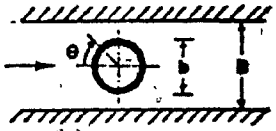

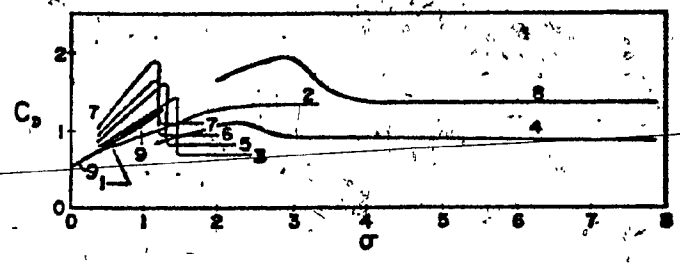

FIG. 13 DRAG COEFFICIENT, CAVITATING CYLINDER

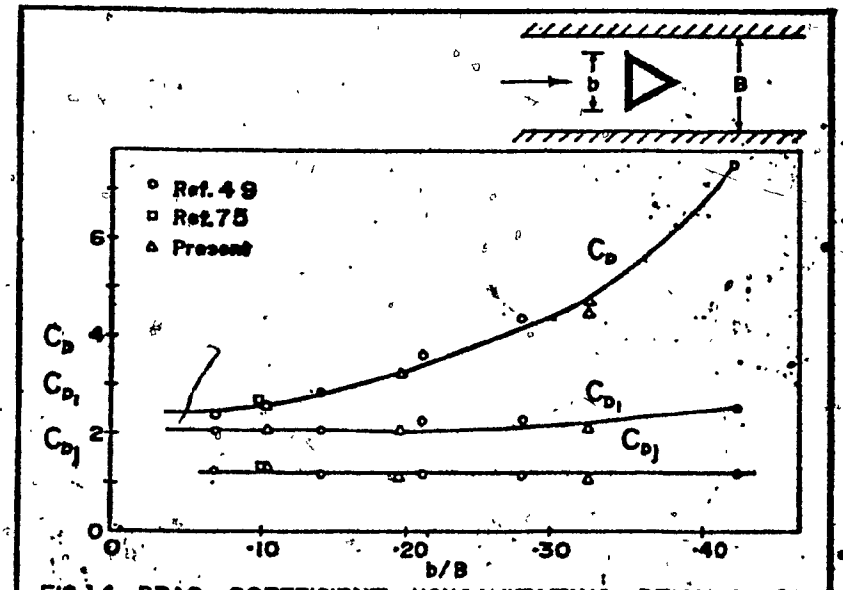

FIG. 14 DRAG COEFFICIENT, NONCAVITATING PRISM θ = 0°

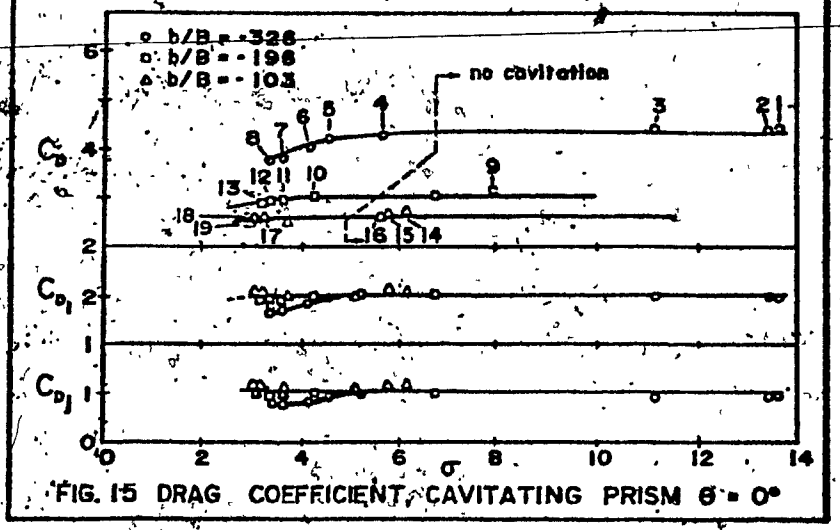

FIG. 15 DRAG COEFFICIENT, CAVITATING PRISM θ = 0°

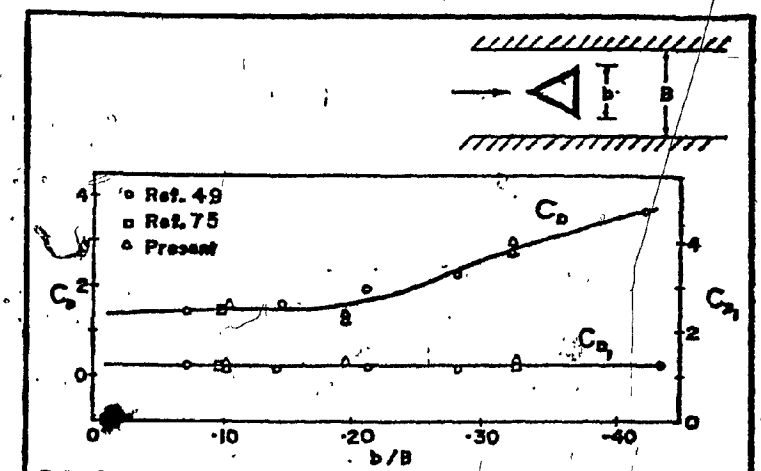

FIG. 16 DRAG COEFFICIENT, NONCAVITATING PRISM θ = 60°

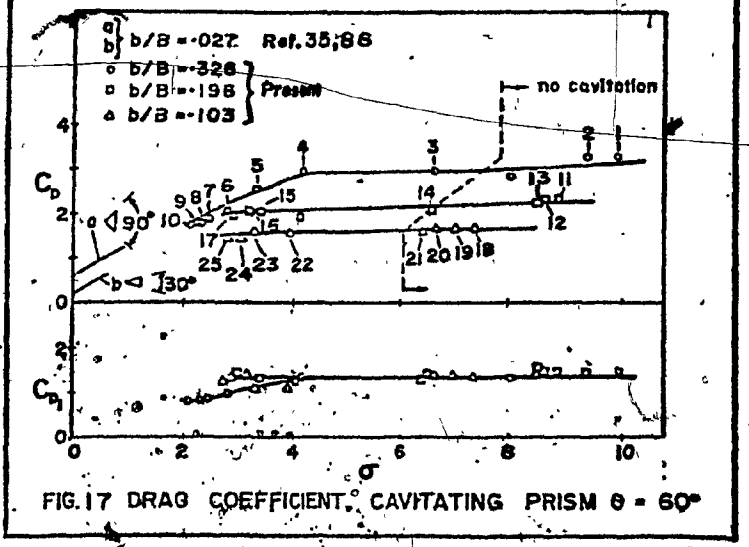

FIG. 17 DRAG COEFFICIENT, CAVITATING PRISM θ = 60°

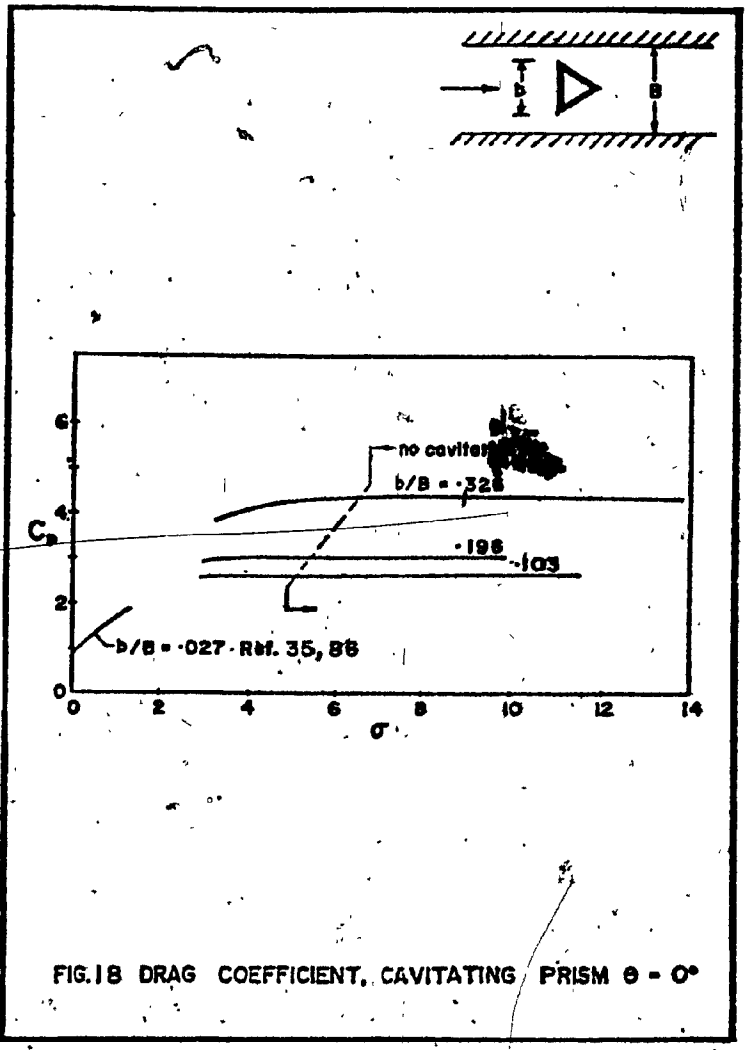

FIG. 18 DRAG COEFFICIENT, CAVITATING PRISM θ = 0°

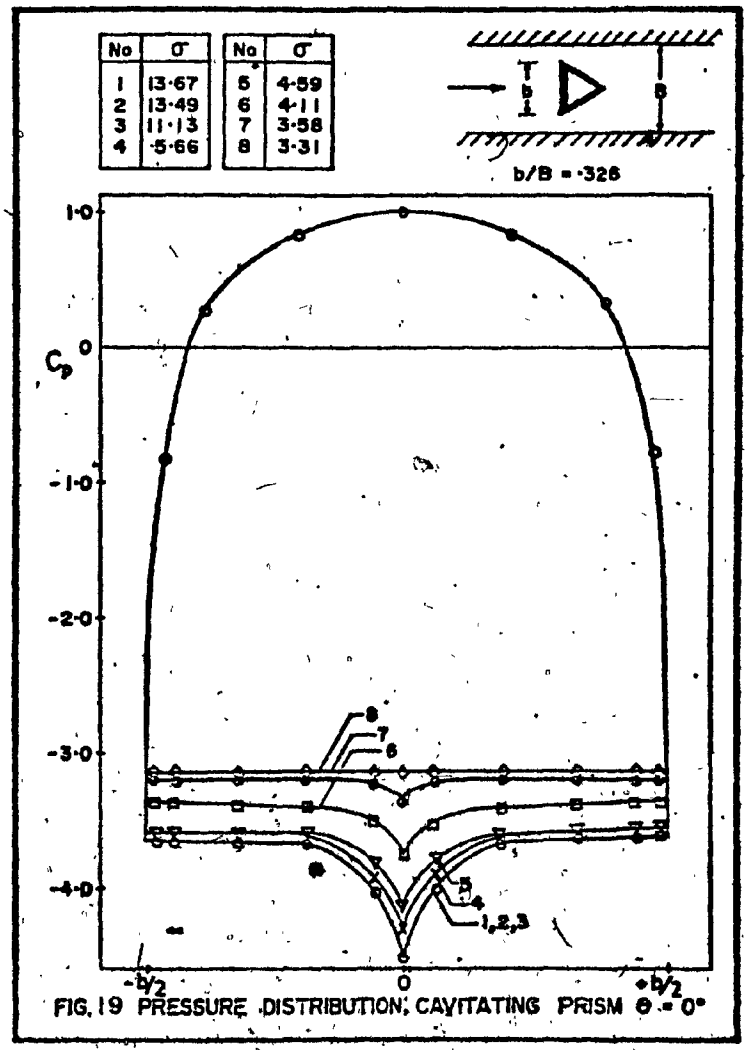

FIG. 19 PRESSURE DISTRIBUTION, CAVITATING PRISM θ = 0°

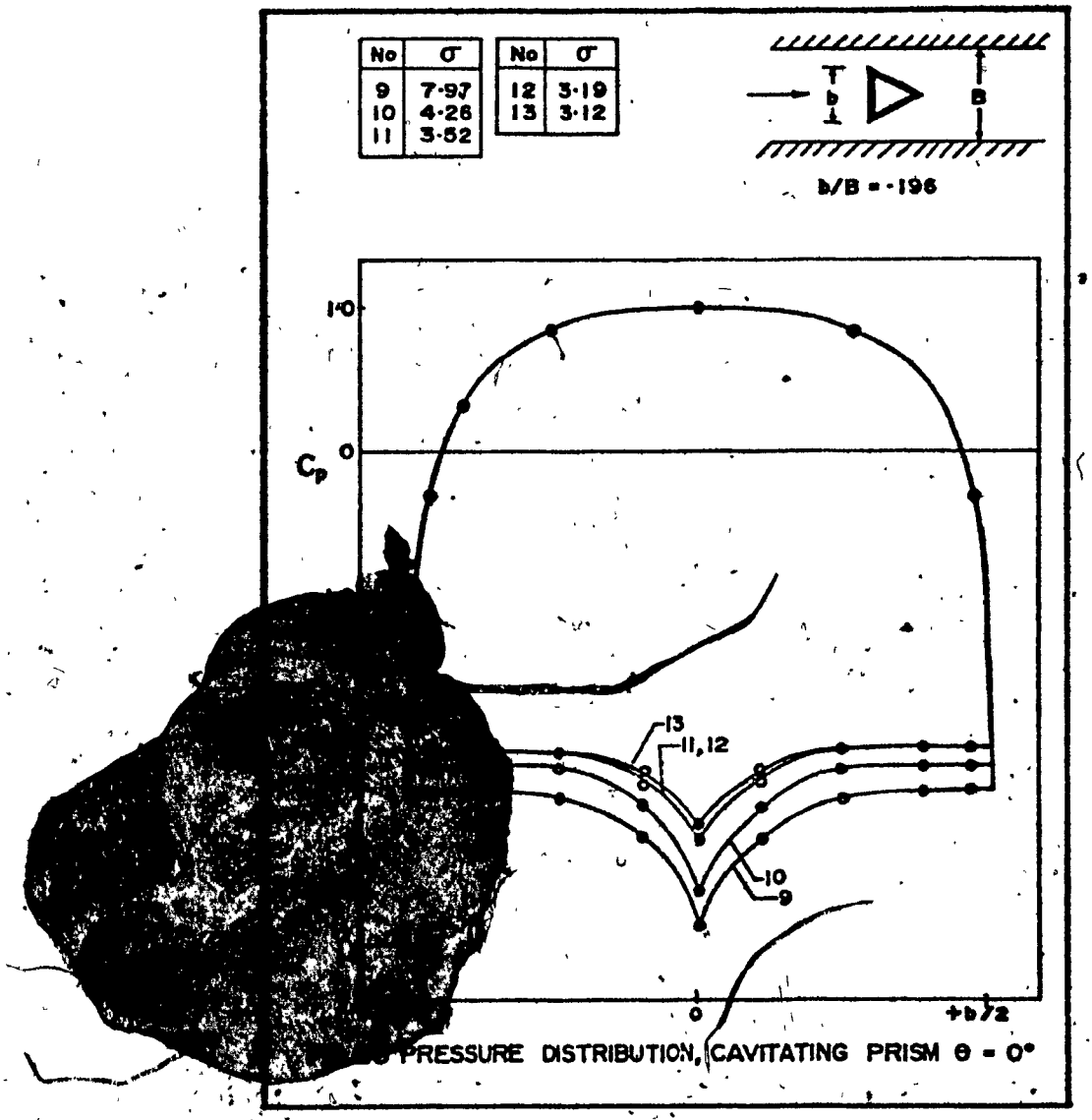

PRESSURE DISTRIBUTION, CAVITATING PRISM θ = 0°

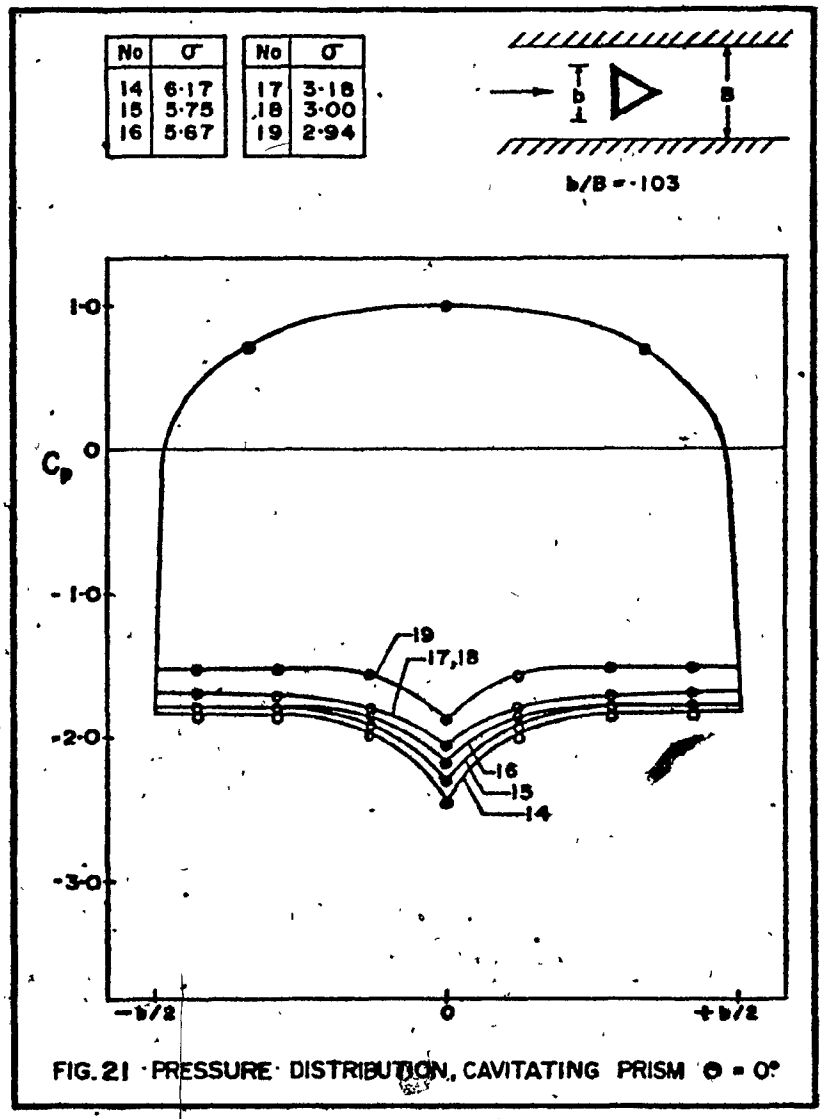

FIG. 21 PRESSURE DISTRIBUTION, CAVITATING PRISM Θ = 0°

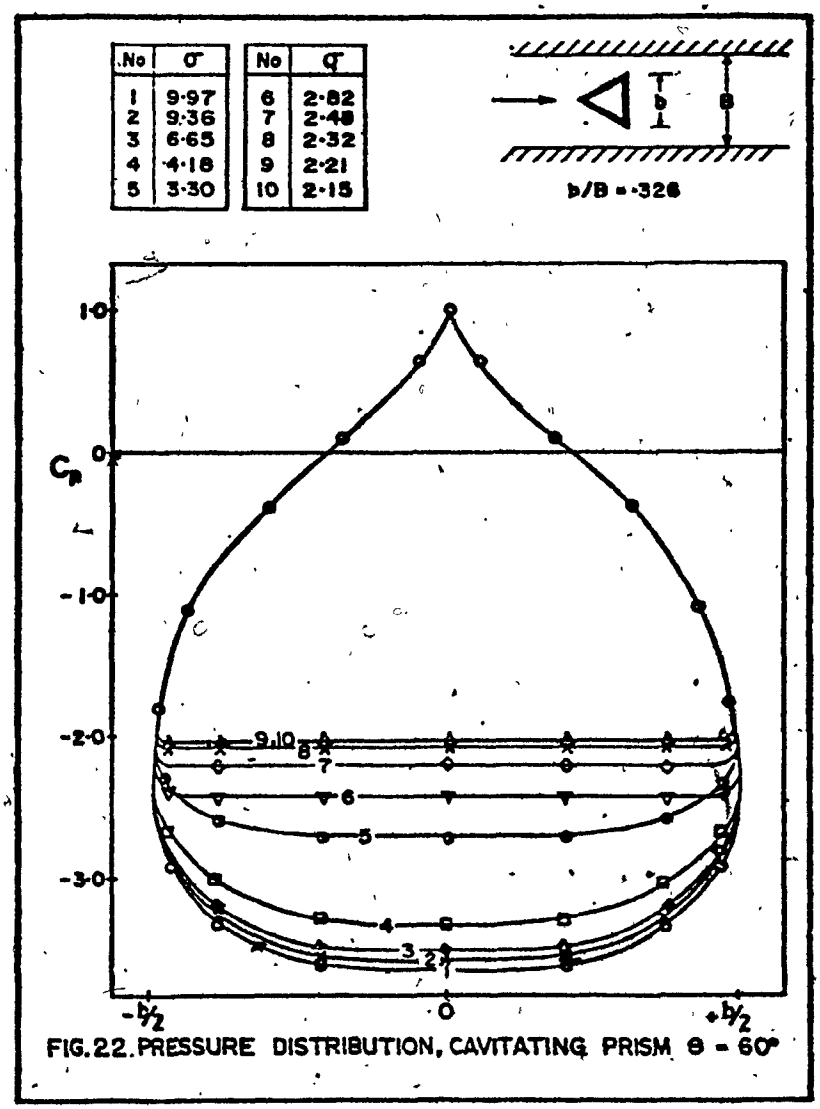

FIG. 22. PRESSURE DISTRIBUTION, CAVITATING PRISM $\theta = 60°$

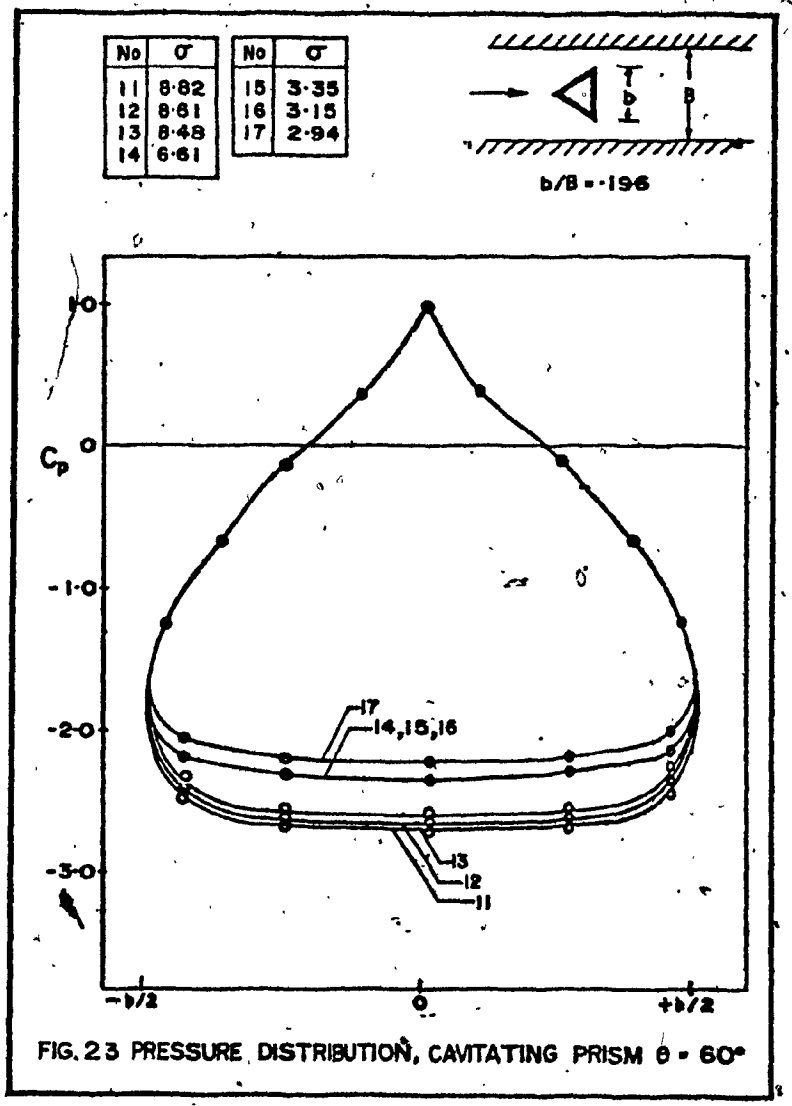

FIG. 23 PRESSURE DISTRIBUTION, CAVITATING PRISM θ = 60°

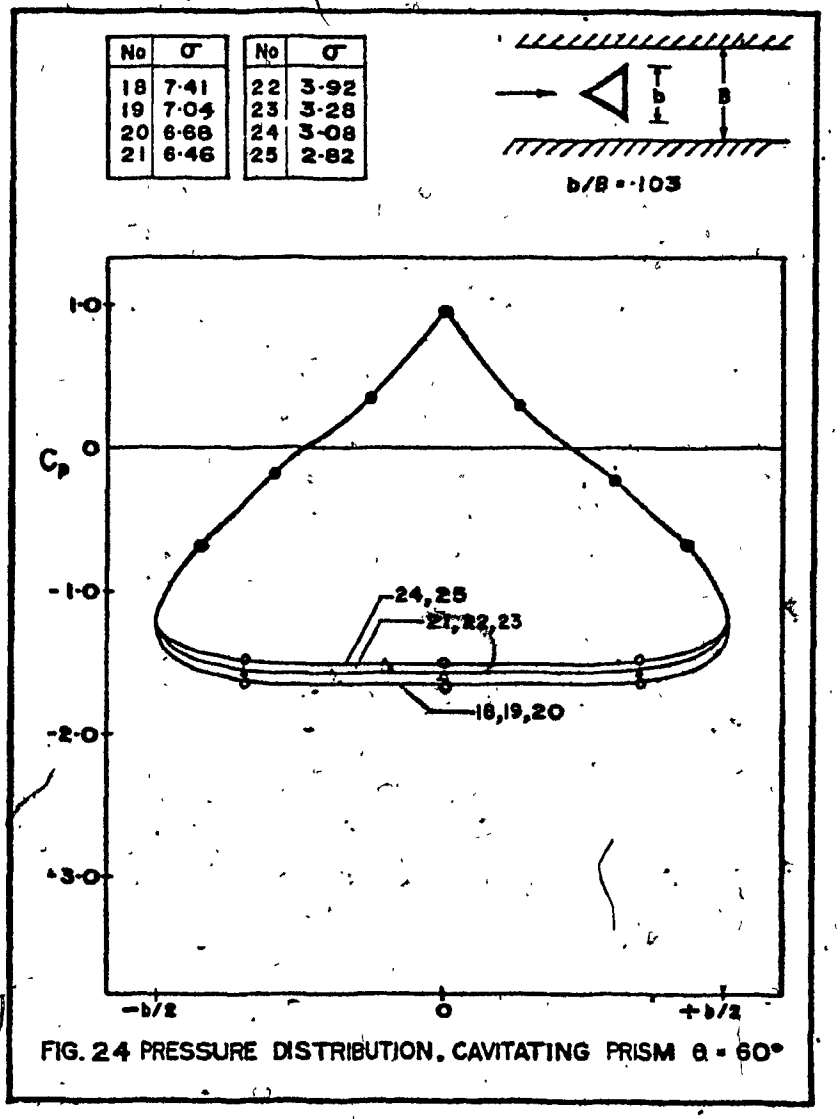

FIG. 24 PRESSURE DISTRIBUTION, CAVITATING PRISM θ = 60°

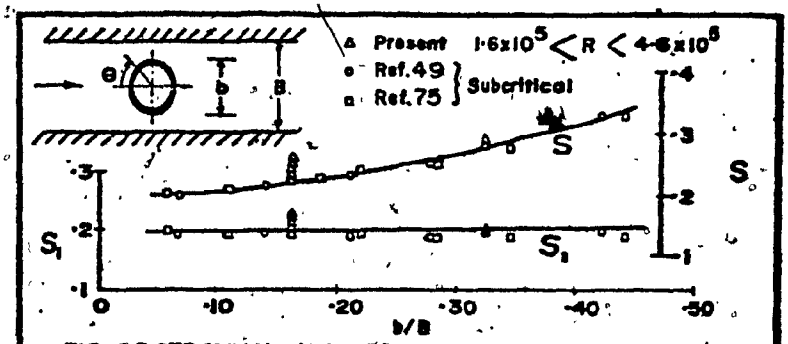

FIG. 25 STROUHAL NUMBER, NONCAVTATING CYLINDER

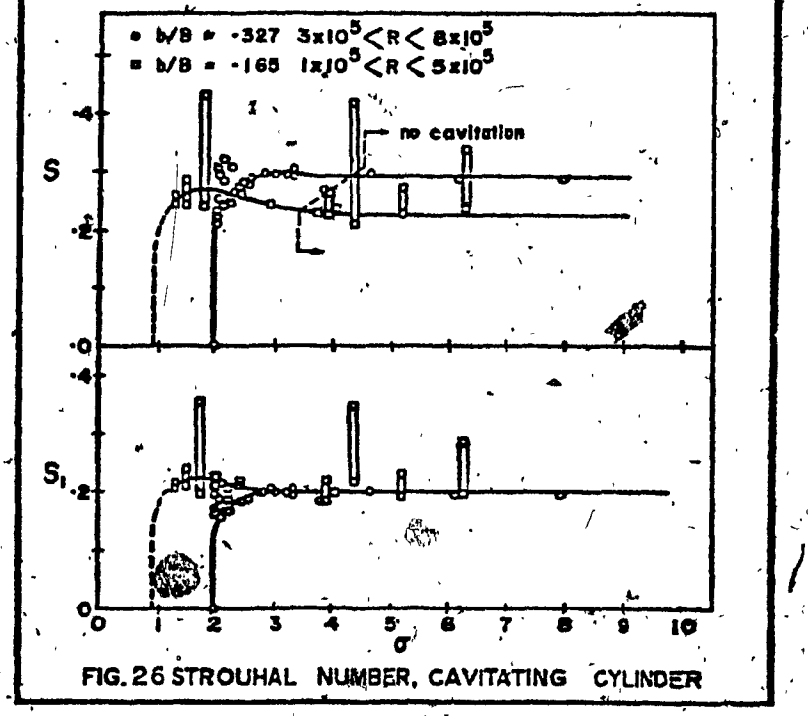

FIG. 26 STROUHAL NUMBER, CAVITATING CYLINDER

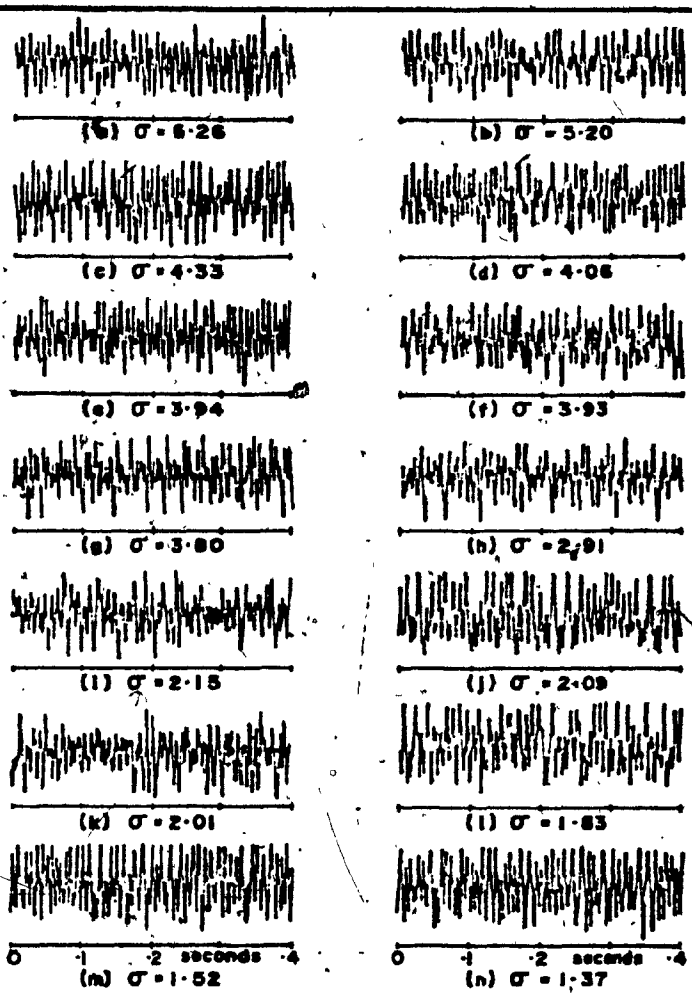

FIG.27 PRESSURE RECORDS, CYLINDER b/B = ·165

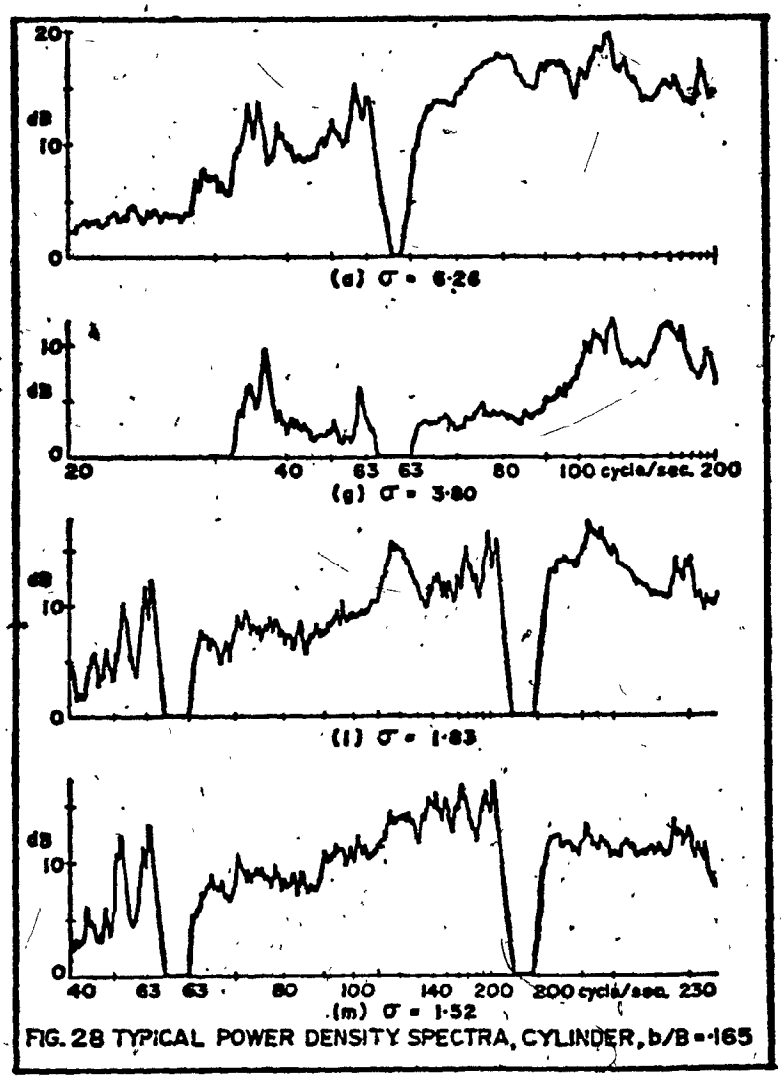

FIG. 28 TYPICAL POWER DENSITY SPECTRA, CYLINDER, b/B = ·165

No	b/B	R x 10^{-5}	REF.
1	·058	2·97	68,70
2	·125	3·97	68,70
3	·165	1·0-5·0	Present
4	·220	6·94	68,70
5	·240	3·28-7·0	81
6	·250	7·92	68,70
7	·327	3·0-8·0	Present

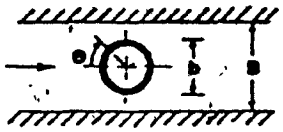

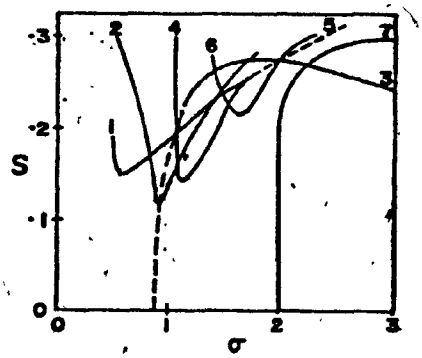

DETAIL. A

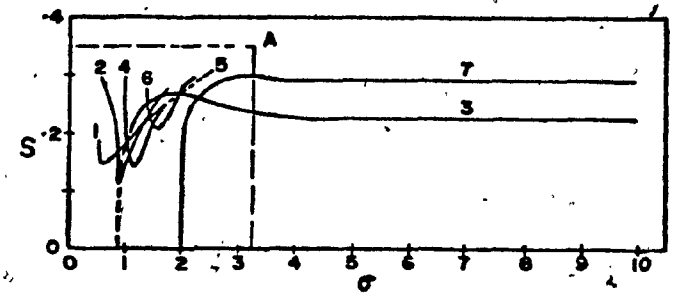

FIG 29 STROUHAL NUMBER, CAVITATING CYLINDER

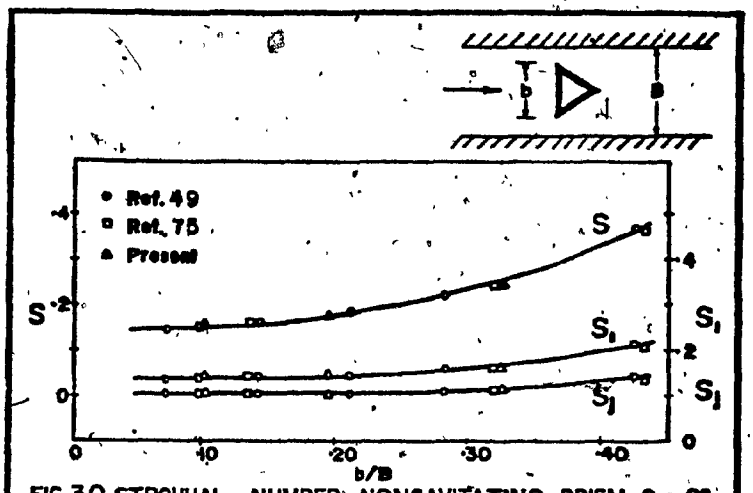

FIG. 30 STROUHAL NUMBER, NONCAVITATING PRISM θ = 0°

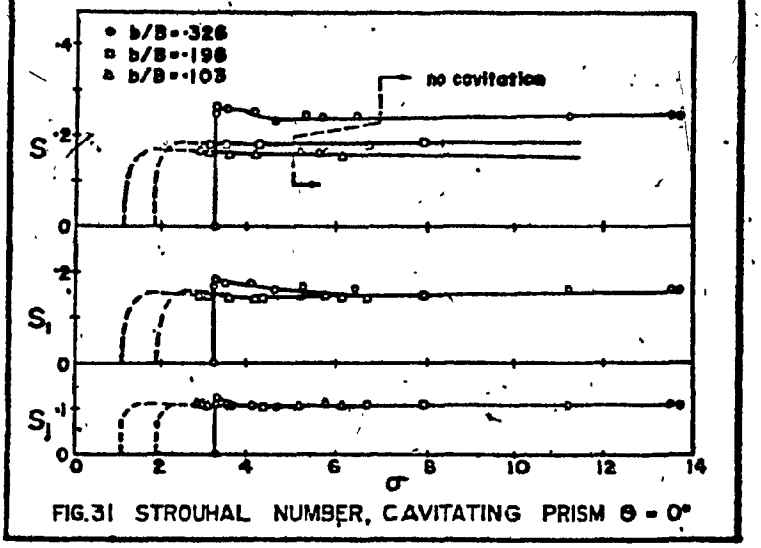

FIG. 31 STROUHAL NUMBER, CAVITATING PRISM θ = 0°

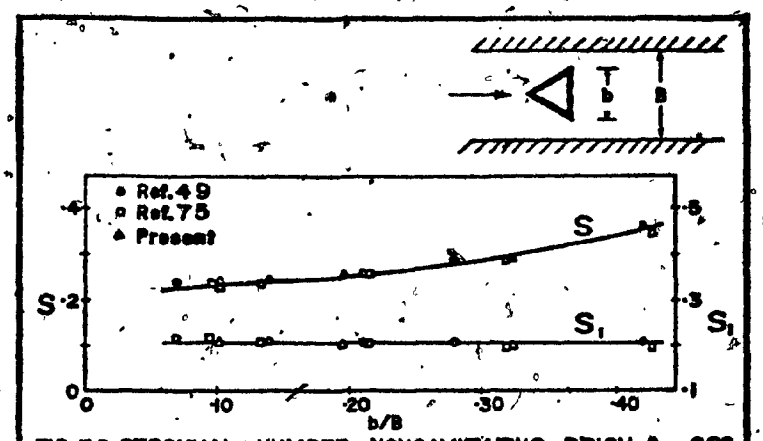

FIG. 32 STROUHAL NUMBER, NONCAVITATING PRISM θ = 60°

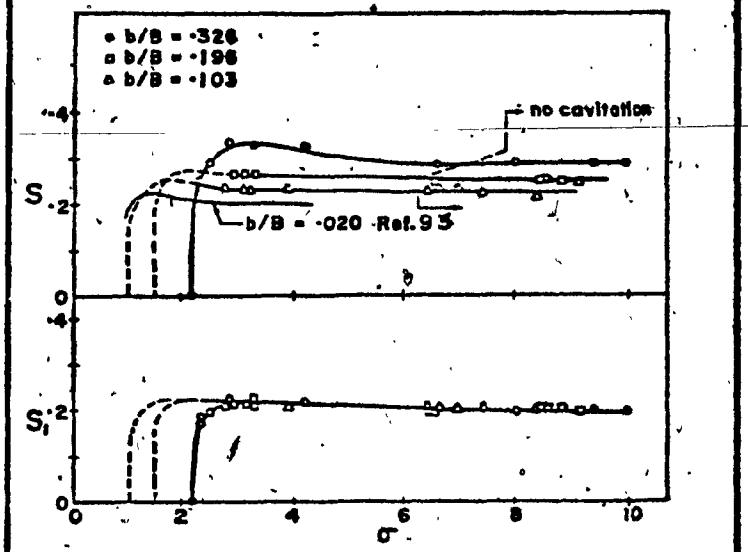

FIG. 33 STROUHAL NUMBER, CAVITATING PRISM θ = 60°

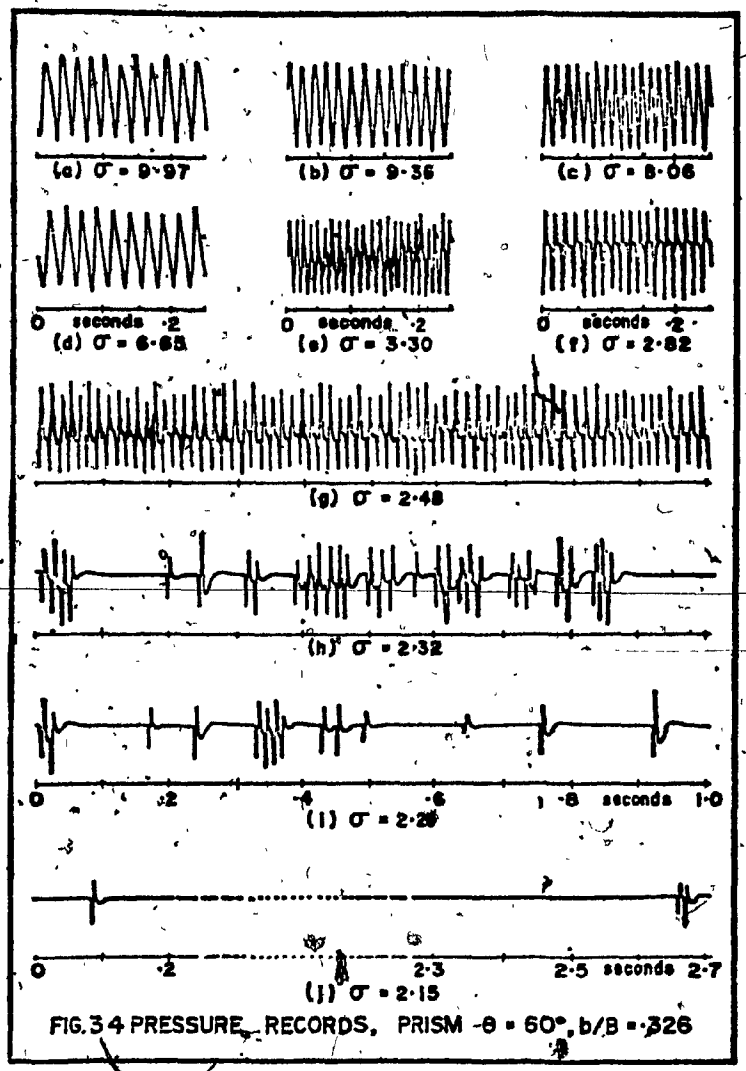

FIG. 34 PRESSURE RECORDS, PRISM θ = 60°, b/B = ·326

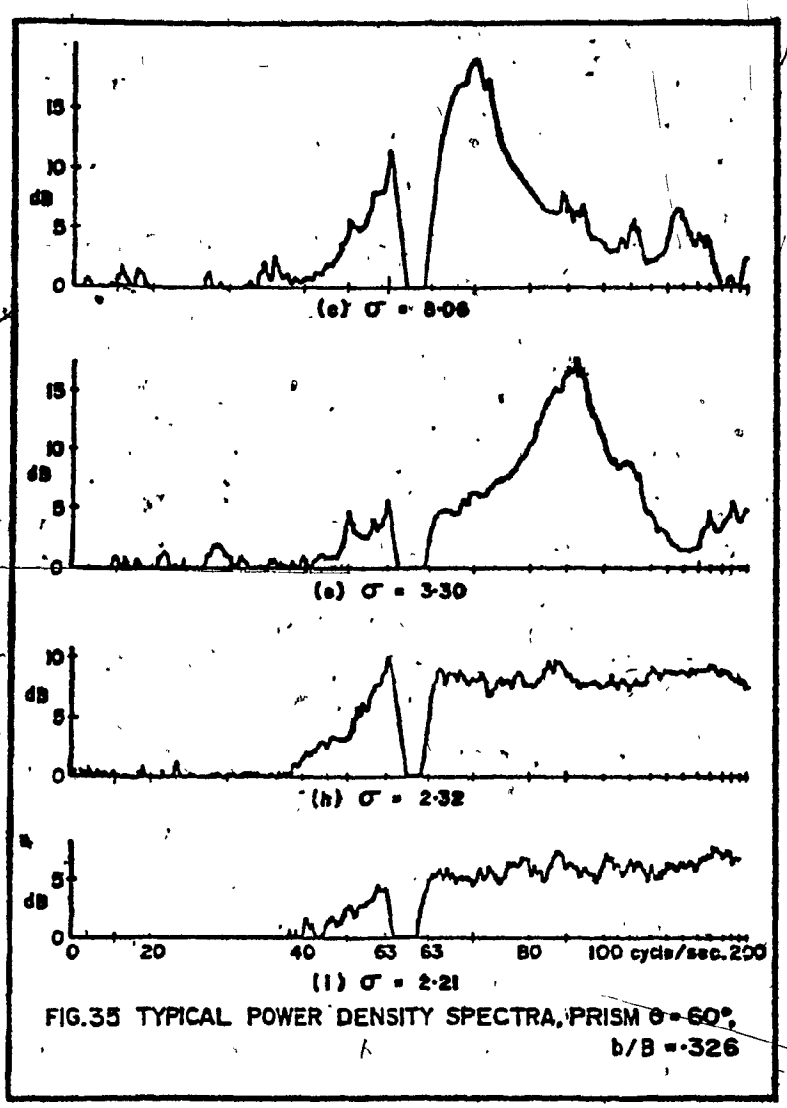

FIG.35 TYPICAL POWER DENSITY SPECTRA, PRISM θ = 60°, b/B = ·326

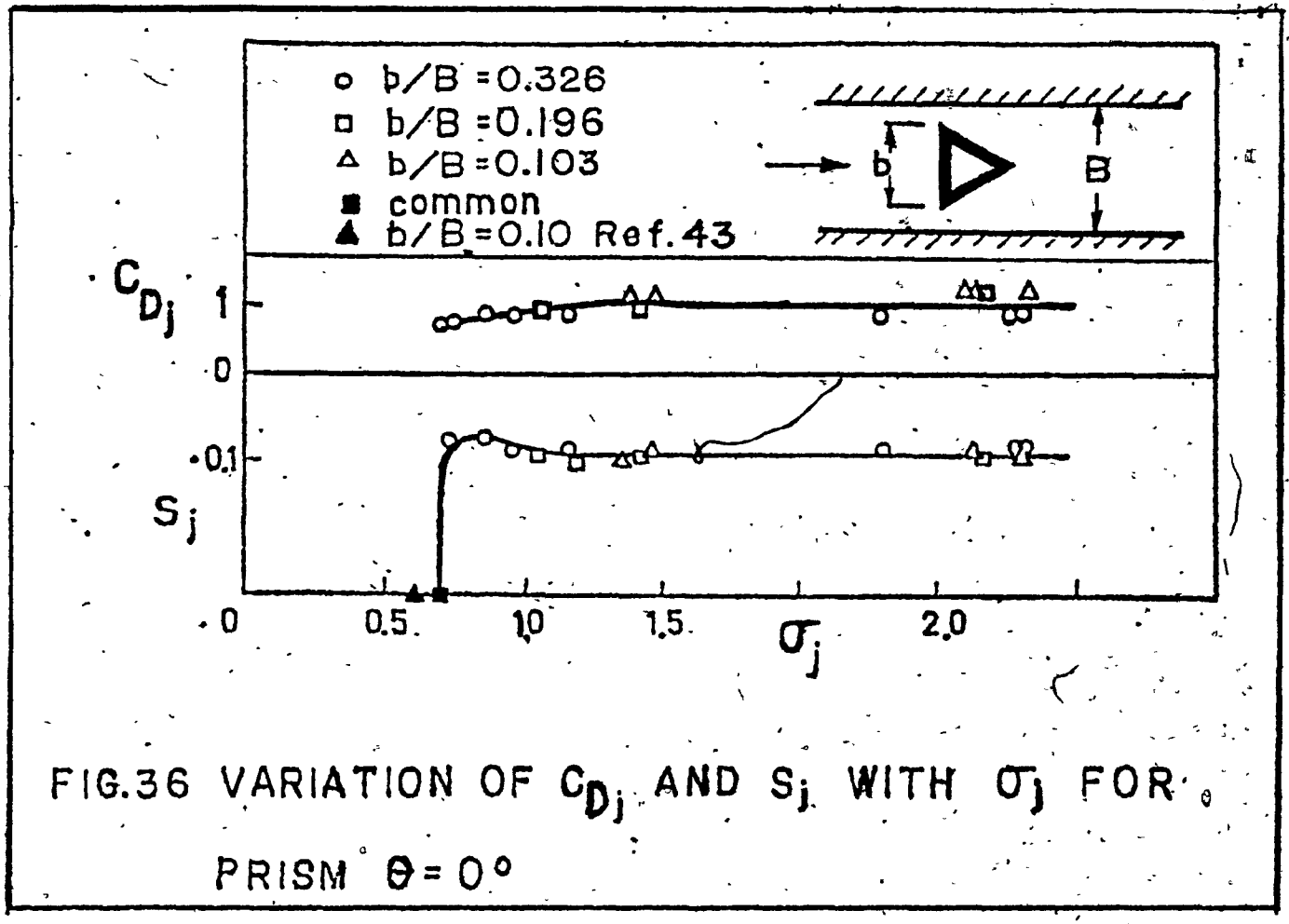

FIG.36 VARIATION OF C_{Dj} AND S_j WITH σ_j FOR PRISM $\theta = 0°$

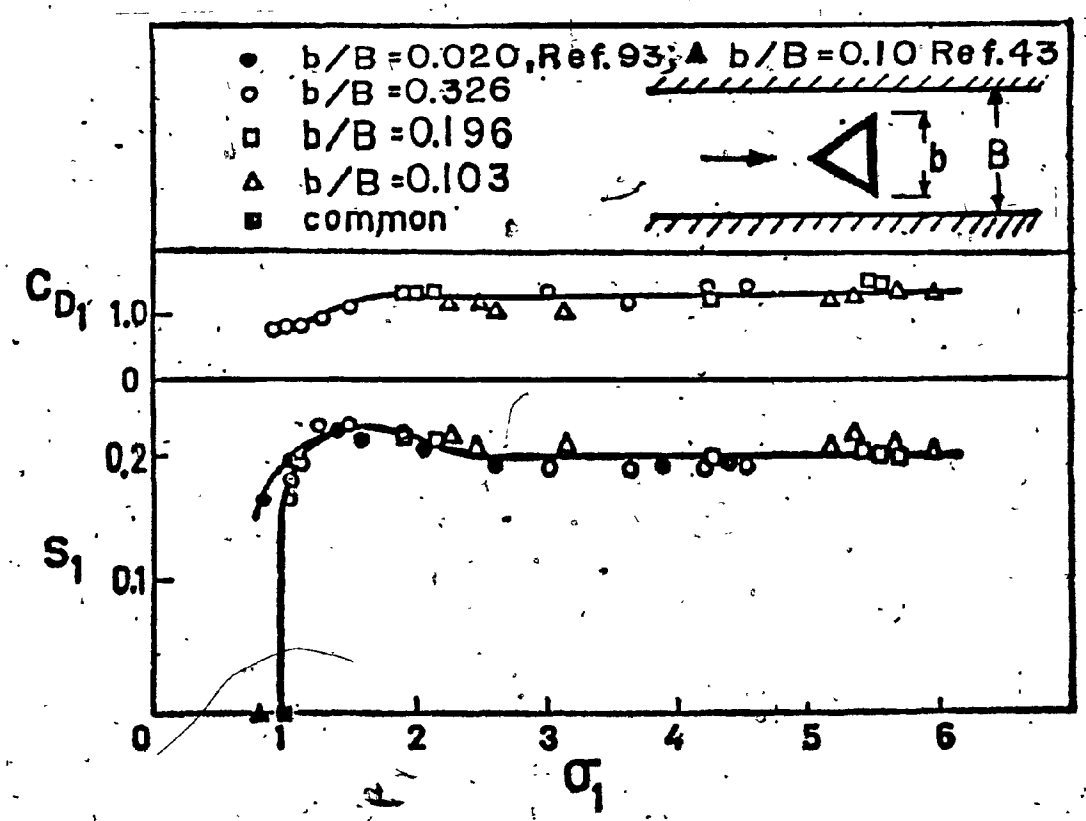

FIG. 37 VARIATION OF C_{D_1} AND S_1 WITH σ_1 FOR PRISM $\theta = 60°$

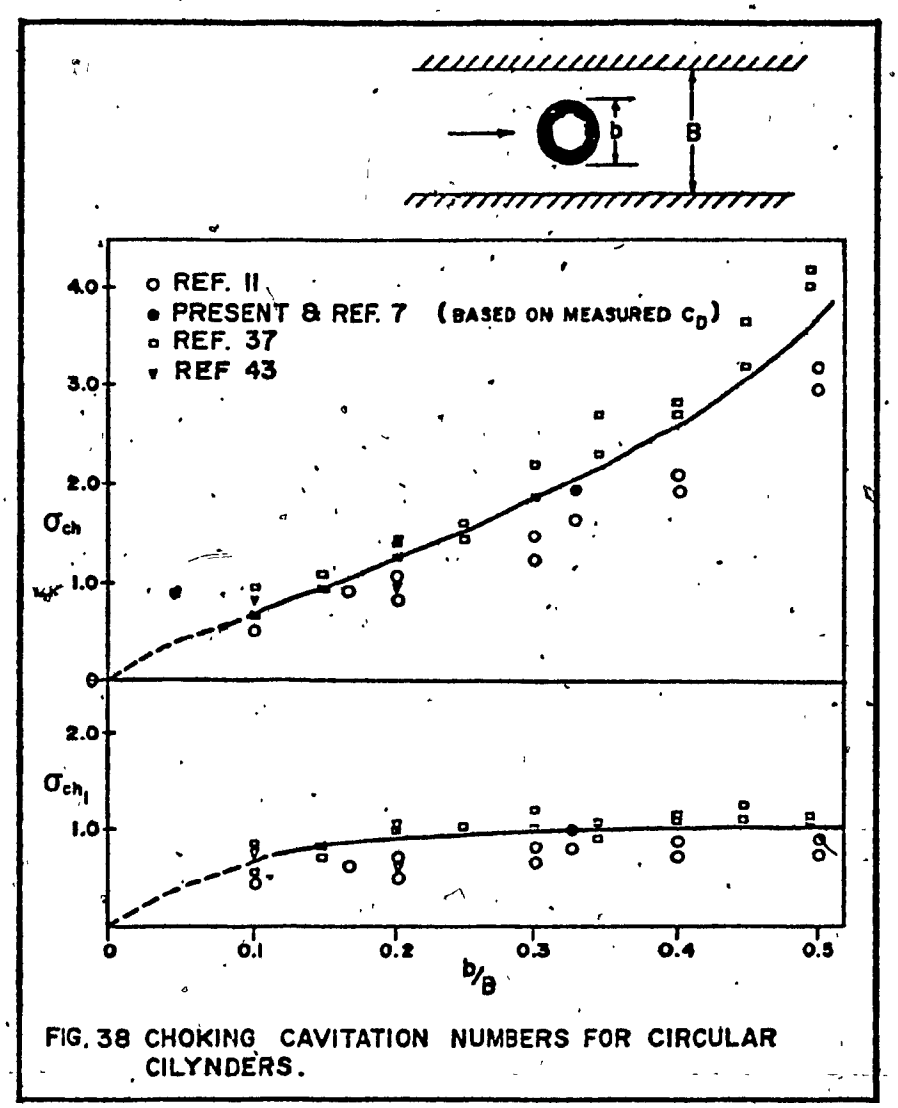

FIG. 38 CHOKING CAVITATION NUMBERS FOR CIRCULAR CILYNDERS.

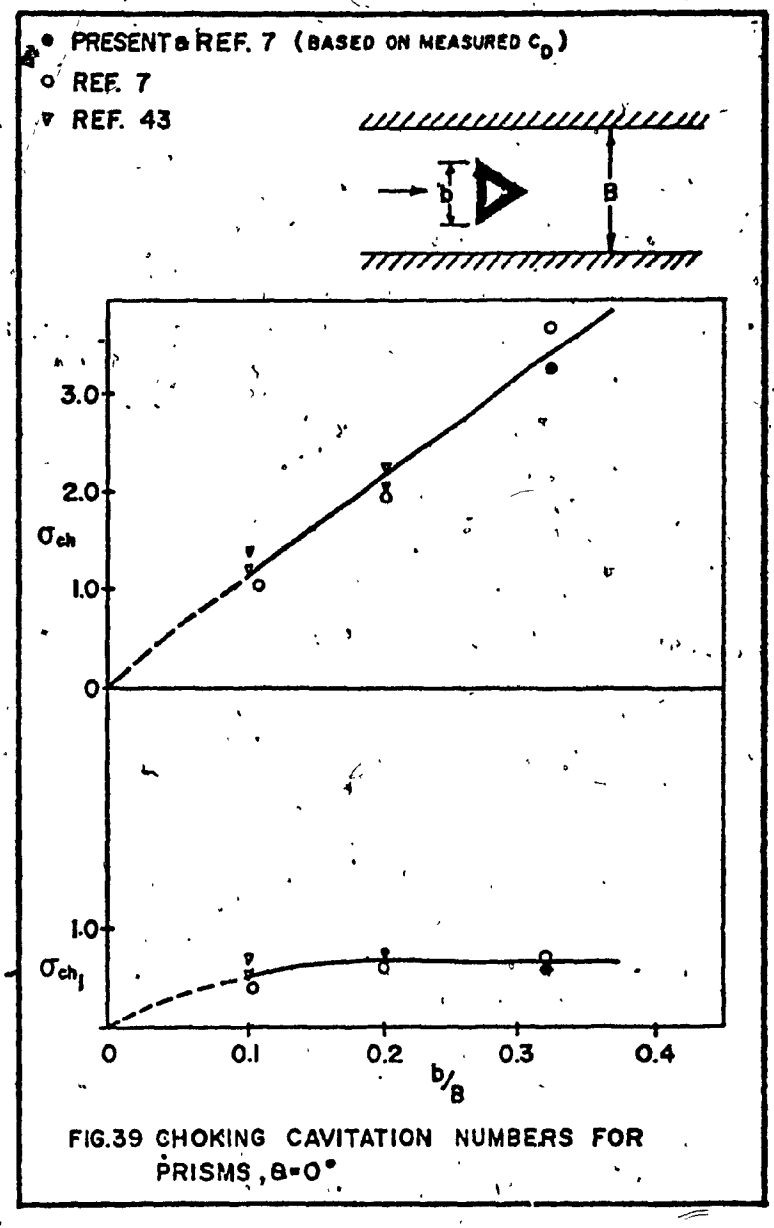

FIG.39 CHOKING CAVITATION NUMBERS FOR PRISMS, $\theta=0°$

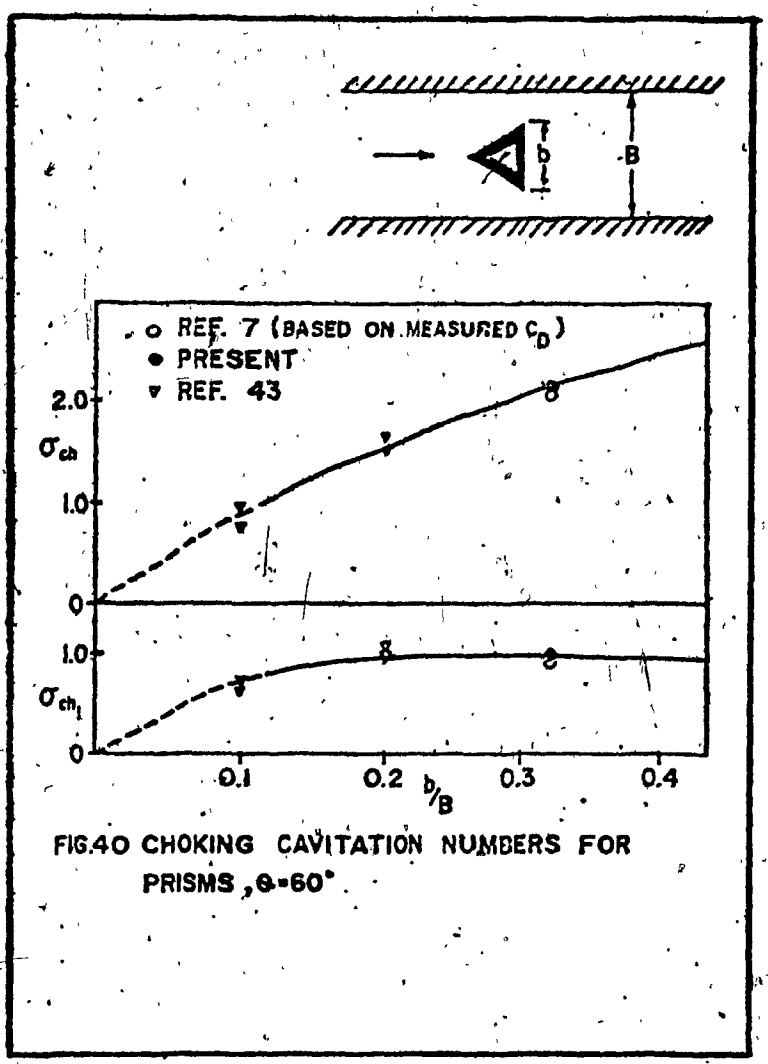

FIG.40 CHOKING CAVITATION NUMBERS FOR PRISMS, $\theta=60°$

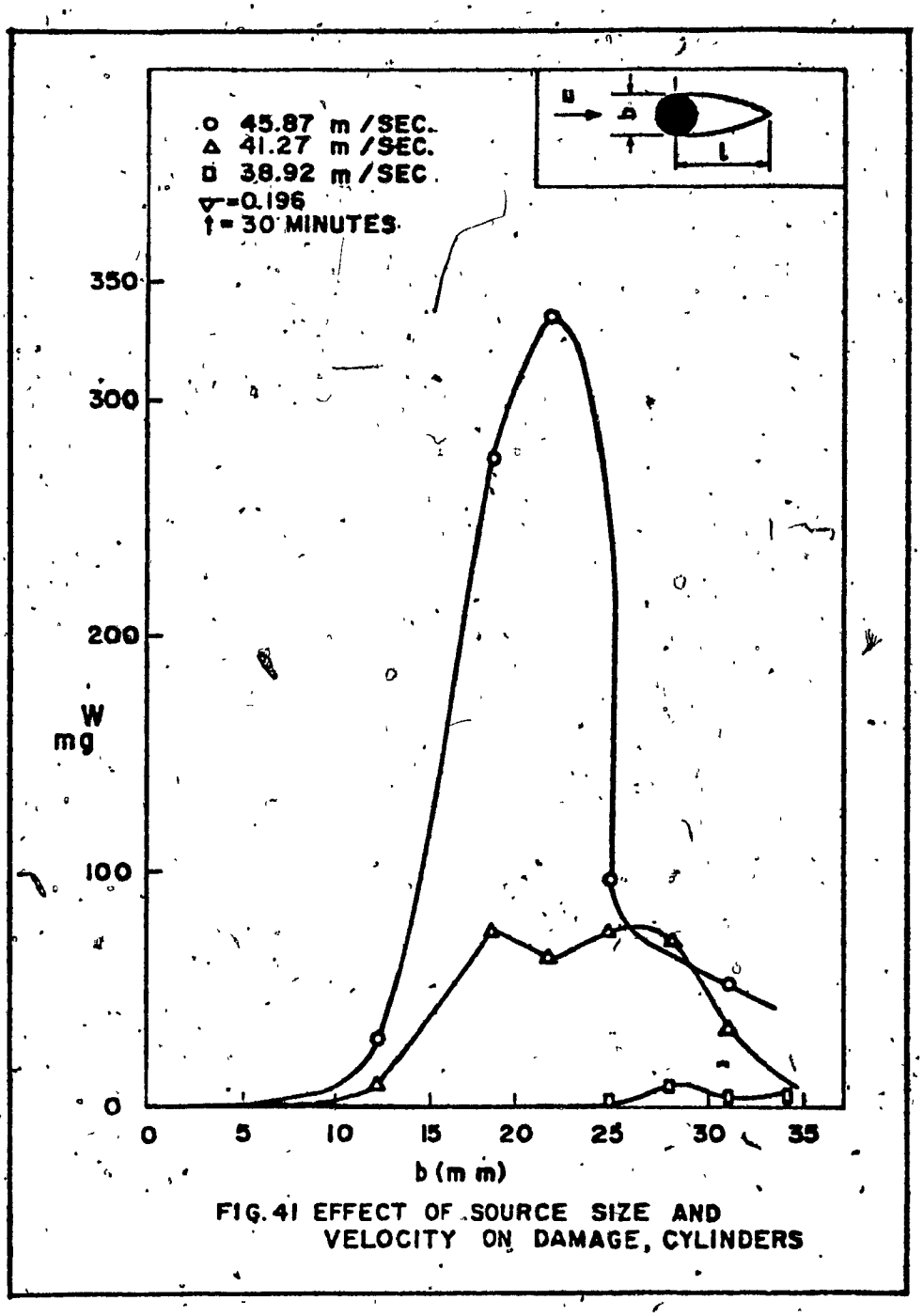

FIG. 41 EFFECT OF SOURCE SIZE AND VELOCITY ON DAMAGE, CYLINDERS

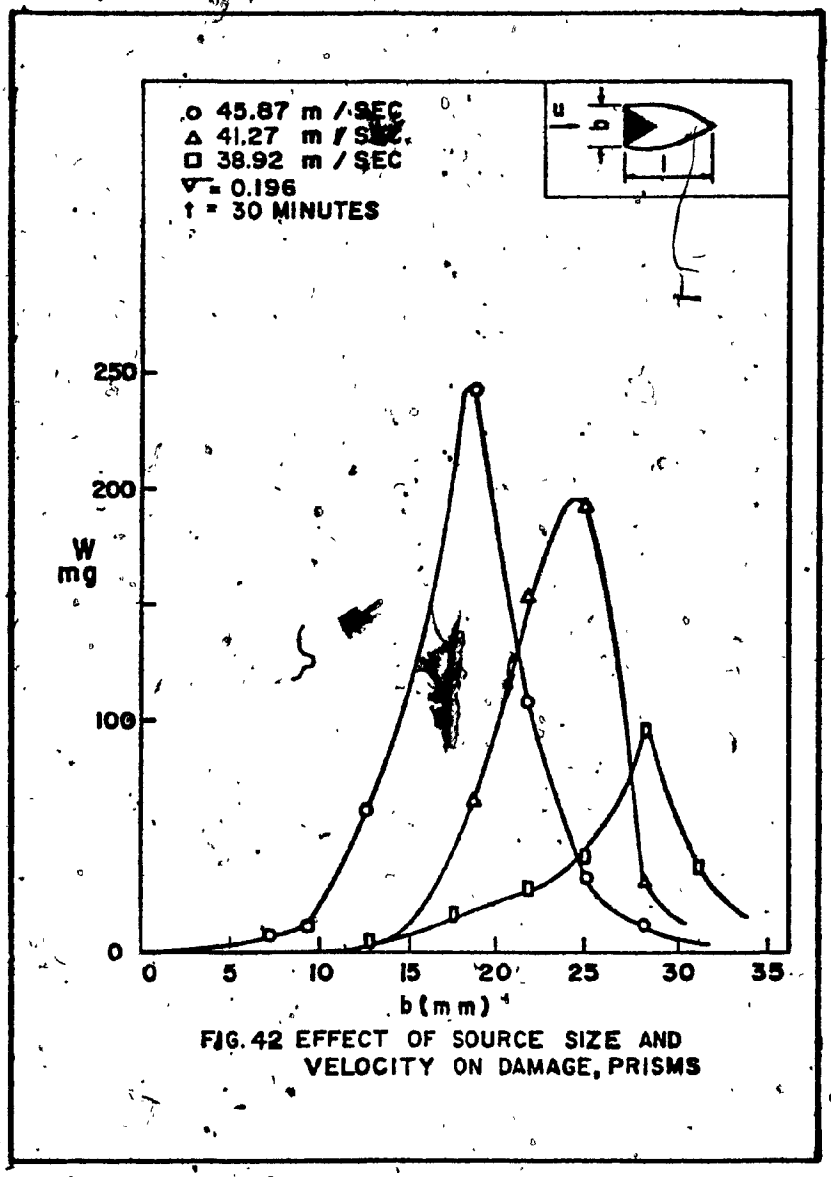

FIG. 42 EFFECT OF SOURCE SIZE AND VELOCITY ON DAMAGE, PRISMS

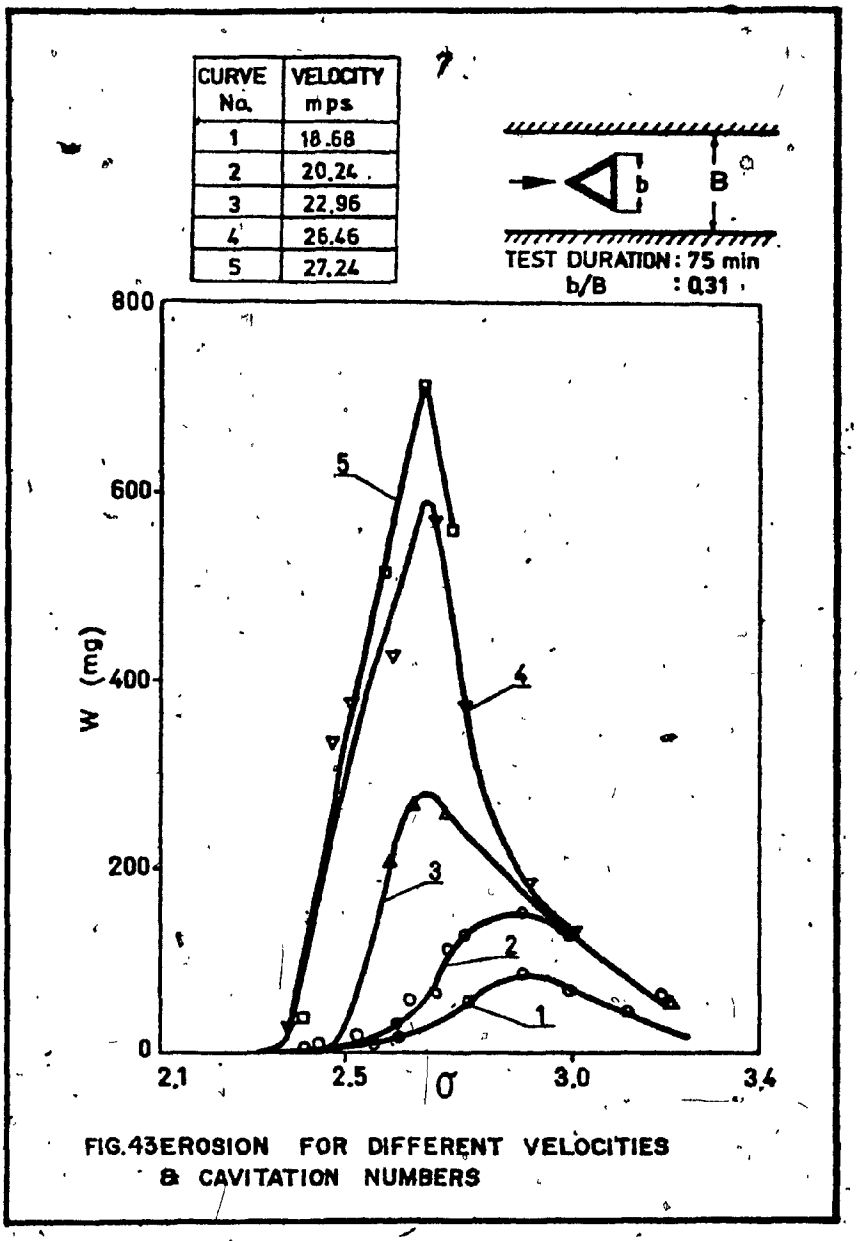

FIG.43EROSION FOR DIFFERENT VELOCITIES & CAVITATION NUMBERS

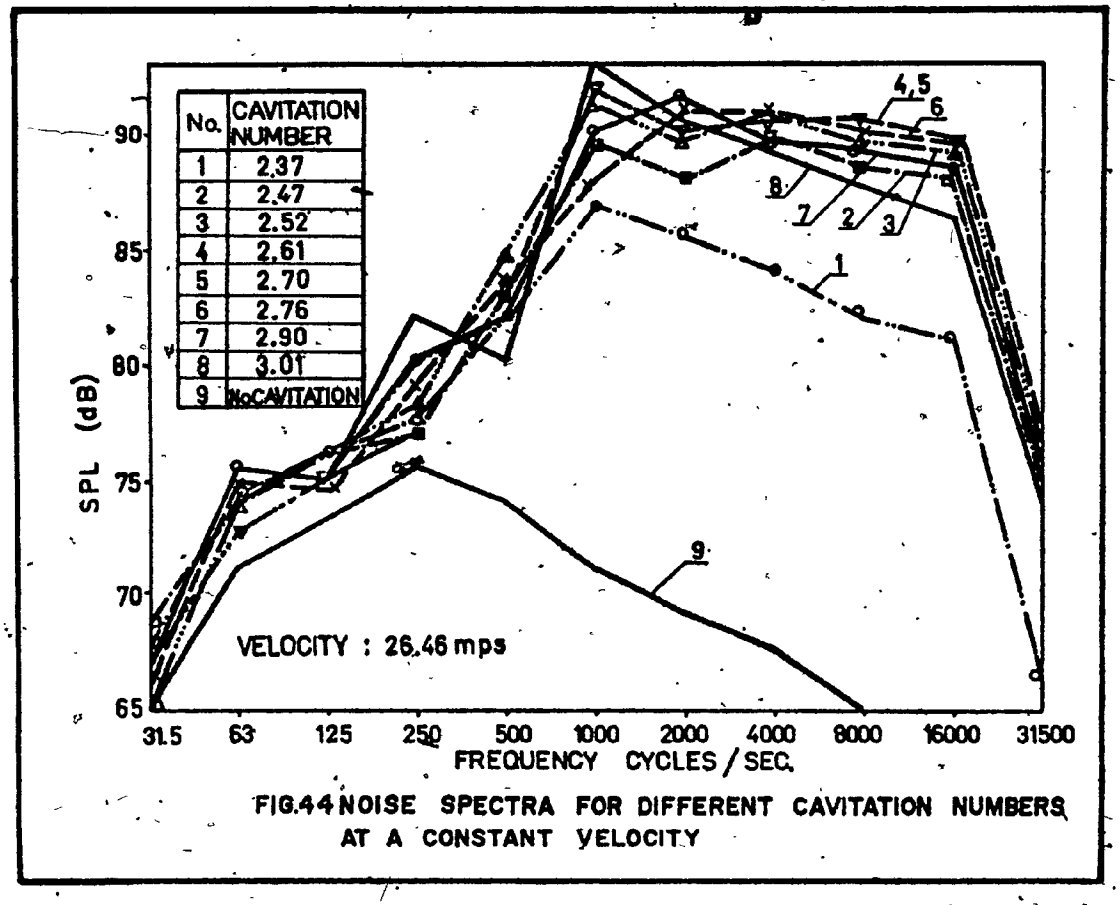

FIG.44 NOISE SPECTRA FOR DIFFERENT CAVITATION NUMBERS AT A CONSTANT VELOCITY

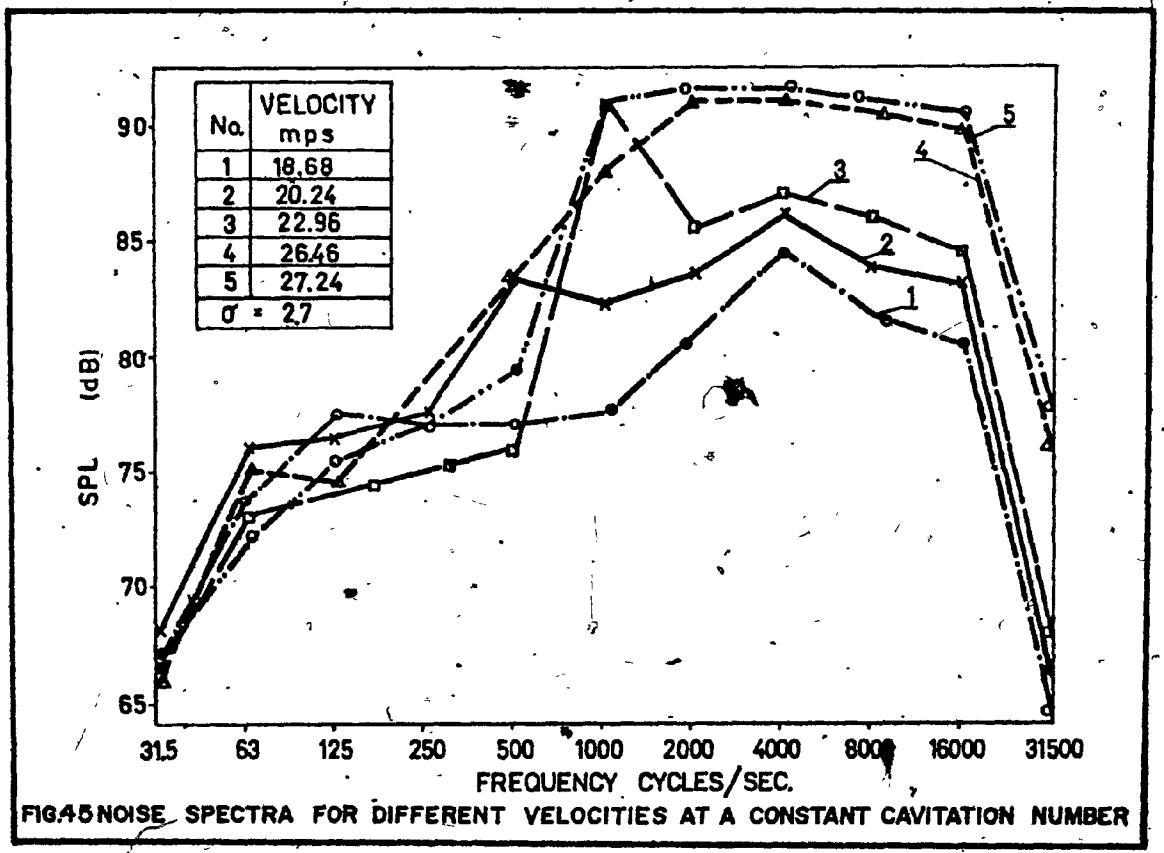

FIG.45 NOISE SPECTRA FOR DIFFERENT VELOCITIES AT A CONSTANT CAVITATION NUMBER

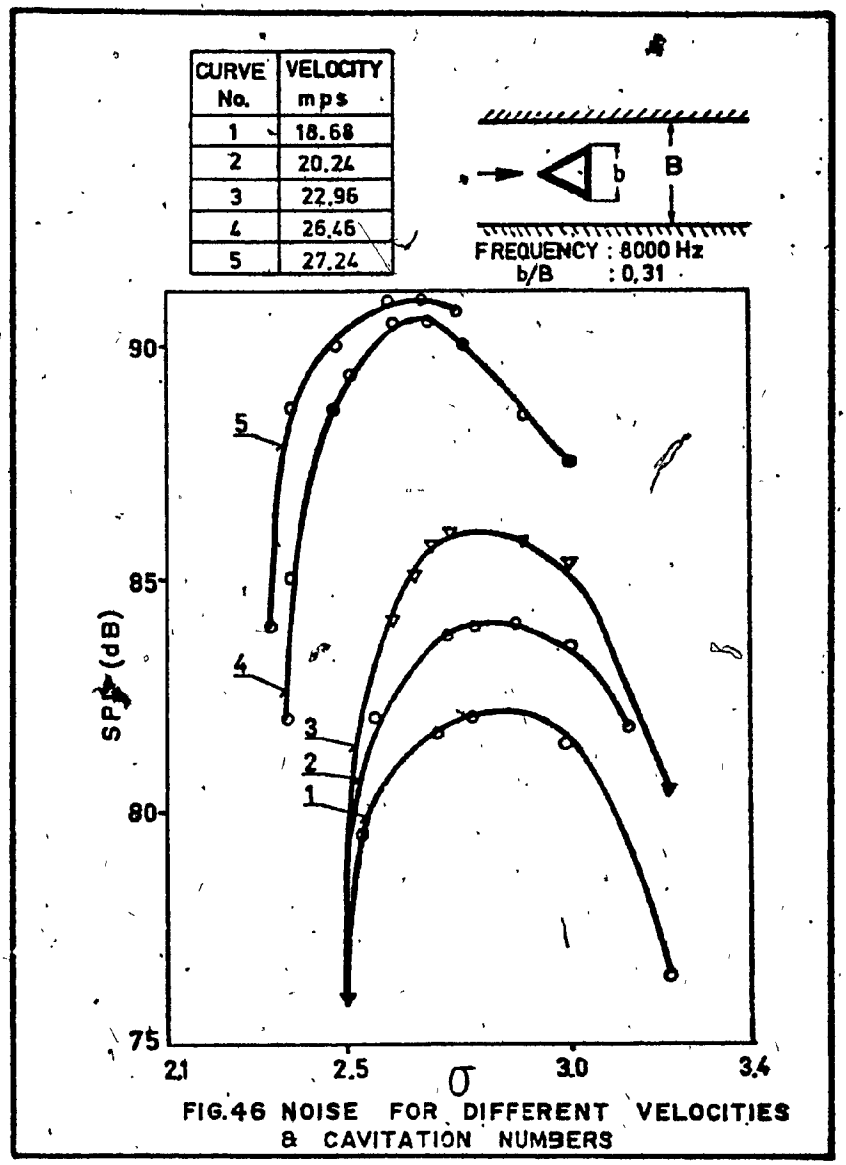

FIG.46 NOISE FOR DIFFERENT VELOCITIES & CAVITATION NUMBERS

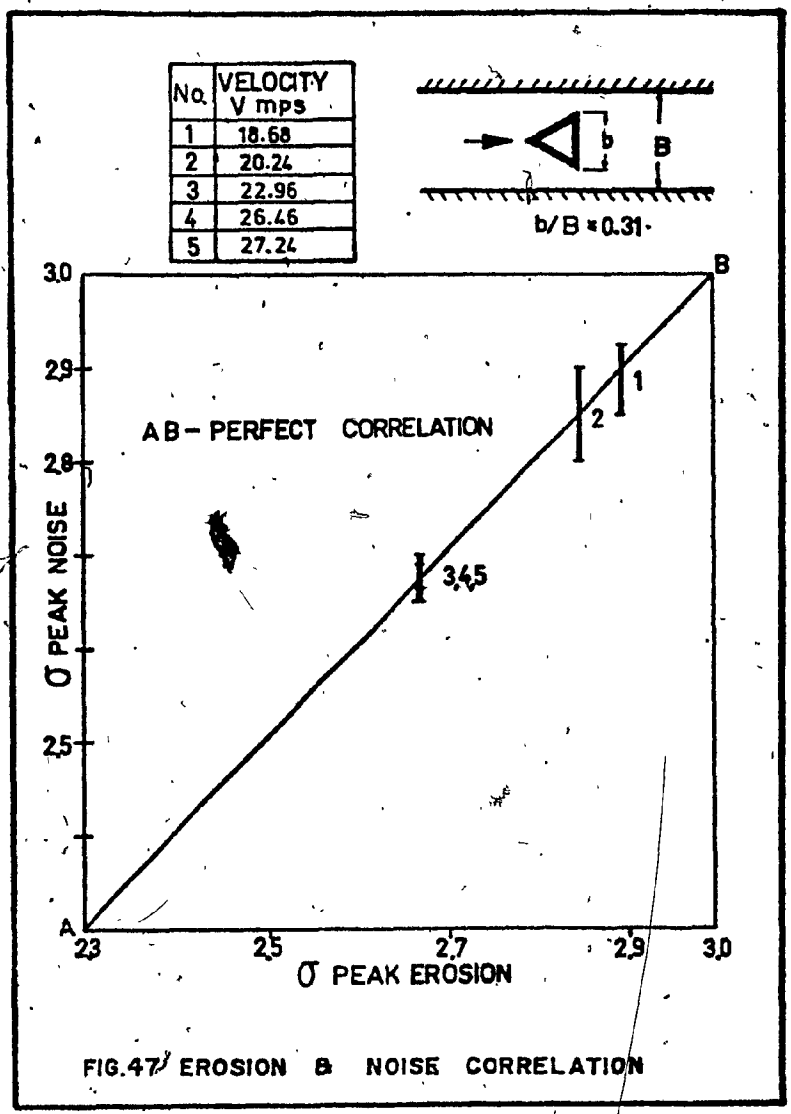

FIG.47 EROSION & NOISE CORRELATION

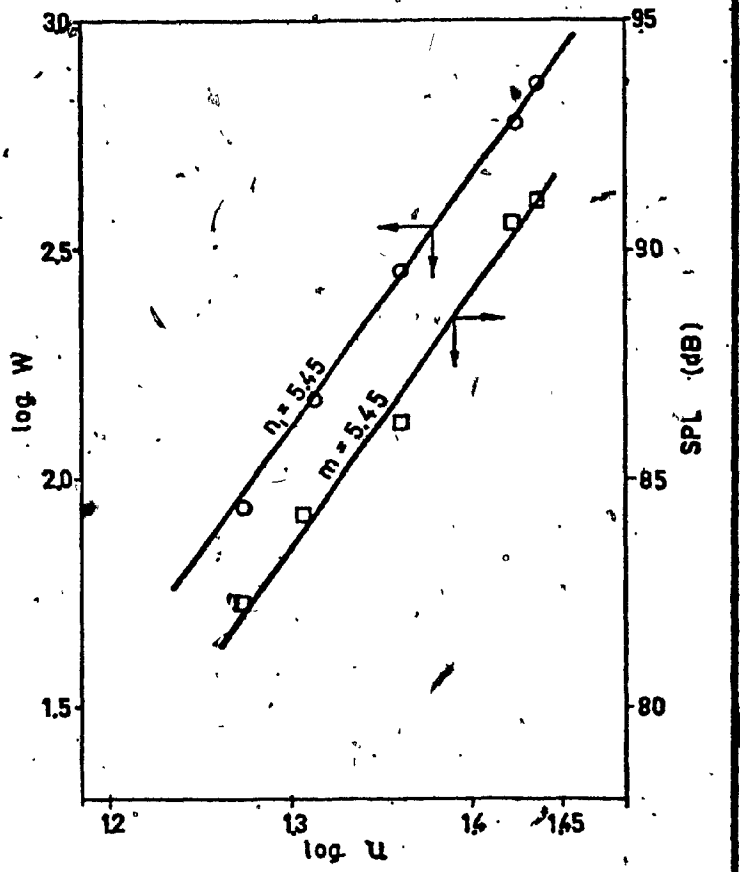

FIG.48 VELOCITY EXPONENT FOR EROSION & NOISE

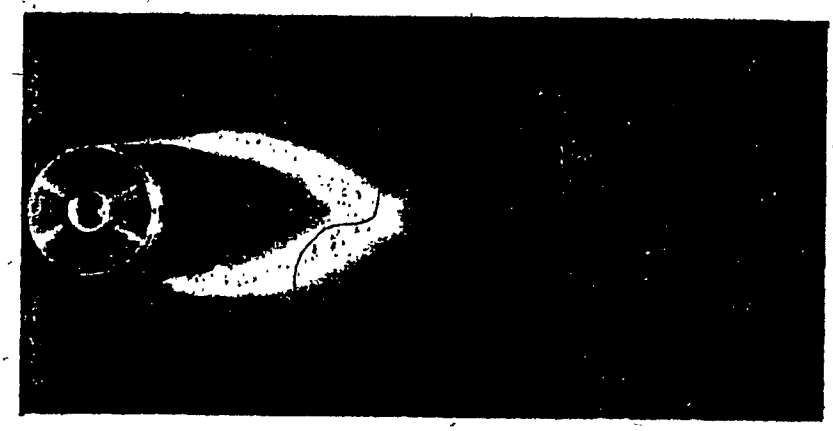

FIG. 49 DAMAGED AREA OF TEST SPECIMEN (NO SPLITTER PLATE)

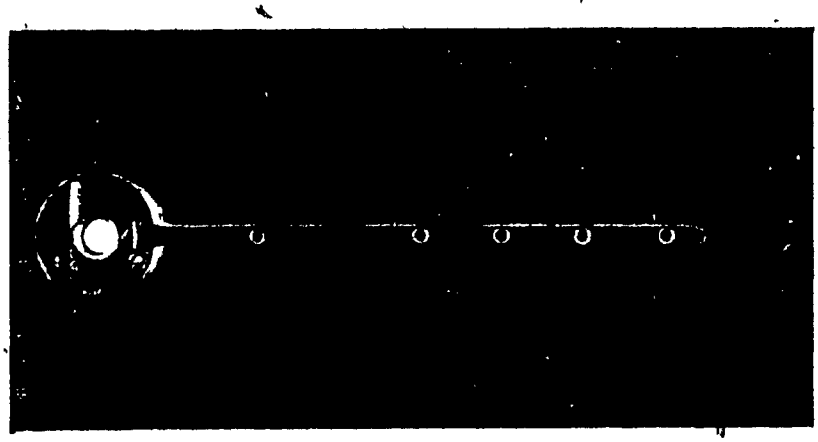

FIG. 50 DAMAGED AREA OF TEST SPECIMEN (WITH SPLITTER PLATE)

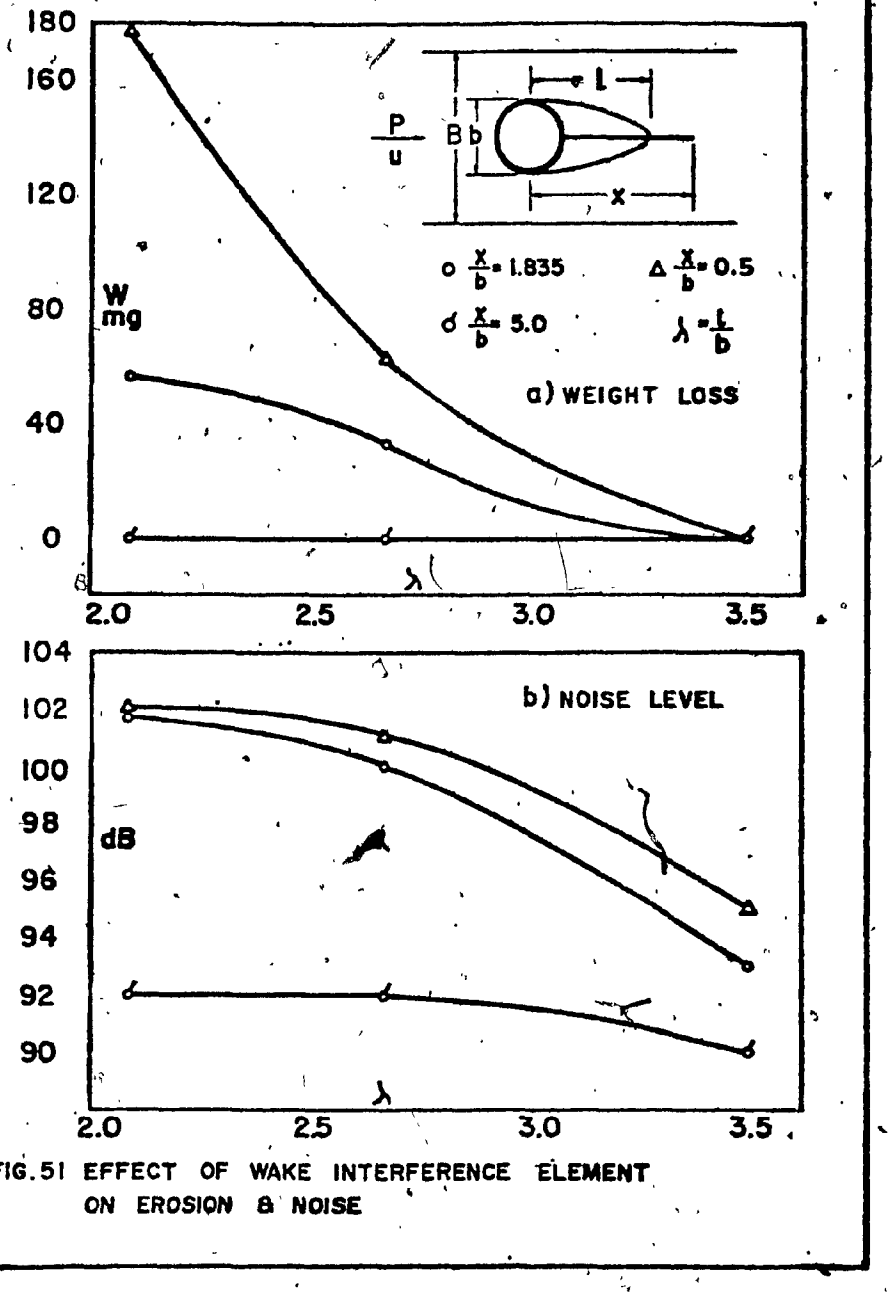

FIG. 51 EFFECT OF WAKE INTERFERENCE ELEMENT ON EROSION & NOISE

TABLE I: SUMMARY OF EXPERIMENTAL STUDIES - VELOCITY EXPONENT FOR CAVITATION EROSION

TYPE OF TEST EQUIPMENT	MATERIAL (TEST SPECIMEN)	CAVITATION NUMBER OR CAVITY LENGTH	TEST DURATION	VELOCITY mps	EROSION CRITERION D	VEL. EXPONENT $D = Ku^{n_1}$ $D = K(u - u_0)^{n_2}$
Axi-symmetric water tunnel, hemispherical nose ogival after body (33)	Aluminium 2S-F	ℓ = 25 mm ℓ = 51 mm	10 min. to 30 min.	18 to 30	Number of pits per second per sq. in.	$n_1 = 6$
Field test on 30,000 KW Francis turbine (34)	Aluminium 2S-0 test piece on runner	ℓ = 152 to 203 mm	5 min. to 20 min.	18 to 30	Number of pits per second per sq. in.	$n_1 = 6$ (5.6 - 6.3)
2-Dimensional water tunnel, cylindrical source. (56)	Lead	$\lambda = 3$ Near peak erosion	--------	14 to 23	Rate of volume erosion	$n_1 = 4$ to 5, Near peak erosion
Field hydraulic turbine (32)	Steel runner	----------	Up to 100 min.	5 to 9	Radio isotope technique	$n_1 = 5$ to 8
Venturi test rig, cylindrical source (22)	Steel, Aluminium and Plexiglass	Near peak erosion	Varied	15 to 30	Volume loss	$n_1 = 1.7$ to 5, n_1 increases with test time
2-Dimensional water tunnel, cylindrical source (80)	Lead	$\lambda = 3$	Varied	9 to 14	Weight loss	$n_1 = 2$ to 5, n_1 increases with test time
Venturi test rig, tapered piece projecting into the venturi, mercury (23)	Stainless steel 302	Varied	30 to 100 hrs	6 to 20	Volume loss	$n_1 = \pm 1$ to 2
Venturi test rig, same as above (24)	Stainless steel 302	Varied	--------	6 to 20	Volume loss	$n_1 = 0$ to 5 depends on σ

cont'd

Venturi test rig (27)	Brass	Constant	--------	37 to 49	Weight loss	$n_1 = 7$
2-Dimensional water tunnel, cylindrical source (58)	Lead	$\lambda = 2.5$ to 3	Incubation period	12 to 20	Volume loss	$D \propto L^3 u^{n_1}$ $n_1 = 5$
Rotating disk in water, holes on the disk to induce cavitation (90)	8 different alloys	$\sigma = .084$ $\sigma = .125$ and $\sigma = .217$	Up to 40 hrs	39 to 63	Volume loss	$1 < n_1 < 12$ $1 < n_2 < 7$ High exponent at low volume loss
Rotating disk, cylindrical source (9)	Lead-Antimony alloy.	$\sigma = 0.25$ $\sigma = 0.5$ and $\sigma = 0.75$	90 min.	23 to 50	Weight loss	$7 < n_1 < 10$ $.25 < \sigma < .75$ u_s depends on static pressure
Rotating disk, holes on the disk to induce cavitation (26)	Aluminium	$\sigma = 0.23$	30 min.	26 to 34	Weight loss	$n_1 = 9.55$
Venturi test rig, cylindrical source (29)	Lead	$\lambda = 1$ to 10	---------	15 to 25	Volume loss	$5 < n_1 < 8$ For noise and erosion
Venturi test rig, cylindrical source, mercury (25)	Stainless steel 304	At peak erosion	For constant rate erosion	7 and 9	Weight loss rate	$n_1 = 3.7$
2-Dimensional water tunnel, cylindrical source (60)	Lead	Near peak erosion	Varied 0-14 hrs	7 to 25	Weight loss	$n_1 = 2$ to 5 n_1 increases with test time
2-Dimensional water tunnel, cylindrical and 30° wedge sources (85)	Lead	Near peak erosion	--------	9 to 14	Volume loss rate	$n_1 = 5$ for erosion and noise, depends on σ

cont'd

Water tunnel (30)	-------	------	Varied up to 5 hrs	-------	Weight loss	n_i = 10 to 2.5, decreases with test time
2-Dimensional water tunnel, cylindrical source (67)	Aluminium	Varied	Varied up to 100 minutes	20 to 30	Volume loss	n_i = 6, initial cavitation n_i = 17, for peak erosion
Venturi test rig, circular pin (65)	Aluminium & copper	---------	1 hour	18 to 27	Weight loss	n_i = 7
Rotating foil facility, hydrofoil (NACA-16-021) source (74)	Aluminium 1100-F	At peak erosion	10 to 70 hrs	49 to 59	Erosion intensity	n_i = 6, Erosion depends on source size & σ
2-Dimensional water tunnel, Cavitation behind a step (21)	Aluminium 1100-F	σ = 0.33	10 min. to 190 min.	17 to 21	Number of pits per second per sq. in.	n_i = 6
Rotating disk, equilateral prism - Apex facing downstream (52)	Aluminium 1100-0	σ = 0.196	30 min.	39 to 46	Weight loss	n_i = 3.5 for peak erosion and optimum source size

Notes: 1. Numbers in paranthesis denote the source reference number.

2. Some columns are blank due to lack of information.

TABLE 2: σ_{ch} FOR THE CAVITATING BODIES

BODY SHAPES	BLOCKAGE RATIO b/B	MINIMUM σ FOR PRESENT TESTS	σ_{ch}	REFERENCE
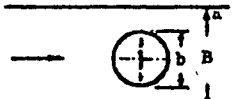	0.165	1.38	0.91	11
	0.327	2.02	2.02 2.0* 1.70	Present 7 11
	0.103	2.82	0.81 to 1.07	43
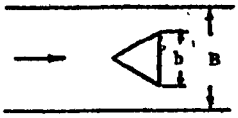	0.196	2.94	1.4 to 1.63	43
	0.326	2.15	2.15 2.09*	Present 7
	0.103	2.94	1.02** 1.06 1.2 to 1.5	7 14,79 43
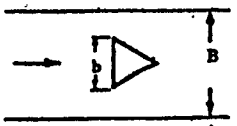	0.196	3.12	1.95** 1.87 2 to 2.2	7 14,79 43
	0.326	3.31	3.31 3.37* 3.69**	Present 7 7

*Using the measured drag and equation (4) of Ref (7) Part I [Flat plate]
**Using drag from fig 4 and equation (4) of Ref (7) Part I

Note: See also section 4.1.4 and figures 38, 39, and 40

TABLE 3

TEST RESULTS OF WAKE INTERFERENCE ELEMENTS

TO REDUCE CAVITATION EROSION AND NOISE

λ	x/b = 0.5		x/b = 1.835		x/b = 5.0	
	W Milligms	NOISE dB	W Milligms	NOISE dB	W Milligms	NOISE dB
2.08	177.4	102	56.6	101.7	0	92
2.67	62.4	101	33.0	100	0	92
3.5	0	95	0	93	0	90

Material: Aluminium 1100.F.
Test Duration: 1 hour
Velocity: 31.79 mps
Reynolds Number: $\frac{Ub}{\nu} = 6.30 \times 10^5$
Blockage: $\frac{b}{B} = 0.312$

λ = Non-dimensional cavity-length = $\frac{x}{b}$
x = Splitter plate length
b = Diameter of cylinder

APPENDIX I.

COMPUTER PROGRAMME OUTPUT AND SPECIMEN COMPUTATIONS.

COMPUTER PROGRAMME AND OUTPUT

(DRAG COEFFICIENT AND STROUHAL NUMBER DATA REDUCTION)

```
      PPOGRAM BHASKAR(INPUT,OUTPUT)
      DIMENSION D(12),P(12),OS(12),PS(12)
      REAL L,NU
C
      ICOC=38  $  ICO60=64  $  ICO=0  $  ICOCS=19
  100 ICO=ICO+1
      IF(ICO.GT.43) STOP
      IF(ICO.EQ.1) PRINT 1001
 1001 FORMAT(1H1,5(/),63X,*TABLE.1*,2(/),46X,*DRAG COEFFICIENT AND STROU
     2HAL NUMBER DATA*,2(/),39X,*FOR CAVITATION SOURCE CIRCULAR CYLINDER
     3 BLOCKAGE 1.165*,)
      IF(ICO.EQ.1) PRINT 1002
      IF(ICO.EQ.20)PRINT 1003
 1003 FORMAT(1H1,5(/),63X,*TABLE.2*,2(/),46X,*DRAG COEFFICIENT AND STROU
     o2HAL NUMBER DATA*,2(/),39X,*FOR CAVITATION SOURCE CIRCULAR CYLINDER
     3 BLOCKAGE 1.327*,)
      IF(ICO.EQ.20) PRINT 1002
 1002 FORMAT(     4(/),8X,*SIZE*,4X,*BLOC-*,4X,*VELO-*,5X,*PRESS-*,5X,
     2*FREQUE-*,5X,*CAVIT.*,4X,*CAVIT.*,4X,*DRAG*,5X,*DRAG*,5X,*STRO.*,
     34X,*STRO.*,5X,*REYNOLDS*,/,16X,*AGE*,5X,*CITY*,6X,*URE*,8X,*NCY*,
     49X,*NUMB.*,5X,*NUMB.*,5X,*COEF.*,4X,*COEF.*,4X,*NUMB.*,4X,*NUMB.*,
     55X,*NUMB.*,//,)
      IF(ICO.EQ.39) PRINT 2001
 2001 FORMAT(1H1,10(/),19X,*TABLE.3.DRAG COEFFICIENT AND STROUHAL NUMBER
     2DATA FOR CAVITATION SOURCE PRISMS 60 DEGREES ORIENTATION*,)
      IF(ICO.EQ.39) PRINT 2002
 2002 FORMAT(     3(/),15X,*SIZE*,5X,*BLOC-*,5X,*VELO-*,6X,*PRESS-*,4X,
     2*FREQUE-*,5X,*CAVIT.*,5X,*CAVIT.*,5X,*DRAG*,6X,*DRAG*,5X,*STRO.*,
     35X,*STRO.*,/,24X,*AGE*,6X,*CITY*,7X,*URE*,9X,*NCY*,4X,*NUMB.*
     4,6X,*NUMB.*,6X,*COEF.*,5X,*NUMB.*,5X,*NUMB.*,5X,*NUMB.*,//)
      IF(ICO.EQ.65) PRINT 3001
 3001 FORMAT(1H1,5(/),63X,*TABLE.4*,2(/),46X,*DRAG COEFFICIENT AND STROU
     2HAL NUMBER DATA*,2(/),42X*FOR CAVITATION SOURCE PRISMS 0 DEGREE OR
     3IENTATION*,)
      IF(ICO.EQ.65) PRINT 3002
 3002 FORMAT(     4(/),8X,*SIZE*,4X,*BLOC-*,3X,*VELO-*,4X,*PPESS-*,4X,
     2*FREQUE-*,3X,*CONTR.*,3X,*CAVIT.*,3X,*CAVIT.*,3X,*CAVIT.*,3X,
     3*DRAG*,4X,*DRAG*,4X,*DPAG*,4X,*STRO.*,3X,*STRO.*,3X,*STRO.*,/,
     416X,*AGE*,4X,*CITY*,5X,*URE*,7X,*NCY*,7X,*COEF.*,4X,*NUMB.*,
     54X,*NUMB.*,4X,*NUMB.*,4X,*COEF.*,3X,*COEF.*,3X,*COEF.*,3X,
     6*NUMB.*,3X,*NUMB.*,3X,*NUMB.*,//,)
      IF(ICO.GE.39) GO TO 2000
      IF(ICO.GT.ICOCS) GO TO 1500
      N=11
      D(1C)=D(11=1C.C*3.14159*1.C/360.C
      DO 1315 I = 2,9
 1315 D(I) = 20[*3.14159*1.C/16[.0
C
      READ 1310,(P(I),I=1,N)
 1310 FORMAT(8F1C.4)
      AREA = (P(1)+P(2))*D(1)*COS(5.0*.01745)/2.C
C
      DO 1315 I =2,9
 1315 APEA=AREA+(P(I)+P(I+1))*C(I)*COS((I-1)*21.0*.01745)/2.0
      APEA=AREA+(P(1C)+P(11))*D(10)*COS(175.*.0174S)/2.0
      DPAG=15.C*APEA/64.
      DRAG=2.*DPAG
```

```
      GO TO 1520
 1500 N=12
      D(1)=9.*3.14159*1.985/360.
      D(11)=D(1)
      DO 1505 I=2,11
 1505 D(I)=18.*3.14159*1.985/360.
C
      READ 1510,(P(I),I=1,N)
 1510 FORMAT (8F10.4)
      AREA=(P(1)+P(2))*D(1)*COS(4.5*.01745)/2.0
      DO 1515 I=2,10
 1515 AREA=AREA+(P(I)+P(I+1))*D(I)*COS((I-1)*18.*.01745)/2.0
C
      DRAG=15.*AREA/64.
      DRAG=2.*DRAG
C
 1520 READ 1525 ,L,P,U
 1525 FORMAT(3F10.4)
     *A=15.*L/64.
      A=A/144.
      CD=DRAG/(.5*A*R*U**2)
      READ1530,PO,PV,F,NU,B
 1530 FORMAT(5F10.4)
      BP=L/P
      RE=(U*L*1E6)/(NU*12)
      SIGMA=(144.0*(PO-PV))/(0.5*R*U**2)
      SIGMA1=SIGMA*(1.-BRY**2
      S=F*L/(12.*U)
      S1=(1.-BP)*S
      CD1=(1.-BP)**2*CD
      PRINT 1535,L,BR,U,PO,F,SIGMA,SIGMA1,CD,CD1,S,S1,RE
 1535 FORMAT(7X,2(F5.3,4X),F6.3,2(4X,F7.3),5X,2(F6.3,4X),4(F5.3,4X),
     2 1PF10.3,/,)
      GO TO 100
 2000 CONTINUE
      READ 2005,N
 2005 FORMAT(I2)
      READ 2010,(P(I),I=1,N)
 2010 FORMAT(8F10.4)
C
      ND=N-1
      READ 2015,(D(I),I=1,ND)
 2015 FORMAT(8F10.4)
      AAREA=0.0
      DO 2020 I=1,ND
 2020 AAREA=AAREA+(P(I)+P(I+1))*D(I)/2.0
C
      READ 2025,M
 2025 FORMAT(I2)
C
      READ 2030,(PS(I),I=1,M)
 2030 FORMAT(8F10.4)
C
      MD=M-1
      READ 2035,(DS(I),I=1,MD)
 2035 FORMAT(8F10.4)
C
```

```
      115               SAREA=0.0
                        DO 2140 I=1,MD
                 2040   SAREA=SAREA+(PS(I)+PS(I+1))*DS(I)/2.0
                   C
                        AREA=0.5*AAA-SAREA
      120               IF(ICD.GT.ICD60) AREA=-AREA
                        DRAG=15.0/64.0*AREA
                        DRAG=2.0*DRAG
                   C
                        READ 2045,L,R,U
      125       2045  FORMAT(3F10.4)
                        A=15.0/64.0*L
                        A=A/144.0
                        CD=DRAG/(0.5*A*R*U**2)
                   C
      130               IF(ICD.LE.ICD60) READ 2050,PO,PV,F,R
                        IF(ICD.GT.ICD60) READ 2050,PO,PV,F,CC,R
                 2050  FORMAT(5F10.4)
                        BR=L/R
                   C
      135               SIGMA=(144.0*(PO-PV))/(0.5*R*U**2)
                        SIGMA1=SIGMA*(1.0-BR)**2
                        S=F*L/(12.0*U)
                        S1=S*(1.0-BR)
                        CD1=CD*(1.0-BR)**2
      140           C
                        IF(ICD.LE.ICD60) GO TO 2065
                   C    L DEGREES PRISM
                        SIGMAJ=SIGMA1*CC*CC
                        SJ=S1*CC
                        CDJ=CD1*CC*CC
      145               IF(ICD.EQ.71) PRINT 2057
                        IF(ICD.EQ.76) PRINT 2057
                 2057   FORMAT(/)
                        PRINT 2060,L,BR,U,PO,F,CC,SIGMA,SIGMA1,SIGMAJ,CD,CD1,CDJ,S,S1,SJ
      150       2060  FORMAT(7X,2(F5.3,3X),F6.3,3X,2(F7.3,3X),F6.4,3(3X,F6.3),
                     2(3X,F5.3),/)
                        GO TO 100
                   C    60 DEGREES PRISM
                 2065   PRINT 2070,L,BR,U,PO,F,SIGMA,SIGMA1,CD,CC1,S,S1
      155       2070  FORMAT(14X,2(F5.3,5X),F6.3,2(5X,F7.3),2(5X,F6.3),4(5X,F5.3),/)
                        GOTO 100
                        END
```

SYMBOLIC REFERENCE MAP (R=1)

ENTRY POINTS
4134 BHASKAR

VARIABLES	SN	TYPE	RELOCATION			
5357	A	REAL		5375	AAREA	REAL
5353	AREA	REAL		5364	B	REAL
5365	BR	REAL		5401	CC	REAL

TABLE. 4

DRAG COEFFICIENT AND STROUHAL NUMBER DATA

FOR CAVITATION SOURCE CIRCULAR CYLINDER BLOCKAGE 0.165

SIZE b	BLOCKAGE b/B	VELOCITY u	PRESSURE P	FREQUENCY f	CAVIT. NUMB. σ	CAVIT. NUMB. σ_1	DRAG COEF. C_D	DRAG COEF. C_{D_1}	STRO. NUMB. S	STRO. NUMB. S_1	REYNOLDS NUMB. R
1.000	.165	28.376	34.232	80.000	6.253	4.360	1.025	.714	.235	.196	2.252E+05
1.000	.165	28.376	34.232	115.000	6.253	4.360	1.025	.714	.338	.282	2.252E+05
1.000	.165	34.660	42.385	94.300	5.200	3.626	.897	.625	.227	.189	2.765E+05
1.000	.165	34.660	42.385	114.800	5.200	3.626	.997	.625	.276	.230	2.765E+05
1.000	.165	24.323	17.476	64.300	4.332	3.021	.924	.644	.210	.175	1.564E+05
1.000	.165	24.323	17.476	122.000	4.332	3.021	.924	.644	.418	.349	1.564E+05
1.000	.165	43.070	50.995	122.000	4.058	2.830	.880	.614	.236	.197	3.461E+05
1.000	.165	48.140	61.791	130.100	3.941	2.748	.865	.603	.225	.188	3.921E+05
1.000	.165	30.913	25.530	97.000	3.933	2.743	1.155	.805	.262	.218	2.017E+05
1.000	.165	53.710	74.084	146.000	3.799	2.649	.926	.576	.227	.189	4.432E+05
1.000	.165	38.511	29.393	112.900	2.909	2.028	1.161	.809	.243	.203	3.095E+05
1.000	.165	32.430	17.133	101.090	2.396	1.663	1.440	1.004	.260	.217	2.181E+05
1.000	.165	36.484	19.005	115.000	2.093	1.460	1.501	1.047	.263	.219	2.492E+05
1.000	.165	40.791	20.766	117.500	1.830	1.276	1.448	1.010	.240	.200	2.863E+05
1.000	.165	40.791	20.766	212.000	1.830	1.276	1.448	1.010	.433	.362	2.863E+05
1.000	.165	47.125	23.625	130.000	1.521	1.061	1.285	.896	.230	.192	3.400E+05
1.000	.165	47.125	23.625	160.000	1.521	1.061	1.285	.896	.283	.236	3.400E+05
1.000	.165	51.686	24.996	160.000	1.374	.958	1.230	.858	.258	.215	3.729E+05
1.000	.165	55.739	29.071	163.000	1.376	.960	1.213	.846	.244	.203	4.079E+05

TABLE.5

DRAG COEFFICIENT AND STROUHAL NUMBER DATA

FOR CAVITATING SOURCE CIRCULAR CYLINDER BLOCKAGE 0.327

SIZE b	BLOCKAGE b/B	VELOCITY u	PRESSURE P	FREQUENCY f	CAVIT. NUMB. σ	CAVIT. NUMB. σ_1	DRAG COEF. C_D	DRAG COEF. C_{D_1}	STRO. NUMB. S	STRO. NUMB. S_1	REYNOLDS NUMB. R
1.985	.327	27.363	40.424	46.988	7.955	3.598	4.218	1.908	.244	.191	4.311E+05
1.985	.327	25.443	28.968	44.388	6.162	2.878	4.364	1.974	.284	.191	4.179E+05
1.985	.327	28.579	25.168	50.775	4.512	2.041	3.425	1.549	.294	.198	4.559E+05
1.985	.327	26.350	18.286	43.000	3.451	1.742	3.837	1.736	.270	.182	3.774E+05
1.985	.327	30.403	21.241	53.666	3.364	1.522	2.816	1.274	.292	.196	4.480E+05
1.985	.327	30.403	21.241	55.600	3.364	1.522	2.816	1.274	.303	.203	4.480E+05
1.985	.327	34.457	26.477	61.538	3.271	1.480	2.173	.983	.295	.199	5.572E+05
1.985	.327	35.471	25.748	63.636	3.004	1.359	1.981	.896	.297	.200	5.227E+05
1.985	.327	37.497	26.809	66.810	2.796	1.265	1.781	.806	.295	.198	5.907E+05
1.985	.327	38.714	25.681	65.476	2.535	1.147	1.672	.756	.280	.188	5.70[illegible]E+05
1.985	.327	41.551	28.351	68.333	2.413	1.091	1.449	.656	.272	.183	6.213E+05
1.985	.327	40.538	25.410	60.000	2.269	1.026	1.518	.687	.245	.165	6.061E+05
1.985	.327	44.794	30.971	81.250	2.270	1.027	1.243	.562	.360	.242	6.798E+05
1.985	.327	51.686	38.504	75.000	2.124	.961	.928	.420	.240	.161	7.844E+05
1.985	.327	45.605	29.982	73.000	2.118	.958	1.194	.540	.265	.178	7.095E+05
1.985	.327	43.071	26.738	83.300	2.116	.957	1.137	.605	.320	.215	6.536E+05
1.985	.327	42.565	25.779	75.300	2.088	.945	1.370	.620	.291	.196	6.364E+05
1.985	.327	42.565	25.779	62.500	2.088	.945	1.370	.620	.243	.163	6.364E+05
1.985	.327	50.672	35.261	0.000	2.019	.913	.966	.437	0.000	0.000	7.690E+05

TABLE 6. DRAG COEFFICIENT AND STROUHAL NUMBER DATA FOR CAVITATION SOURCE PRISMS 60 DEGREES ORIENTATION

SIZE b	BLOCKAGE b/B	VELOCITY u	PRESSURE P	FREQUENCY f	CAVIT. NUMB. σ	CAVIT. NUMB. σ_1	DRAG COEF. C_D	DRAG NUMB. C_{D_1}	STRO. NUMB. S	STRO. NUMB. S_1
.625	.103	25.843	33.720	112.500	7.410	5.961	1.641	1.320	.227	.203
.625	.103	28.376	38.549	127.340	7.037	5.661	1.713	1.378	.234	.210
.625	.103	33.950	52.219	158.330	6.681	5.375	1.631	1.312	.243	.218
.625	.103	32.430	46.146	145.000	6.462	5.198	1.570	1.263	.233	.209
.625	.103	26.350	18.793	116.100	3.924	3.157	1.290	1.038	.229	.206
.625	.103	29.900	20.257	133.000	3.282	2.640	1.343	1.081	.232	.208
.625	.103	32.937	22.923	146.000	3.077	2.475	1.473	1.185	.231	.207
.625	.103	53.713	55.095	245.000	2.818	2.267	1.534	1.234	.238	.213
1.190	.196	35.471	75.011	89.371	8.818	5.696	2.315	1.495	.250	.201
1.190	.196	28.376	47.048	72.046	8.610	5.562	2.317	1.497	.252	.202
1.190	.196	32.430	61.395	82.105	8.488	5.478	2.422	1.564	.251	.202
1.190	.196	22.296	22.618	55.461	6.614	4.272	1.862	1.203	.247	.198
1.190	.196	36.991	31.272	97.727	3.348	2.163	2.118	1.368	.262	.211
1.190	.196	41.551	37.120	112.069	3.157	2.039	2.090	1.350	.267	.215
1.190	.196	46.618	43.376	126.119	2.936	1.896	2.035	1.314	.268	.216
1.975	.326	24.829	41.817	42.855	9.973	4.533	3.255	1.480	.284	.192
1.975	.326	29.497	56.737	51.454	9.369	4.255	3.223	1.465	.285	.192
1.975	.326	40.538	89.428	70.000	8.857	3.663	2.769	1.259	.284	.192
1.975	.326	23.309	24.808	40.331	6.652	3.024	2.938	1.358	.285	.192
1.975	.326	31.417	28.336	61.714	4.185	1.903	2.918	1.322	.323	.218
1.975	.326	44.592	44.622	89.097	3.299	1.500	2.557	1.162	.329	.222
1.975	.326	35.471	24.233	71.875	2.815	1.280	2.345	.948	.334	.225
1.975	.326	38.714	25.388	67.813	2.481	1.128	1.863	.847	.288	.194
1.975	.326	43.031	25.441	66.663	2.325	1.057	1.761	.801	.274	.185
1.975	.326	41.045	26.040	68.750	2.317	1.053	1.774	.807	.276	.186
1.975	.326	46.112	31.179	0.000	2.153	.979	1.766	.803	0.000	0.000

TABLE.7

DRAG COEFFICIENT AND STROUHAL NUMBER DATA

FOR CAVITATION SOURCE PRISMS 0 DEGREE ORIENTATION

SIZE b	BLOCKAGE b/B	VELOCITY u	PRESSURE P	FREQUENCY f	CONTR. COEF. C_c	CAVIT. NUMB. σ	CAVIT. NUMB. σ_1	CAVIT. NUMB. σ_j	DRAG COEF. C_D	DRAG COEF. C_{D_1}	DRAG COEF. C_{D_j}	STRO. NUMB. S	STRO. NUMB. S_1	STRO. NUMB. S_j
.625	.103	30.910	43.035	95.000	.7550	6.175	4.967	2.831	2.769	2.228	1.270	.160	.144	.108
.625	.103	41.855	68.189	132.500	.7550	5.756	4.631	2.640	2.651	2.132	1.216	.165	.148	.112
.625	.103	38.516	56.993	120.000	.7550	5.677	4.567	2.603	2.609	2.099	1.196	.162	.146	.110
.625	.103	37.750	30.886	117.000	.7550	3.180	2.558	1.458	2.615	2.104	1.199	.161	.145	.109
.625	.103	43.071	37.750	127.000	.7550	2.992	2.407	1.372	2.623	2.110	1.203	.154	.138	.104
.625	.103	57.766	66.308	179.000	.7550	2.937	2.363	1.347	2.420	1.947	1.110	.161	.145	.109
1.190	.196	28.376	43.546	52.480	.7185	7.969	5.148	2.657	3.366	2.175	1.123	.183	.147	.106
1.190	.196	51.179	75.364	92.000	.7185	4.254	2.750	1.420	3.043	1.965	1.015	.178	.143	.103
1.190	.196	36.990	32.762	65.000	.7185	3.521	2.274	1.174	2.924	1.889	.975	.174	.140	.101
1.190	.196	56.246	68.216	101.250	.7185	3.188	2.059	1.063	3.000	1.938	1.003	.179	.143	.103
1.190	.196	45.605	43.987	81.926	.7185	3.117	2.014	1.040	2.986	1.929	.996	.178	.143	.103
1.975	.326	28.579	75.470	43.000	.6740	13.670	6.214	2.823	4.384	1.993	.905	.248	.167	.113
1.975	.326	30.910	87.040	45.800	.6740	13.488	6.131	2.785	4.337	1.971	.896	.244	.164	.111
1.975	.326	36.475	94.507	52.000	.6740	11.127	5.058	2.298	4.151	1.887	.857	.241	.163	.110
1.975	.326	27.363	28.926	39.000	.6740	5.663	2.573	1.169	4.245	1.930	.877	.235	.158	.107
1.975	.326	36.484	41.521	52.200	.6740	4.588	2.086	.948	4.247	1.930	.877	.235	.159	.107
1.975	.326	46.112	59.186	72.220	.6740	4.119	1.868	.849	4.026	1.830	.831	.258	.174	.117
1.975	.326	34.710	29.361	54.383	.6740	3.578	1.626	.739	3.703	1.724	.783	.258	.174	.117
1.975	.326	41.551	38.862	0.000	.6740	3.312	1.506	.684	3.804	1.729	.786	0.000	0.000	0.000

SPECIMEN COMPUTATIONS

COMPUTATION OF VELOCITY EXPONENTS

a) Erosion

Weight loss,

$$W \alpha u^{n_1} \tag{1}$$

or

$$\log_{10} W \alpha n_1 \log_{10} u \tag{2}$$

At peak erosion conditions, from figure 48, the slope of the line $\log_{10} W$ versus $\log_{10} u$ gives, $n_1 = 5.45$.

b) Noise

Noise intensity,

$$I = \frac{p^2}{\rho c^2} \tag{3}$$

At peak erosion conditions,

$$I \alpha u^m \tag{4}$$

or

$$\log_{10} I \alpha m \log_{10} u \tag{5}$$

For constant p and c,

$$2 \log_{10} p \alpha m \log_{10} u \tag{6}$$

Measured sound pressure level (SPL),

$$\text{SPL (dB)} = 20 \log_{10} \frac{p}{P_{ref}} \tag{7}$$

Hence, for a constant reference pressure, from equations (6) and (7),

$$\frac{\text{SPL (dB)}}{10} \propto m \log_{10} u \qquad (8)$$

From figure 48, the slope of the line $\log_{10} u$ versus SPL (dB) gives $m = 5.45$.

APPENDIX II

EXPERIMENTAL UNCERTAINTIES

EXPERIMENTAL UNCERTAINTIES

FIGURE	TITLE	REMARKS-ERROR RANGE.
1	Venturi Apparatus	-
2	Cavitating Bodies	b/B = .165 $\pm$ $^{.0001}_{.0002}$
		.327 $\pm$ .0005
		.103 $\pm$ $^{.0003}_{.0001}$
		.196 $\pm$ .0005
		.326 $\pm$ .0006
		R(Typical): $\pm$ 2.5%, θ $\pm$.5°
3	Cavitation Test Section	Linear measurement $\pm$ .02 mm Angular measurement $\pm$ .5°
4	Instrumentation	-
5	Test Section for Erosion and noise studies.	As in fig. 3
6	Effect of Test Duration on Erosion, Venturi Apparatus.	Time: $\pm$ 1 second Weight Loss: $\pm$ .05 mg
7	Rotating Disk Facility.	Linear measurement $\pm$ .02 mm Angular measurement $\pm$ .05 mg σ $\pm$ .05 R(Typical): $\pm$ 2.5%
8	Effect of Test Duration on Damage, Rotating Disk Apparatus.	Time: $\pm$ 1 second Weight loss: $\pm$ .05 mg u $\pm$ .05 mps σ $\pm$ .05
9	Drag Coefficient, Noncavitating cylinder.	Present: R: as in fig. 2 Present: C_D $\pm$ .06 Present: C_{D_1} $\pm$ .04 Present: b/B $\pm$ .0005 (max.)

FIGURE	TITLE	REMARKS—ERROR RANGE.
10	Drag Coefficient, Cavitating Cylinder.	C_D ± .06 C_{D_1} ± .04 σ ± .05
11	Pressure Distribution for Cylinder.	R: as in fig. 2 σ ± .05 C_p ± .02
12	Pressure Distribution for Cylinder	As in fig. 11
13	Drag Coefficient, Cavitating Cylinder.	Present: R: as in fig. 2 σ ± .05 C_D ± .06
14	Drag Coefficient, Noncavitating Prism $\theta = 0^o$	Present: C_D ± .06 C_{D_1} ± .04 C_{D_j} ± .02
15	Drag Coefficient, Cavitating Prism $\theta = 0^o$	C_D ± .06 C_{D_1} ± .04 C_{D_j} ± .02 σ ± .05
16	Drag Coefficient, Noncavitating Prism $\theta = 60^o$	Present: C_D ± .06 C_{D_1} ± .04
17	Drag Coefficient, Cavitating Prism $\theta = 60^o$	Present: C_D ± .06 C_{D_1} ± .04 σ ± .05
18	Drag Coefficient, Cavitating Prism $\theta = 0^o$	C_D ± .06 σ ± .05

FIGURE	TITLE	REMARKS-ERROR RANGE
19	Pressure Distribution Cavitating Prism $\theta = 0^o$	$\sigma \pm .05$ $C_p \pm .03$
20	Pressure Distribution Cavitating Prism $\theta = 0^o$	As in fig. 19
21	Pressure Distribution Cavitating Prism $\theta = 0^o$	As in fig. 19
22	Pressure Distribution Cavitating Prism $\theta = 60^o$	As in fig. 19
23	Pressure Distribution Cavitating Prism $\theta = 60^o$	As in fig. 19
24	Pressure Distribution Cavitating Prism $\theta = 60^o$	As in fig. 19
25	Strouhal Number, Non-cavitating Cylinder.	Present: $S \pm .0025$ $S_1 \pm .0023$ R: as in fig. 2
26	Strouhal Number, Cavitating Cylinder.	$S \pm .0025$ $S_1 \pm .0023$ R: as in fig. 2 $\sigma \pm .05$
27	Pressure Records, Cylinder b/B = .165	$\sigma \pm .05$ Time ± .25%
28 *	Typical Power Density Spectra Cylinder, b/B = .165	dB: sought only relative value $\sigma \pm .05$ frequency ± .25%

FIGURE	TITLE	REMARKS-ERROR RANGE.
29	Strouhal Number, Cavitating Cylinder.	$\sigma \pm .05$ R: as in fig. 2 $S \pm .0025$
30	Strouhal Number, Non-cavitating Prism $\theta = 0^o$	$S \pm .0025$ $S_1 \pm .0023$ $S_j \pm .0017$
31	Strouhal Number, cavitating Prism $\theta = 0^o$	$S \pm .0025$ $S_1 \pm .0023$ $S_j \pm .0017$ $\sigma \pm .05$
32	Strouhal Number, Non-cavitating Prism $\theta = 60^o$	$S \pm .0025$ $S_1 \pm .0023$
33	Strouhal Number, Cavitating Prism $\theta = 60^o$	$S \pm .0025$ $S_1 \pm .0023$ $\sigma \pm .05$
34	Pressure Records, Prism $\theta = 60^o$, $b/B = .326$	$\sigma \pm .05$ time: 0.25%
35	Typical Power Density Spectra Prism $\theta = 60^o$, $b/B = .326$	$\sigma \pm .05$ frequency ± .25% dB: sought only relative value
36	Variation of C_{D_j} & S_j with σ_j for Prism $\theta = 0^o$	$C_{D_j} \pm .02$ $S_j \pm .0017$ $\sigma_j \pm .016$
37	Variation of C_{D_1} & S_1 with σ_1 for Prism $\theta = 60^o$	$C_{D_1} \pm .04$ $S_1 \pm .0023$ $\sigma_1 \pm .03$

FIGURE	TITLE	REMARKS-ERROR RANGE.
38	Choking Cavitation Numbers for cylinders.	σ_{ch} ± .05 σ_{ch_1} ± .03
39	Choking Cavitation Numbers for Prisms $\theta = 0^o$	σ_{ch} ± .05 σ_{ch_1} ± .03 σ_{ch_j} ± .016
40	Choking Cavitation Numbers for Prisms $\theta = 60^o$	σ_{ch} ± .05 σ_{ch_1} ± .03
41	Effect of Source Size and velocity on Damage, cylinders.	b ± .02 mm u ± .05 mps W ± .05 mg t ± 1 second σ ± .05
42	Effect of Source Size and Velocity on Damage, Prisms.	as in fig. 41
43	Erosion for Different velocities and cavitation numbers.	time ± 1 second b/B ± .0005 u ± .05 mps W ± .05 mg σ ± .05
44	Noise Spectra for Different cavitation Numbers at a constant velocity.	σ ± .05 u ± .05 mps SPL(dB) ± .05
45	Noise Spectra for Different velocities at a constant cavitation number.	σ ± .05 SPL(dB) ± 0.5 velocity ± .05 mps

FIGURE	TITLE	REMARKS-ERROR RANGE.
46	Noise (SPL) for Different velocities at constant cavitation numbers	σ ± .05 SPL (dB) ± 0.5 velocity ± .05 mps b/B ± .0005
47	Erosion and Noise Correlation.	σ ± .05 SPL(dB) ± 0.5 velocity ± .05 mps b/B ± .0005
48	Velocity expinent for erosion and noise.	Weight loss w ± .05 mg Velocity ± .05 mps SPL (dB) ± 0.5
49	Damaged Area of Test specimen (No splitter Plate)	
50	Damaged Area of Test specimen (With splitter plate)	
51	Effect of Wake Interference Element on Erosion and Noise.	SPL (dB) ± 0.5 W ± .05 mg x/b ± .004 (max) λ ± .056 (max)

* Note: Power Density Spectra information is used as a check on the direct strip chart measurements.